RHEOLOGICAL MEASUREMENTS AND CORE FLOOD DATA ANALYSIS IN SUPPORT OF CHEMICAL ENHANCED OIL RECOVERY FORMULATION DESIGN

by

Huiling Tang

A Thesis

Submitted to the Faculty of Purdue University

In Partial Fulfillment of the Requirements for the degree of

Master of Science in Civil Engineering

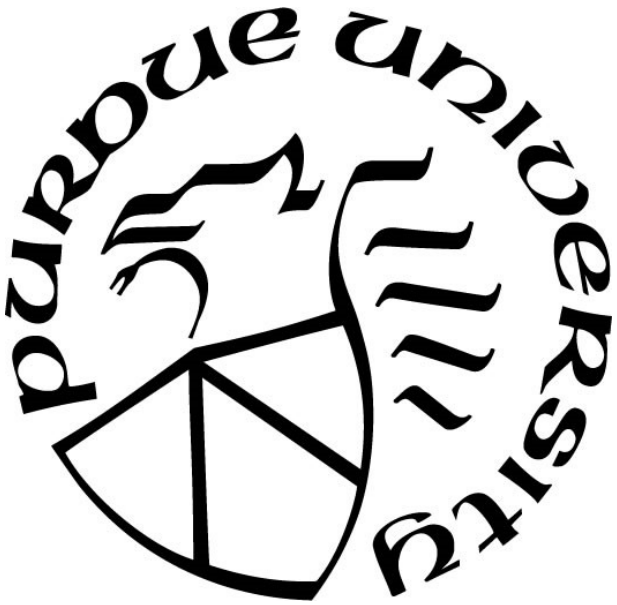

Lyles School of Civil Engineering

West Lafayette, Indiana

August 2017

THE PURDUE UNIVERSITY GRADUATE SCHOOL
STATEMENT OF COMMITTEE APPROVAL

Dr. Maria C. Santagata, Chair

Department of Civil Engineering

Dr. Cliff T. Johnston

Department of Agronomy

Dr. Antonio Bobet

Department of Civil Engineering

Approved by:

Dr. Dulcy M. Abraham

Head of the Graduate Program

For my father Ying-qi Tang, my mother Xiao-hui Wang.

ACKNOWLEDGMENTS

Firstly, I would like to express my sincere gratitude to my advisor Professor Marika Santagata for her continuous support of my research. Her guidance helped me in all the time of research and writing of this thesis. Besides my advisor, I would like to thank the rest of my thesis committee: Professor Cliff Johnston and Professor Antonio Bobet for their insightful comments and encouragement.

I gratefully acknowledge the funding received from Pioneer Oil Company that allowed me to pursue my graduate school studies. My sincere thanks also go to the following people: Dr. Rituraj Borgohain in Purdue EOR laboratory, Mohammadhasan Sasar and Yung-Jih Yang for their help and assistance with the experimental work; Professor Elias Franses in Purdue University's Chemical Engineering Department for his valuable comments. Without their support, it would not be possible to conduct this research.

Last but not the least, I would like to thank my parents for supporting me spiritually throughout writing this thesis and my life in general.

TABLE OF CONTENTS

LIST OF TABLES

LIST OF FIGURES

ABSTRACT

Author: Tang, Huiling. MSCE
Institution: Purdue University
Degree Received: August 2017
Title: Rheological Measurements and Core Flood Data Analysis in Support of Chemical Enhanced Oil Recovery Formulation Design
Major Professor: Maria Caterina Santagata

This research involved rheological measurements and the analysis of core flood test data in support of the design of a formulation for Chemical Enhanced Oil Recovery (cEOR) at the Pioneer Rock Hill reservoir, a site characterized by relatively low formation brine salinity and temperature. Extensive and systematic rheological measurements identified viscosity values and rheological behaviors of different polymers, surfactants and polymer-surfactant solutions over a range of concentrations, salinities, and temperatures relevant to the targeted field conditions. The results were used to support formulation design in combination with phase behavior studies and interfacial tension measurements, provide information relevant to in-tank mixing/pumping operations, and maximize sweep efficiency and mobility control in the core flood tests. Further rheological measurements were conducted on the primary surfactant, Petrostep® S13D, over a broad range of concentrations in both deionized water and two synthetic brines, up to neat solution. The results of these tests indicate that different structures (micellar solution, hexagonal liquid crystal, and lamellar liquid crystal) form at different concentrations, supporting SAXS observations performed by another research group.

In a separate effort, data obtained from core flood tests conducted in the Purdue EOR laboratory to evaluate and optimize formulations, were collected and organized. Five performance parameters: recovery factor in terms of %ROIP, oil saturation after chemical flood (S_{orc}), maximum injection pressure during chemical flood, surfactant sorption, and total injectant cost, were selected to evaluate test efficiency, based on technical and economic feasibility. Performance analysis of the core flood data and comparison with data from the literature show average to very good performance of the Purdue core flood tests.

1. INTRODUCTION

1.1 Overview of Chemical EOR

Enhanced oil recovery, also called tertiary oil recovery, is defined as the stage of oil production after secondary recovery (waterflooding in most cases) in which a fluid or combination of fluids, or, most recently, microbes, are injected into a reservoir in order to displace additional oil [1][2]. About 70% of original oil in place (OOIP) is likely to remain in the reservoir after the waterflood as discontinuous oil drops trapped by capillary forces [3]. EOR processes fall into 4 main categories based on the injectant: thermal, gas, chemical, and microbial methods. Data for 652 EOR projects performed worldwide between 1959 and 2010 were collected and summarized to construct a database in [4]. As shown in Figure 1.1, only about 11% of these projects adopted chemical EOR. It is also reported in [5] that, based on biannual EOR Surveys published by Oil & Gas Journal (1976-2010), oil production from chemical EOR processes has been negligible since the 1990's everywhere in the world except in China, because of the volatility of oil markets and the high cost associated with the injected chemicals. However, due in part to the developments in alkali-surfactant-polymer (ASP) technology and surfactant chemistry, there has been growing interest in the past few years in chemical EOR [5].

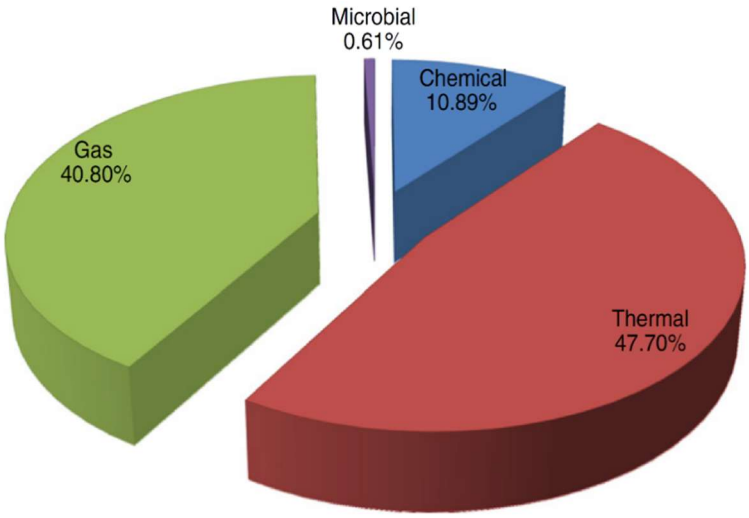

Figure 1.1 Methods used in 652 EOR projects worldwide (1959–2010) [4]

As shown in Figure 1.2, a typical chemical flooding consists of an optional preflush water flood (to adjust salinity and condition the reservoir), a chemical solution, a polymer solution for mobility control and a driving water flood for displacing the chemicals and the resulting oil bank to the production wells.

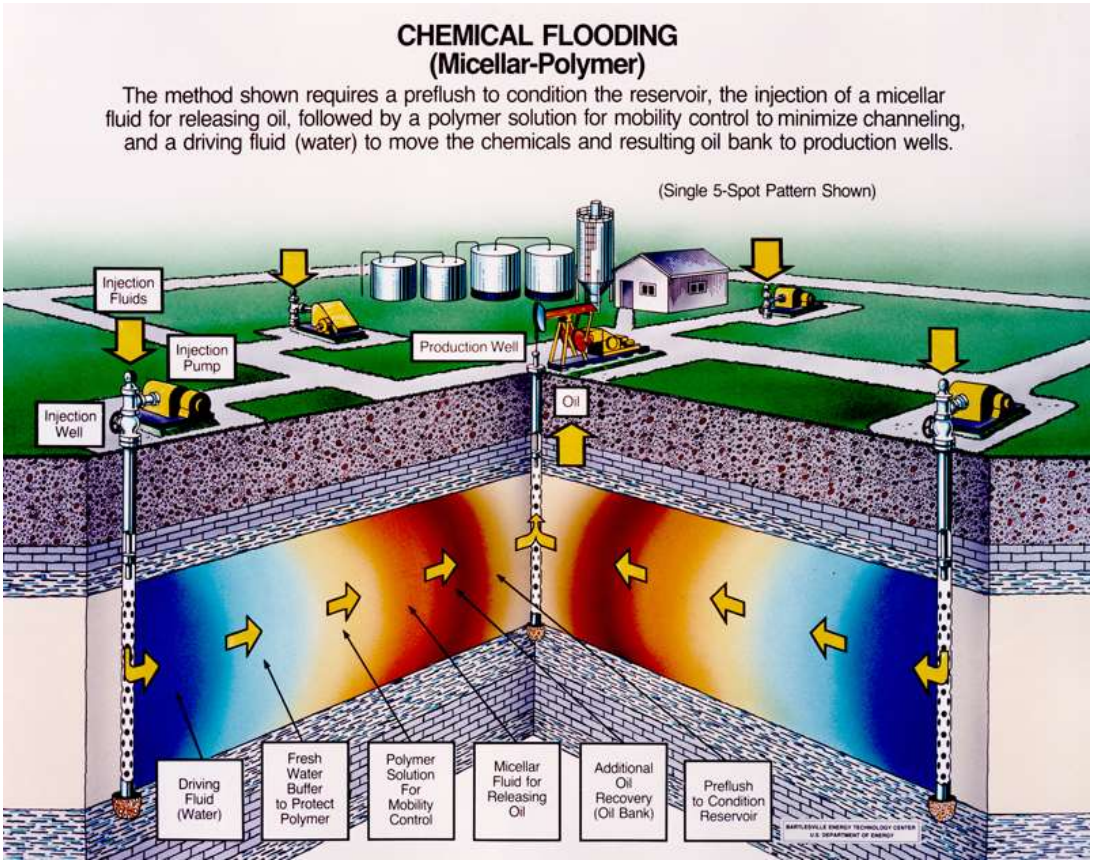

Figure 1.2 Chemical flooding process (Courtesy of U.S. DOE)

Chemical EOR methods fall in different categories: alkali flooding, polymer flooding, surfactant flooding or combinations of chemicals (i.e. ASP/SP flooding). Chemical EOR is considered to work better for mature fields (oil fields where production has reached its peak and has started to decline [6]) and waterflooded fields [5]. This research focuses on surfactant-polymer (SP) flooding of a previously waterflooded sandstone reservoir located in the Illinois basin in Indiana.

The overall displacement efficiency (E) of an EOR process is the product of microscopic (E_d) and macroscopic (E_v) displacement efficiencies (see Equation (1.1)) [1]. The microscopic displacement efficiency (E_d) reflects the extent of the mobilization

of trapped oil at the pore scale that is greatly dependent on factors such as rock wettability, relative permeability, interfacial tension (IFT) and capillary pressure [7]. The macroscopic displacement efficiency (E_v) relates to the volumetric sweep efficiency of the displacing fluids in contact with the reservoir which is controlled by the rock matrix heterogeneities and anisotropy, displacing and displaced fluid mobility ratio and positions of injection and production wells [1][8] .

$$E=E_dE_v \tag{1.1}$$

In surfactant-polymer (SP) flooding, a surfactant is injected to reduce the interfacial tension between displacing fluid and crude oil so as to improve the microscopic displacement efficiency; the use of the polymer is instead aimed at increasing the viscosity of the slug to achieve the desired mobility ratio, which is essential to achieve favorable sweep efficiency and prevent fingering.

Favorable oil recovery highly depends on the chemical formulation with surfactant(s) and polymer type and concentration and salinity playing a critical role. The design of a chemical formulation is therefore a complex process that must rely on knowledge of the site and data of screened chemicals. Prior to field deployment, laboratory scale core flood experiments are critical to examine and optimize the formulation and obtain preliminary assessments of the ultimate recovery achievable in the field.

A three-stage procedure (see Figure 1.3) was developed at the University of Texas at Austin to provide a systematic laboratory approach for chemical formulation design [9][10]. First, a list of chemicals is selected based on properties of crude oil and reservoir conditions. Then the efficiency of these chemicals is screened in a phase behavior study and related IFT and viscosity measurements. Once an optimal formulation is developed, core flood experiments are performed to test and optimize the formulation prior to field implementation.

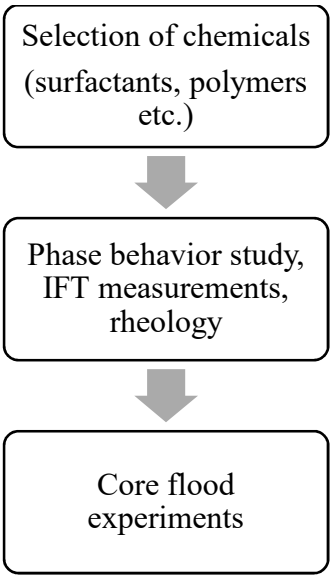

Figure 1.3 Three-stage laboratory procedure for chemical formulation design

1.2 Project Background

The work presented in this thesis was in part funded by a grant from Pioneer Oil Company based in Vincennes, Indiana, as part of a broad research initiative aimed at enhancing oil recovery efforts in the Illinois basin. The partnership between Pioneer Oil and a Purdue team of faculty and students from the Colleges of Engineering, Science and Agriculture was forged in 2014, with the first primary goal of developing an optimal formulation for chemical EOR to be implemented at Pioneer Oil's Rock Hill site in southern Indiana (see Figure 1.4).

The oilfield is a sandstone reservoir in the Illinois basin which has an average depth of approximately 1000 ft. and low reservoir temperature (18-24 ºC). The reservoir has a porosity of about 20% and is highly heterogeneous in terms of permeability, ranging from less than 100 mD to around 1500 mD. The formation brine salinity is relatively low (9400-9700 ppm). Crude oil in the reservoir is light (API 30-32) with viscosity in the 13-23 cP range at 24 ºC.

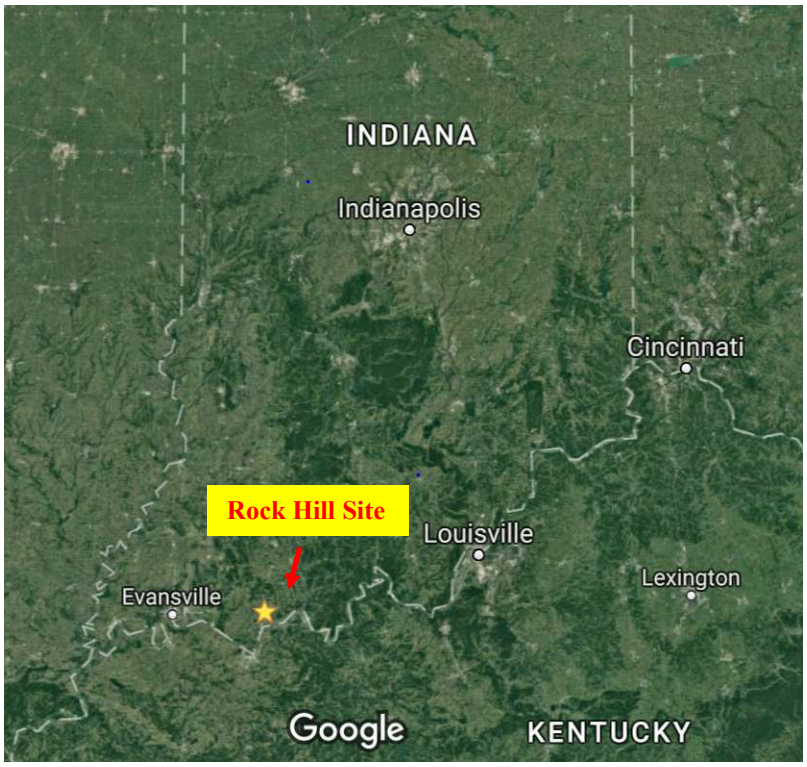

Figure 1.4 Rock Hill field location

Water flood has been previously conducted at the Rock Hill oilfield (see Figure 1.5) and according to field surveys residual oil saturation is currently about 25-30%, posing significant challenges for the intended subsequent chemical flood. In addition, the shallow depth of the reservoir limits the injection pressures that can be utilized during the chemical oil recovery process.

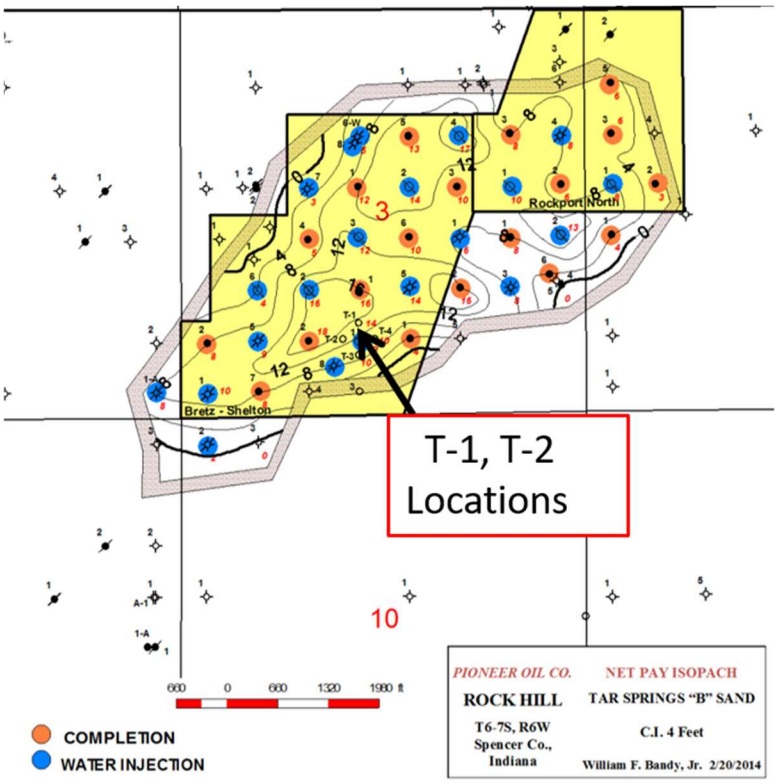

Figure 1.5 Detailed wells information of Rock Hill site

The Purdue Pioneer partnership was implemented through the creation of Purdue's Enhanced Oil Recovery (EOR) Lab located in Discovery Park and funding of research projects aimed at exploring a range of aspects related to chemical EOR at the Rock Hill site, including reservoir characterization, multiphase flow numerical and physical modeling, surfactant and polymer evaluation, crude oil analysis. The partnership benefits from the experimental facilities available in the Purdue EOR Lab, including an apparatus for core flood testing, and in the laboratories associated with the individual faculty part of the EOR team.

The research presented in this thesis was performed during the second year of the agreement (January-December 2016) as part of a one-year project entitled "Pore fluid engineering for enhanced oil recovery: coreflood test analysis and supporting rheological measurements."

1.3 Research Objectives

Within the broad scope of contributing to the design of a formulation for chemical EOR at the Pioneer Rock Hill site, the specific objectives of the work presented in this thesis were to:

a) Conduct an extensive and systematic rheological study of different polymer, surfactant and polymer-surfactant solutions over a range of concentrations, salinities, and temperatures.

   This work, which was conducted in the Rheology Laboratory of Purdue's Lyles School of Civil Engineering, made use of chemicals selected based on a previous phase behavior study and interfacial tension measurements, and was intended to both support the design of an optimal formation-specific formulation and address issues associated with the operations of mixing and pumping of the chemicals at the site.

b) Analyze and interpret data from core flood tests performed in the Purdue EOR laboratory.

   This work, which focused on collecting and organizing data collected by other members of the Purdue EOR research team, was aimed at assessing the efficiency of the formulations examined in the core flood tests and comparing the results obtained to those documented in the literature.

c) Study the rheology of solutions of the primary surfactant, Petrostep® S13D, over a broad range of concentrations in both deionized water and a synthetic brine. This portion of the research, which was performed in the Rheology Lab of the Lyles School of Civil Engineering, was intended to provide insight on the phase diagram of the surfactant, complementing SAXS observations performed by another research group.

1.4 Organization of Thesis

As discussed above, this research addressed three different aspects related to the design of a formulation for chemical (SP) EOR at the Pioneer Rock Hill site, and the organization of this thesis reflects these three efforts.

Chapter 2 presents experimental methods and results related to the rheology testing program conducted in support of formulation design and field mixing/pumping operations. The chapter discusses the impact on the rheological measurements of key influencing factors including chemical (polymer and/or surfactant) type and concentration, temperature, salinity, shear rate and time on the measured values of viscosity, and provides viscosity data for optimal formulations identified from the phase behavior study.

Chapter 3 summarizes the data from core flood tests conducted between November 2015 and March 2017 in Purdue's EOR laboratory and accesses the oil recovery efficiency for these tests. Additionally, data of tests documented in the literature are used to put the Purdue core flood results in context.

Chapter 0 presents the results of the rheological study of DI water and brine solutions of the primary surfactant (S13D) utilized in this research. The different rheological responses observed as a function of concentration and salinity are used, in conjunction with SAXS (Small-angle X-ray Scattering) results obtained by the chemical engineering group of Purdue EOR research team, to draw inferences on the structure of the surfactant solutions.

Finally, Chapter 5 presents a summary of the key insights provided by all experimental results and provides recommendations for future work in the three different areas of research.

2. RHEOLOGICAL MEASUREMENTS

2.1 Introduction

This chapter focuses primarily on the rheological measurements conducted on aqueous surfactant, polymer and polymer-surfactant solutions. These measurements were intended to complement IFT measurements, phase behavior studies and core flood tests performed to identify the optimal slug formulation to be used for chemical EOR at the Pioneer Rock Hill site. Additional tests on pure surfactants conducted to address issues related to mixing/pumping operations at the site are also presented. The chapter is organized in two primary sections, beyond this introduction. Section 2.2 describes the materials and the experimental methods and outlines the experimental program. The results of the experiments are presented in Section 2.3, which examines the impact of key influencing factors including chemical (polymer and/or surfactant) type and concentration, temperature, salinity, shear rate and time on the measured values of viscosity. The section concludes with the presentation of viscosity data for optimal (high salinity) formulations identified from the phase behavior study.

2.2 Materials and Experimental Methods

2.2.1 Materials

The anionic polymers used in this study are partially hydrolyzed polyacrylamide (HPAM) with molecular weights of 6-8 million Dalton (Flopaam 3230S) and 8-10 million Dalton (Flopaam 3330S). Figure 2.1(a) shows the molecular structure of HPAM. There is a synthetic straight chain consists of acrylamide monomers, some of which have been hydrolyzed. m and n are the numbers of amide and carboxylate groups, respectively. When hydrolyzed in water, the polyacrylamide chain of HPAM is stretched to enhance the viscosity due to the electrostatic repulsion between the negative charges in the carboxylate groups on the chain[11]. Both polymers have 30% hydrolysis. Chemicals were provided by SNF Floerger (Cedex, France) in solid form.

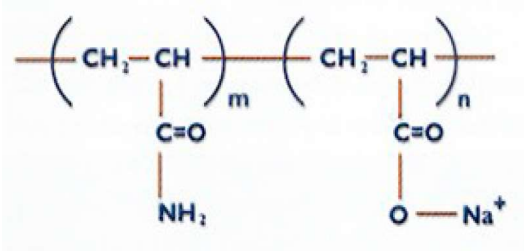

(a) HPAM

C_{13} Hydrocarbon-PPO_{13}-$SO_4^-Na^+$

(b) S13D-HA

Figure 2.1 Polymer and surfactant molecules

Two surfactants were used: an anionic surfactant of alcohol alkoxy sulfate (Petrostep® S13D-HA) and an alkyl benzene sulfonate with sodium salts (Petrostep® A6) supplied by Stepan. Petrostep® S13D-HA has an approximately 80% activity and its chemical structure is proprietary, 'HA' refers to high activity. Surfactants have both hydrophilic and hydrophobic groups to lower the surface tension or interfacial tension between two liquids or between a liquid and a solid. For S13D-HA (see Figure 2.1(b)**),** the hydrophobic part is a long hydrocarbon chain (could be branched), while the hydrophilic part is anionic (SO_3^-). Petrostep® A6 has an activity of about 55%. In addition, n-butanol + 2 EO (Surfonic® L4-2) provided by Huntsman was employed as co-solvent. All evaluated chemicals are listed in Table 2.1.

Synthetic Rock Hill brine, herein referred to as RH brine, was used to prepare chemical solutions (see Section 2.2.2.1 for the procedure followed to prepare the brine). Table 2.2(a) shows the major components of this brine, which was intended to mimic the natural brine existing at the Rock Hill site. Four fresh water samples were taken on March 18th,2014 at two different Rock Hill facilities-BRETZ SHELTON and ROCKPORT NORTH (two independent samples for each facility), which were regarded as representative, and sent to SRC Inc. for analysis immediately after sampling. Their composition is summarized in Table 2.2(a) alongside the data for the

synthetic brine. It is seen that the total dissolved solids (TDS) of the natural Rock Hill brine fall between 8,800 and 10,800 mg/L, with chloride, sodium, and bicarbonate being the primary contributors. The ionic composition of the synthetic brine closely mimics that of the original brine, with the exception of the iron ions. Iron was measured in both natural samples, albeit at rather different concentrations (3 and over 70 mg/L, respectively). The presence of iron in solution in consistent with the reducing conditions of the aquifer. Iron was not included in the synthetic brine as it would precipitate due to the oxidizing conditions present when preparing the brines. This is a potentially significant difference between the two brines, as iron concentrations in reduced brines as low as 1 ppm are known to cause degradation to the polymer when exposed to oxygen[12].

Table 2.1 List of evaluated chemicals

Name	Common chemical name	Type	Supplier
Surfactants			
Petrostep® S13D-HA	Alcohol Alkoxy Sulfate (79.68% Active)	Anionic	Stepan
Petrostep® A6	Alkyl-benzene sulfonate, sodium salts (55.80% Active)	Anionic	Stepan
Co-solvent			
Surfonic® L4-2	n-butanol + 2 EO		Huntsman
Polymers			
Flopaam 3330S	Polyacrylamide (8-10 million Dalton,30% hydrolysis)	Anionic	SNF
Flopaam 3230S	Polyacrylamide (6-8 million Dalton, 30% hydrolysis)	Anionic	SNF

2.2.2 Experimental Methods

2.2.2.1 Sample Preparation

RH brine was prepared by dissolving the salts (purity>98%) shown in Table 2.2(b), in the order they are reported in the table, into degassed, deionized DI water (conductivity: 18MΩ) while stirring using a magnetic stirrer with control of temperature at 24 °C. The DI water was degassed for 1 hour before adding salts (see Figure 2.2). Each salt was not added before the previous one was completely dissolved. 1-1.5 liters of solution were prepared at one time. Normally, polymer/surfactant solutions were prepared immediately after brine preparation. The rest of the fresh brine, if any, was stored at room temperature (close to 24 °C). Storage duration was limited to one week.

A 5000ppm polymer mother solution was used to prepare all other polymer solutions. It was prepared by slowly adding the targeted amount of polymer powder to the shoulder of the vortex of the fresh RH brine. To ensure complete dissolution of the polymer, the solutions were stirred continuously using a magnetic stirrer with control of temperature at 24 °C for at least 24 hours. The mother solution was then diluted to the desired concentration. When preparing solutions at higher salinity (HTDS solutions), NaCl was added to reach the required salinity. Similarly, surfactant/polymer-surfactant samples were made by adding surfactant into brine/polymer solutions while stirring to guarantee the dissolution. These solutions were stored at room temperature (close to 24 °C) and tested within a week after preparation unless the effect of time was examined.

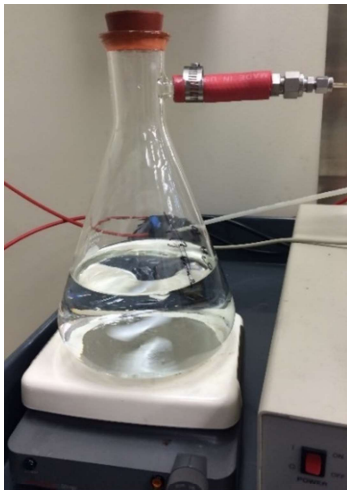

Figure 2.2 DI water (Conductivity: 18MΩ) degassing

2.2.2.2 Rheometer

All rheological tests were conducted using the Physica MCR 301 rotational rheometer, an air bearing, stress-controlled device manufactured by Anton Paar GmbH, which can also operate in strain rate controlled mode through a feedback control loop. The Physica MCR 301 is equipped with a permanent magnet synchronous drive (minimum torque=0.1 μN m, torque resolution= 0.001 μNm), and an optical incremental encoder for measuring the shear strain (resolution < 1 μrad). It can be used to perform a variety of oscillatory and monotonic, stress-controlled, and strain-rate controlled tests including amplitude sweeps, frequency sweeps, time sweeps, rate ramps, stress ramps and creep and recovery tests. The rheometer is equipped with a Peltier temperature control system that can control the temperature in the 40 to 200 °C range. An automated computer software system is used to program the testing variables and to compute and store the experimental results.

Double gap (DG) and cone-plate (CP) geometries (See Figure 2.3) were used to conduct the tests. The double gap geometry has the largest surface area so it is ideal for testing low viscosity solutions while the cone- plate geometry was adopted for higher viscosity solutions.

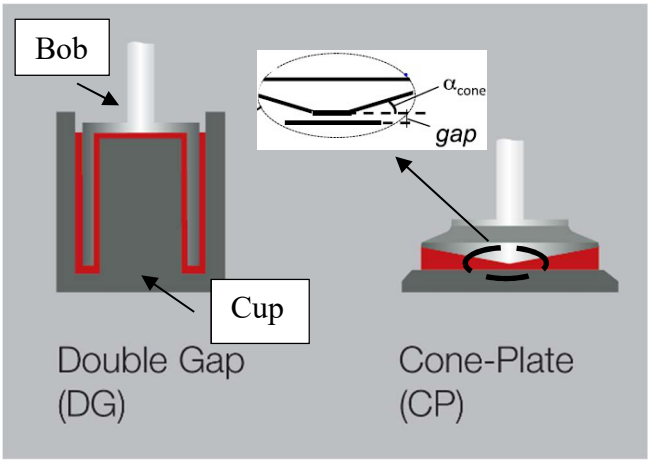

V_{sample}=3.6mL	V_{sample}=1mL
Bob: D_{inner}=24.66mm	D_{cone}=60mm
D_{outer}=26.66mm	α_{cone}=0.981°
$L_{effective}$=40mm	gap=0.046mm

Cup: D_{inner}=23.826mm, D_{outer}=27.592mm

Figure 2.3 Schematics of DG and CP geometries

Table 2.2 Composition Rock Hill brine

(a) Rock Hill brine composition (From SRC Analytical Report) (b) Brine preparation

	Units	Rock Hill Brine		
		Original		Synthetic
		BRETZ SHELTON SAMPLE	ROCKPORT NORTH SAMPLE	
Bicarbonate	mg/L	1660-1670	2050-2110	1664.7
Chloride		4420-4680	5080-5160	4358.5
Calcium		104-106	170	104.8
Magnesium		38-39	58	38.1
Potassium		6.5	8	6.5
Sodium		3170-3190	3630-3780	3197.3
Sulfate		6.1-6.2	4	3.2
Barium		124	270-320	124.5
Iron		3	74-92	0.0
Manganese		0.48	0.88-1.0	1.2
TDS		8790-8870	10200-10800	9400

Synthetic Rock Hill Brine	
Salt(added)	mg/L
Follow the order	
NaCl	6531.96
KCl	12.39
$MnCl_2 \cdot 4H_20$	4.414
$MgCl_2 \cdot 6H_20$	321.96
$BaCl_2 \cdot 2H_20$	221.44
$FeCl_2$	0
$FeCl_3$	0
$SrCl_3$	0
$Na_2SO_4 \cdot 10H_20$	10.61
$NaHCO_3$	2292.31
$CaCl_2 \cdot 2H_20$	385.04
TDS	9400

Two types of tests were performed to measure the viscosity: constant shear rate tests in which the resulting shear stress is measured as a function of time (typically for one minute) as the sample is sheared, and shear rate ramps in which the shear rate is increased in steps, again measuring the resulting shear stress. In these tests, the duration of each measurement point is 10s. The data acquisition system of the MCR301 rheometer takes 0.02s per data point. The first 30% of the duration is for adjustment to reach a steady state and raw data points are generated within the rest 70% of duration. The final measurement point reported is the average number of the last 50% of the raw data. For shear rate ramp tests, at least 4 measurement points are obtained per decade. In select tests on polymer solutions, measurements were also conducted while decreasing the applied shear rate after the maximum value had been reached.

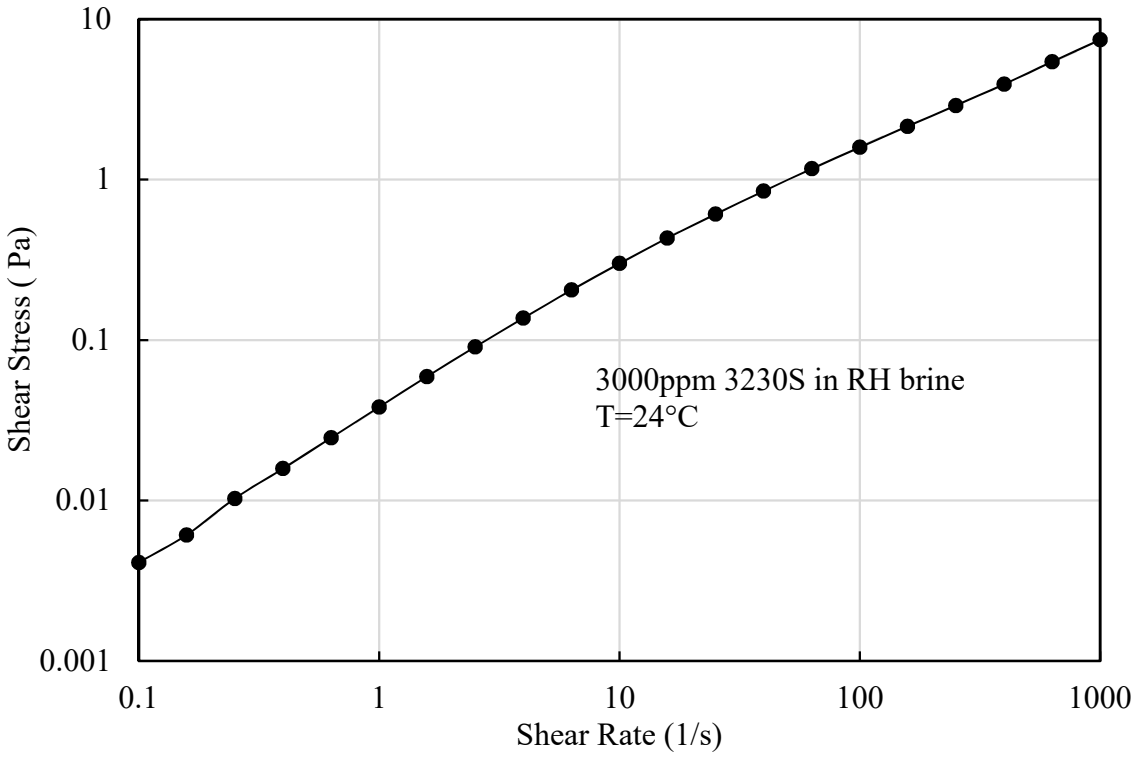

Figure 2.4 Shear rate ramp test for 0.3wt% 3230S in RH brine at 24°C

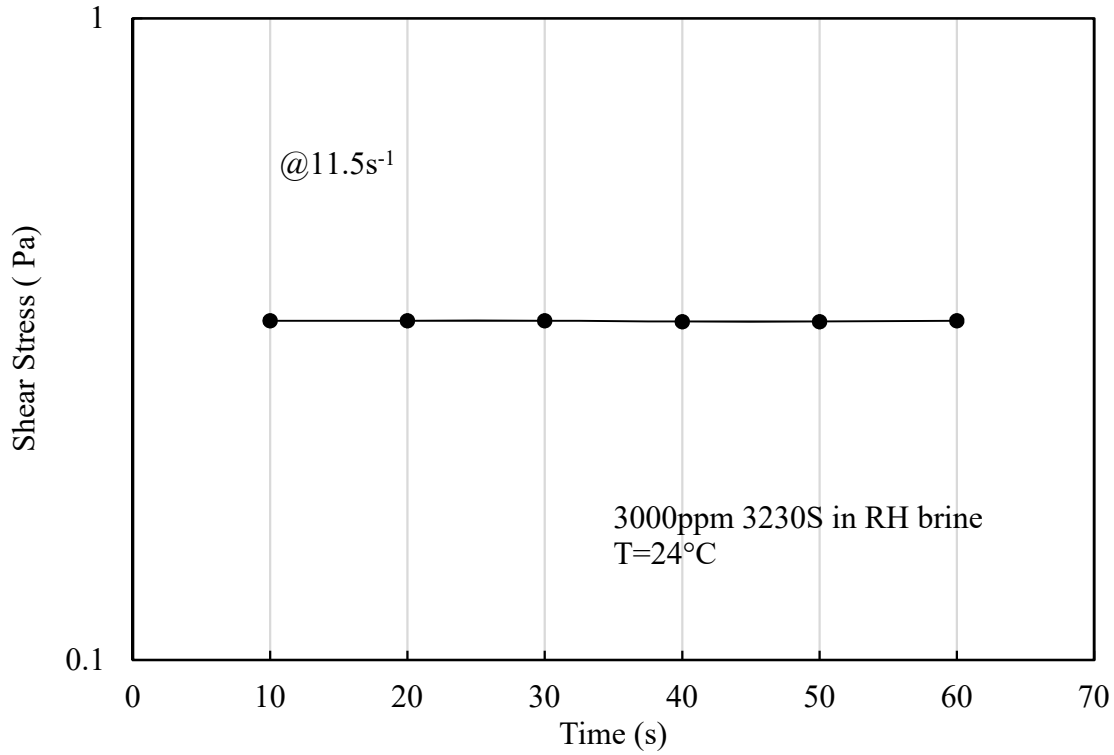

Figure 2.5 Constant shear rate test (at 11.5s^{-1}) for 0.3wt% 3230S in RH brine at 24°C

Figure 2.4 and Figure 2.5 show examples of the results of the two tests described. In both tests, the viscosity is derived as shear stress divided by shear rate.

In the shear rate ramps, measurements of the viscosity were obtained for values of the shear rate in the 0.1 to 1000 s^{-1} range. As the accuracies of viscosity data at low shear rates for different samples are not the same, results with different shear rate ranges are presented in this report. 0.1-10 s^{-1} is the shear rate range associated with chemical flooding [11]. In the constant shear rate tests, measurements were obtained at 10/11.5 s^{-1}. The first value represents the upper end of the range associated with chemical flooding, while the second (11.5 s^{-1}) was adopted in select tests to allow a comparison with viscosity measurements obtained in Purdue's EOR lab using a Brookfield viscometer. These tests measured the viscosity of injected chemical solutions and effluents of core flood tests at 3 rpm (which correspond to 11.52 s^{-1}).

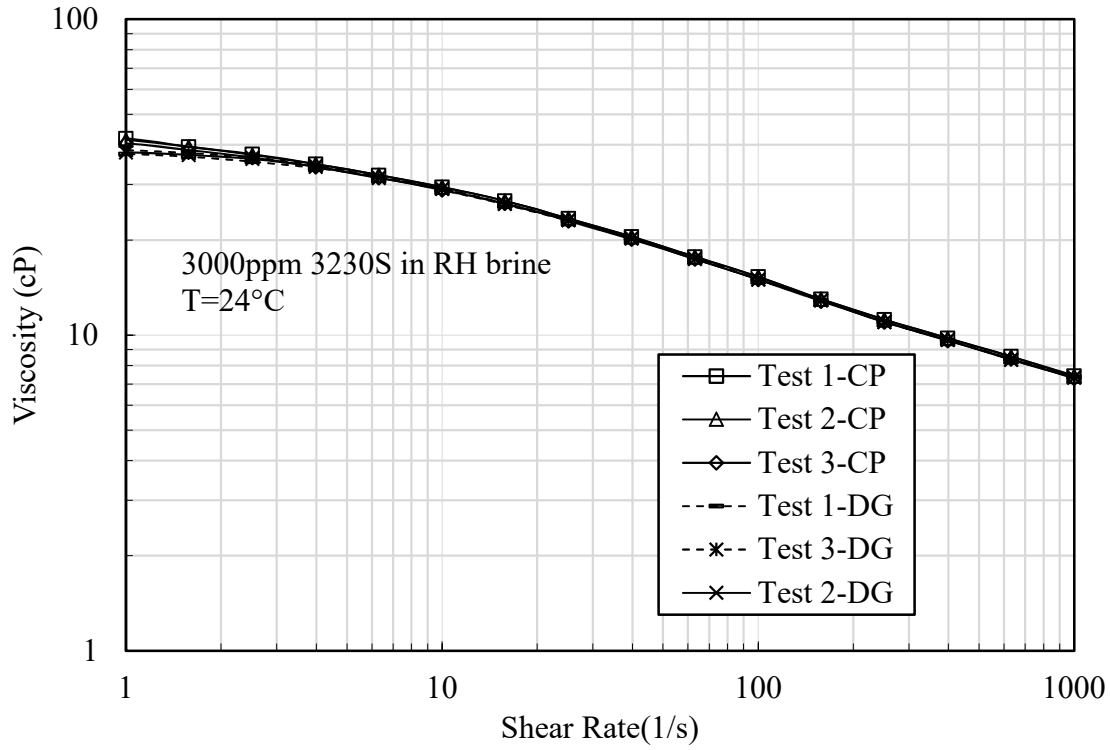

Figure 2.6 Test repeatability with the two geometries

As an example of the test to test repeatability and the consistency of the data obtained using the two geometries employed in this study, Figure 2.6 presents flow curves obtained from shear rate ramps performed on a 3000 ppm 3230S solution in RH brine. The viscosity of this sample (between about 7 and 40cP over the shear rate range examined) is suitable for testing with both geometries. The six curves shown, which pertain to tests on independent samples, show a less than 5% deviation. Note that through most of the testing program a single geometry was used for each sample. In general, the double gap geometry was adopted for testing solutions with viscosity lower than 10cP.

2.2.2.3 Testing Program

As summarized in Table 2.3, the testing program included tests on the pure surfactants, on surfactant only solutions, on polymer only solutions, and on polymer surfactant solutions. The tests on the pure surfactants were aimed at addressing issues related to the handling, pumping and storage of these materials at the site, in particular the dependence of the viscosity on temperature, given the variability in temperature conditions expected at the site. The remaining tests were in support of the design of the chemical formulation to be used for the laboratory core flood tests, and ultimately in the field. Key variables examined in this second group of tests were: the concentration of the various chemicals, the chemistry of the mixing water and the testing temperature.

93 samples in total were tested under different temperatures in this program. The majority of the tests were conducted at 24°C, the temperature at which all core flood tests were performed in Purdue's EOR lab. Additional tests were performed at 18°C. These two values of temperature bracket the values observed in the Rock Hill reservoir. Also, to provide information relevant to in situ EOR deployment, a wider range of temperature 4-35°C was adopted for some tests.

The ranges in the concentrations of the chemicals in general bracketed those explored in the core flood tests (e.g. 0.18wt%-0.34wt% for 3330S, 0.25wt%-0.36wt% for 3230S and 0.4wt%-1.0wt%A for surfactant/surfactant mixtures).

With regard to the salinity of the mixing water, the testing program utilized primarily synthetic Rock Hill brine (RH) with TDS = 9,400 ppm (see Section 2.2.2.1 above). For reference additional tests were also performed utilizing deionized water and the original Rock Hill brine. Finally, having established from the phase behavior studies and the coreflood tests conducted in the EOR lab, that high salinity conditions would improve oil recovery, higher values of the salinity (17.5k-22k) were employed for tests on both polymer and polymer-surfactant solutions. In particular, the last set of tests focused on the formulation that appeared to be most promising for field application: a polymer-surfactant slug with fixed surfactant mixture of 0.8wt% S13D+A6+L4-2(7:2:2) at optimal salinity of 17.5k.

Table 2.3 Testing Program

	Salinity	Polymer	Surfactant	Temp.	Status
Pure surfactant	--	--	S13D	4°C-35°C	Fresh
			A6		
			S13D+A6(7:2)		
			S13D+A6+L4-2(7:2:2)		
Surfactant-only solutions	RH brine	--	0.4-3.0wt%A S13D	24°C	Fresh
	17.5k		0.8wt%A S13D+A6+L4-2(7:2:2)	4°C-35°C	
Polymer-only solutions	RH brine	0.05-0.5wt% 3330S	--	18°C	Fresh (only 0.35wt% 3330S was stored for months to examine time effect)
		0.05-0.5wt% 3330S/3230S		24°C	
	"Original" RH brine	0.2-0.5wt% 3330S		18°C 24°C	
	DI water	0.2-0.5wt% 3330S		24°C	
	18,20,22k	0.2-0.35wt% 3330S		24°C	
Polymer+ surfactant	RH brine	0.3wt% 3330S/3230S	0.4-3.0wt%A S13D	24°C	Fresh
	18,20,22k	0.3wt% 3330S	0.4-3.0wt%A S13D+A6+L4-2(7:2:1)		
	17.5k	0.15-0.5wt% 3330S/3230S	0.8wt%A S13D+A6+L4-2(7:2:2)	4°C-35°C	

Note that in Table 2.3, 'A' refers to active and 'Fresh' status means that samples were tested within a week after preparation. Additional tests on higher concentration S13D solutions are discussed in Chapter 0.

2.3 Experimental Results and Discussion

2.3.1 Viscosity of Pure Surfactants and Surfactant Mixtures

To examine the sensitivity of the rheological behavior of the pure surfactants to site temperature conditions and provide information relevant to mixing/pumping operations in tank, the viscosity of the pure surfactants (S13D, A6) and of the surfactant mixtures [S13D+A6(7:2), S13D+A6+L4-2(7:2:2)] examined in this research was measured at temperatures of 4-35°C. These temperatures reflect the range that is expected to be encountered in the field tanks over the course of a year. Note that, as summarized in Table 1, the two surfactants used here - S13D and A6 - are 79.68% active and 55.8% active, respectively. Figure 2.7 shows pictures of the tested samples.

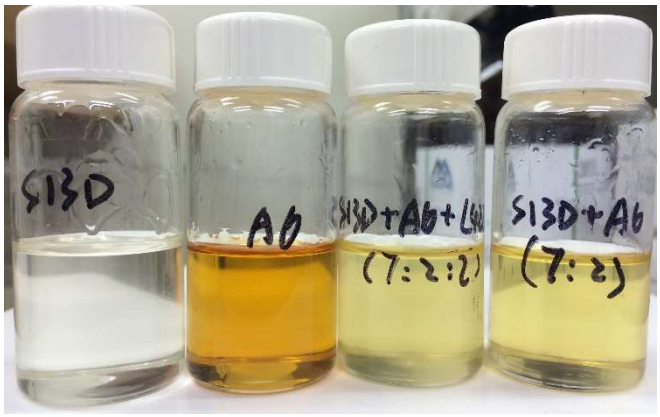

Figure 2.7 Pure surfactant samples
(From left to right: S13D, A6, S13D+A6+L4-2(7:2:2), S13D+A6(7:2))

Figure 2.8 presents the results of the shear rate ramps performed at of 4, 15 and 25°C. As shown in Figure 2.8(a), over the shear rate range examined, S13D exhibits Newtonian behavior with viscosity markedly increasing with decreasing temperature (from about 1600 cP at 25°C, to about 2900 cP at 15°C, to over 5900 cP at 4°C). This over threefold increase in viscosity suggests increased challenges in mixing and pumping the surfactant at the lower site temperatures expected for the winter months.

In contrast to S13D, the A6 surfactant (Figure 2.8(b)) shows viscosity decreasing with increasing shear rate, with values generally lower than those observed for the primary surfactant. Over the shear rate range examined (1-100 s^{-1}) the viscosity of the A6 surfactant decreases by as a much as a factor of 7 at 25°C, with reduced sensitivity to shear rate with decreasing temperature. Above 5 s^{-1}, the data show the expected trend

of decreasing viscosity with increasing temperature at any shear rate. At the lowest shear rate values examined the data show no clear trend with the highest value of viscosity measured on the sample tested at 25°C. The two surfactant mixtures, S13D+A6(7:2) (Figure 2.8(c)), and S13D+A6+L4-2(7:2:2) (Figure 2.8(d)), all show Newtonian behavior over the 1 to 100 s^{-1} shear rate range.

For the testing conditions examined, S13D is quite more viscous than A6, and therefore adding co-surfactant A6 into S13D to reach the targeted ratio causes a reduction in viscosity. The reduction is around 50% for all three temperatures. With the addition of the co-solvent (mixture S13D+A6+L4-2(7:2:2) in Figure 2.8(d)), the reduction in viscosity compared to S13D exceeds 85%, again independent of temperature. Note that according to the information provided by the manufacturer, water accounts for 20-40% of A6 apart from the 55.8% active components. Thus, when mixed with A6 and L4-2, S13D is effectively diluted, contributing to the decreased viscosity of the mixtures.

As seen for the pure S13D, the viscosity of the mixtures is markedly dependent on temperature with the value measured at 4°C over three times greater than that measured at 25°C. This again indicates that increased challenges in handling and pumping are to be expected in the field operations during cold weather periods.

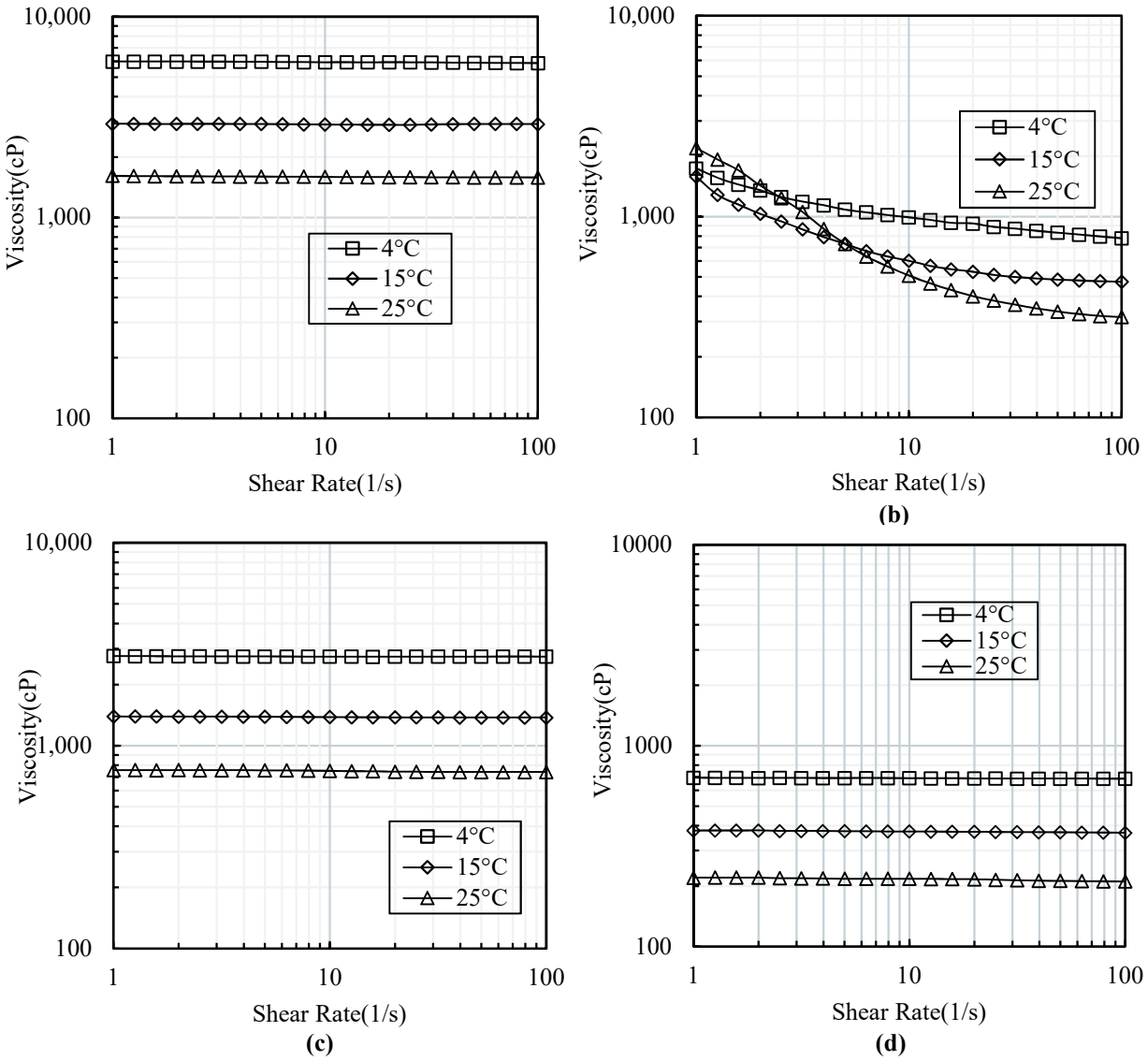

(a) S13D (b) A6 (c) S13D+A6(7:2) (d) S13D+A6+L4-2(7:2:2)

Figure 2.8 Pure surfactant rheology at 4°C, 15°C, 25°C

2.3.2 Viscosity of Surfactant-only Solutions

As summarized in Table 2.3, viscosity measurements were performed on surfactant solutions that were considered most promising for field application following extensive testing in Purdue's EOR laboratory. They are 0.4wt%-3.0wt%A solutions of S13D in RH brine and a 0.8wt%A solution of S13D+A6+L4-2(7:2:2) in 17.5k brine. Measurements on solutions of the surfactant mixture were conducted at temperatures

in the 4-35°C range. All tests in this section used the double gap geometry. Due to the low viscosity of the solutions and the resolution of the geometry, viscosity data from the shear rate ramp tests on these solutions are presented in Figure 2.9 only for shear rates exceeding $10s^{-1}$. For reference this figure also presents data for the RH brine. Close to Newtonian behavior is observed for all solutions, with viscosity increasing with surfactant concentration. At the reference shear rate ($10s^{-1}$), the viscosity increases from 0.94cP for the RH brine to 1.30cP when adding 2.0wt%A S13D.

As shown in Figure 2.10, viscosity of 0.8wt%A S13D+A6+L4-2(7:2:2) in 17.5k at $10s^{-1}$ decreases with testing temperature.

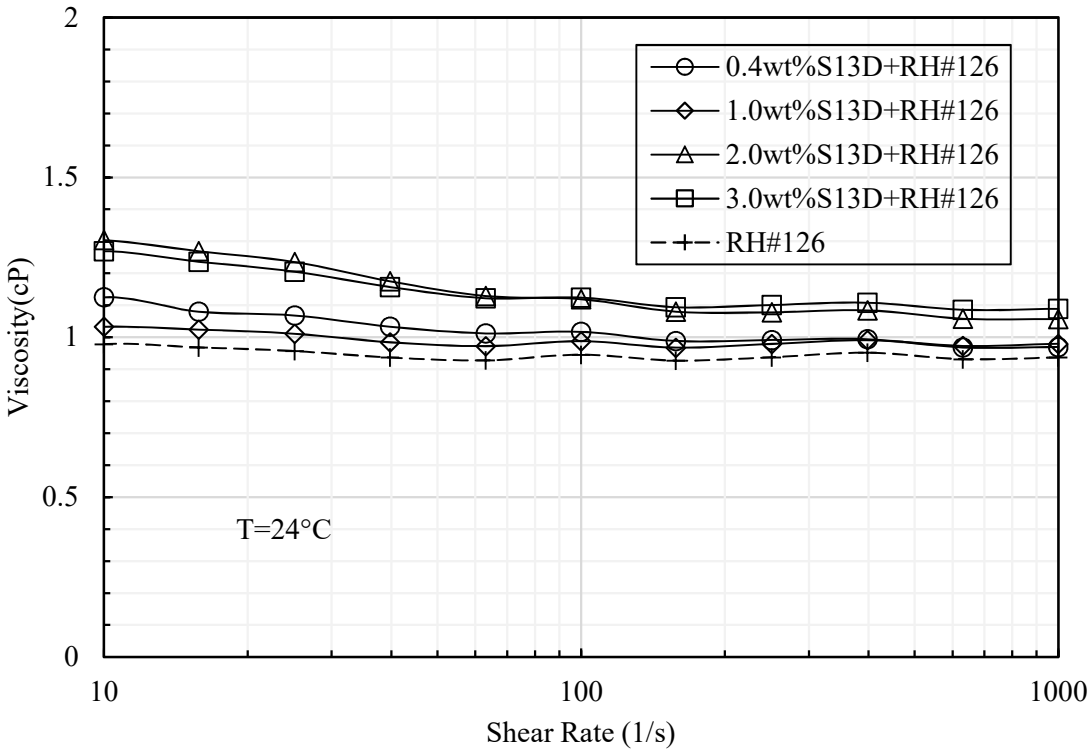

Figure 2.9 Viscosity of 0.4wt%-3.0wt%A S13D solutions in RH brine at 24°C

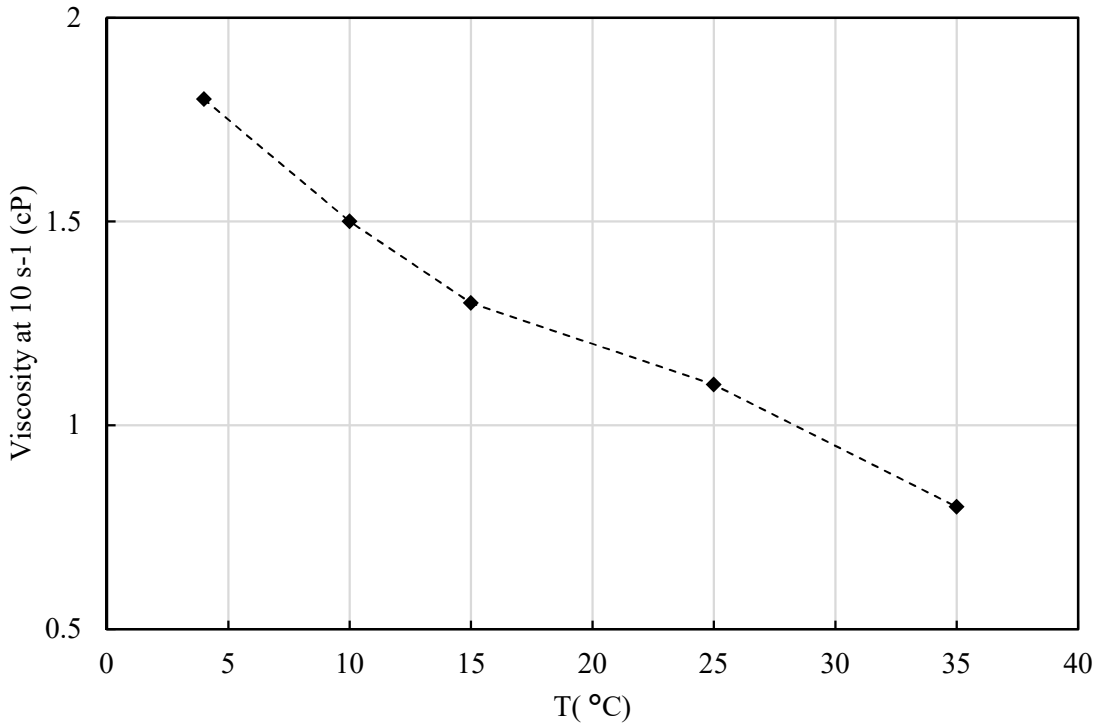

Figure 2.10 Effect of temperature (4-35°C) on the viscosity of 0.8wt% S13D+L4-2+A6(7:2:2) at 17.5k

2.3.3 Viscosity of Polymer-only Solutions

2.3.3.1 Effect of Polymer Concentration on Polymer Viscosity

Figure 2.12 presents loading curves for the two polymers examined in this study at 24°C. These curves show the variation in the viscosity at 10 s^{-1} measured in constant shear rate tests on polymer solutions prepared in synthetic RH brine with concentrations ranging from 500 ppm to 5000 ppm. These results were obtained to provide baseline viscosity data against which to evaluate the effects of the addition of a surfactant, and of changes in salinity. As expected, due to its lower molecular weight, Flopaam 3230S shows lower viscosity than Flopaam 3330S at any concentration. For both polymers, the increase in viscosity with polymer concentration is well described by a second order polynomial equation.

Shear rate tests (see Figure 2.13, Figure 2.14) show the variation of viscosity as a function of shear rate in the 1-1000 s^{-1} range, with shear thinning behavior observed in all polymer solutions, At all shear rates, the higher the polymer concentration, the

higher the solution viscosity. On select solutions viscosity measurements were performed not only while increasing the shear rate (loading ramp) but also in the unloading stage. As illustrated in Figure 2.11, there is excellent consistency in the data from the loading and unloading ramps, especially after the shear rate exceeds 1 s^{-1}.

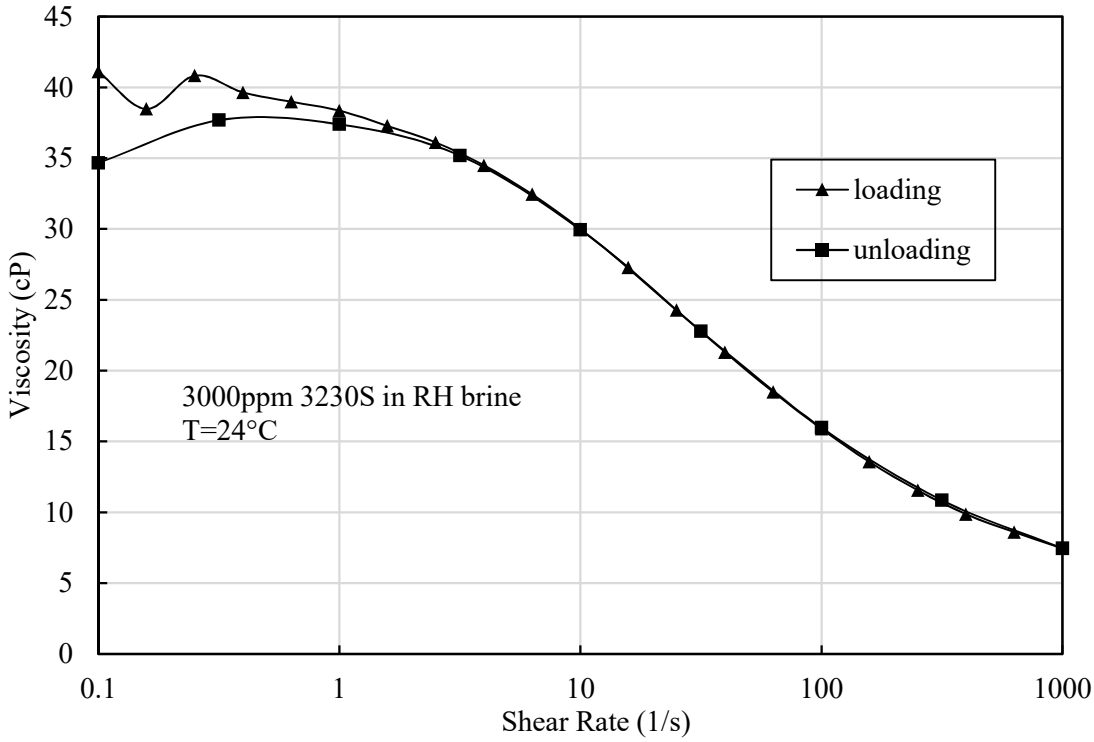

Figure 2.11 Loading and unloading ramps for 0.3wt% 3230S in RH brine at 24°C

2.3.3.2 Effect of Temperature on Polymer Viscosity

It is established [11][13][14] that the viscosity of polymer solutions is highly dependent on temperature. This effect was investigated on a limited basis for solutions of Flopaam 3330S in RH brine, conducting tests at 18°C and 24°C (reservoir temperature). The results, which are shown in Figure 2.14, indicate a reduction in viscosity in the 7-15% range with the decrease in testing temperature from 24°C to 18°C for all polymer solutions over the range of shear rates examined.

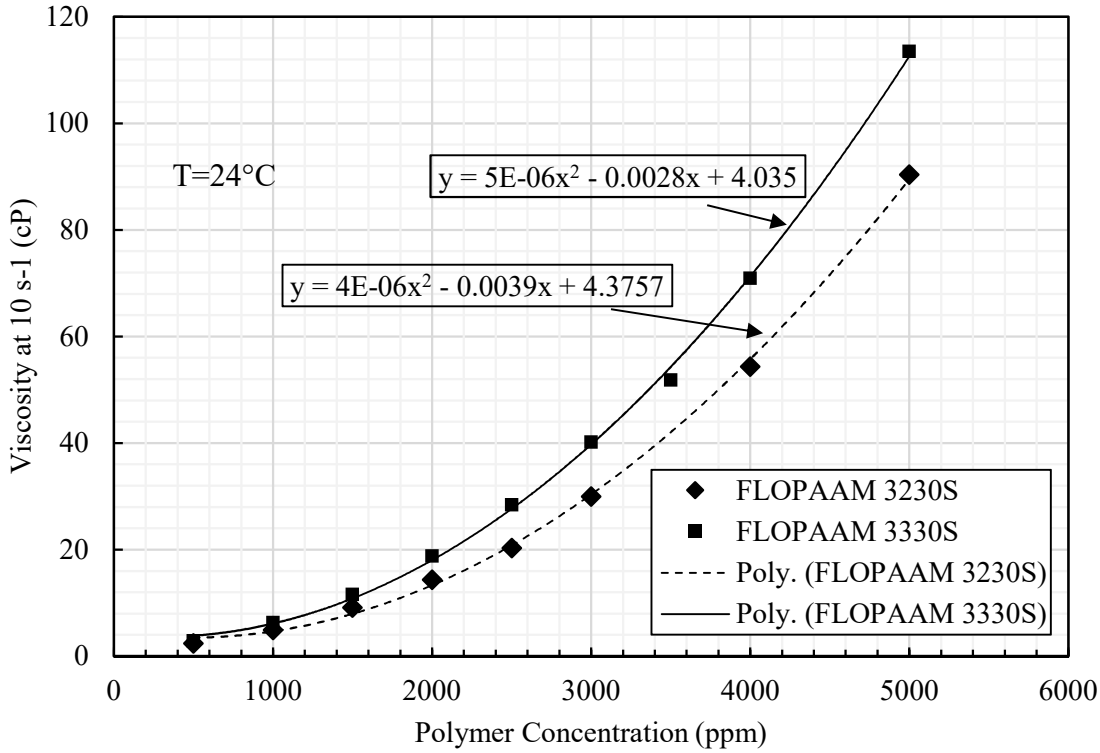

Figure 2.12 Loading curves for polymers-3230S,3330S

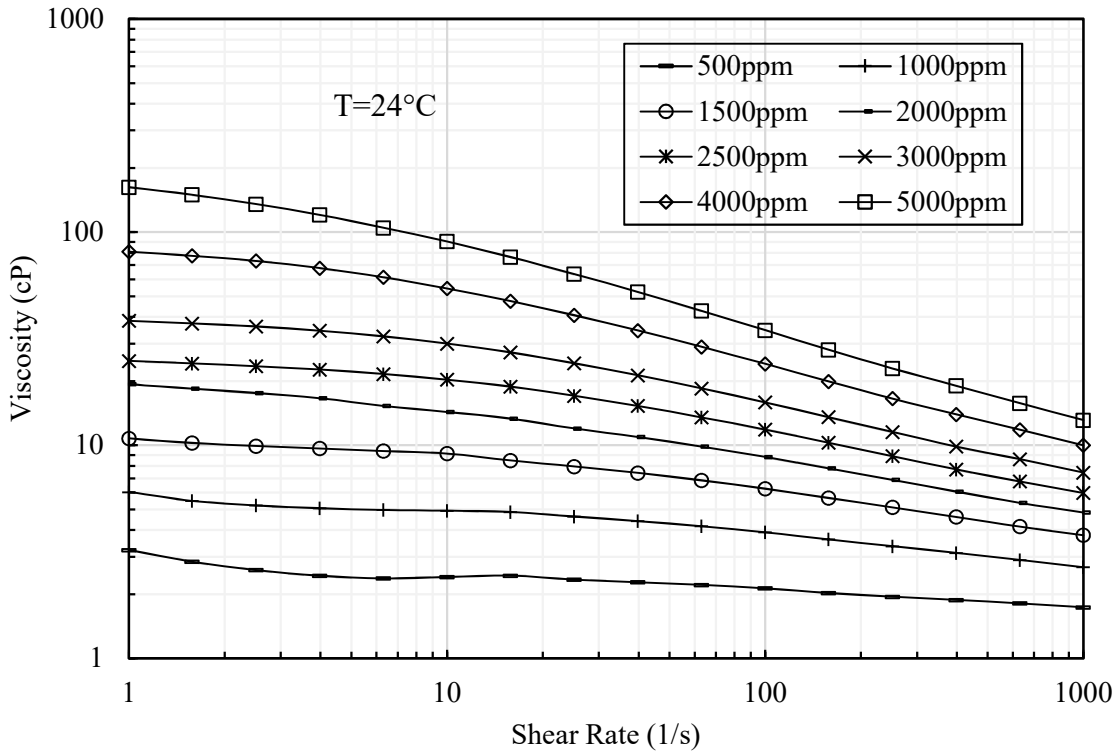

Figure 2.13 Viscosity of Flopaam 3230S in RH brine

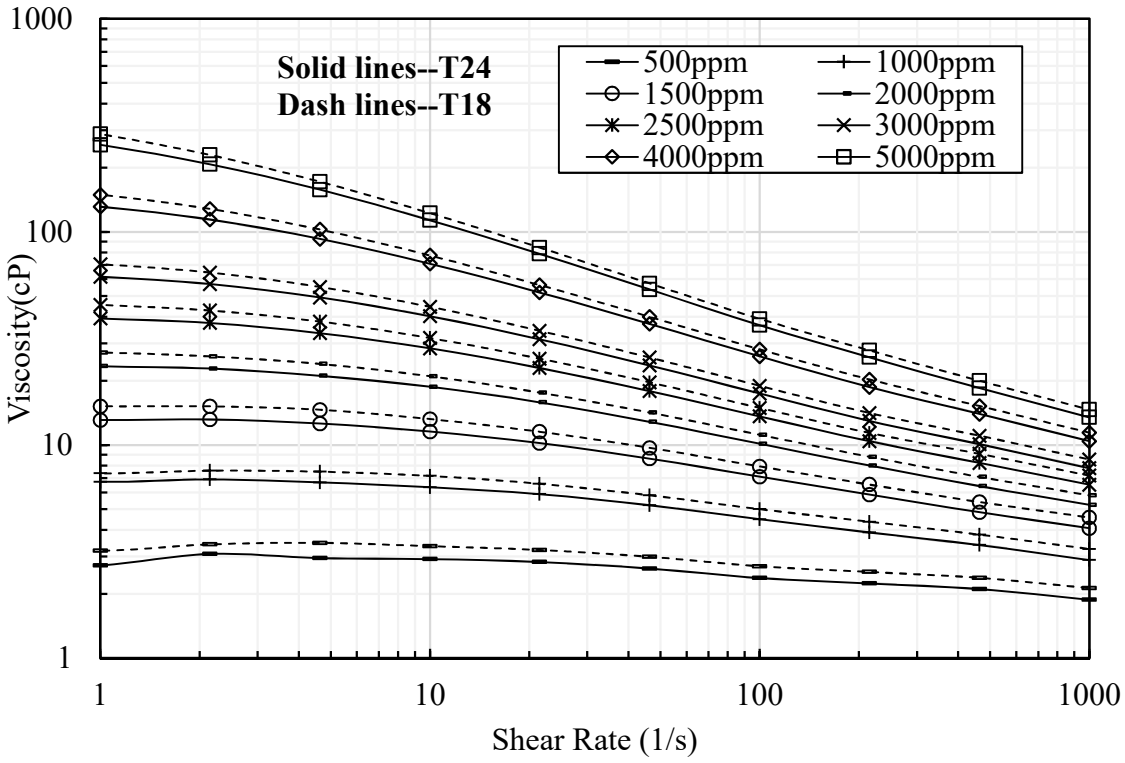

Figure 2.14 Viscosity of Flopaam 3330S in RH brine

2.3.3.3 Effect of Salinity on Polymer Viscosity

As summarized in Table 2.3, viscosity measurements were conducted on high salinity (HTDS) polymer solutions with total dissolved solids of 18,000, 20,000 and 22,000 ppm (indicated in the following as 18k, 20k, and 22k solutions). These values of salinity (reached adding the required amount of NaCl to the polymer solutions in RH brine) were selected based on phase behavior studies on oil-surfactant mixtures conducted in the EOR laboratory during the process of designing the chemical EOR formulation for the Rock Hill site. As an example of the results obtained from shear rate ramps, Figure 2.15 shows the effect of salinity on the viscosity of 0.35wt% Flopaam 3330S solutions at 24°C. Shear thinning behavior is observed in all the curves. At any shear rate the viscosity is found to decrease with increasing salinity due to a charge shielding mechanism, which arises due the addition of the sodium ions. The presence of these ions results in the decrease of the repulsive forces between the negative charges of the carboxylate groups due to a screening effect, causing the polymer chains to coil up and the degree of polymer chain entanglement to diminish [11].

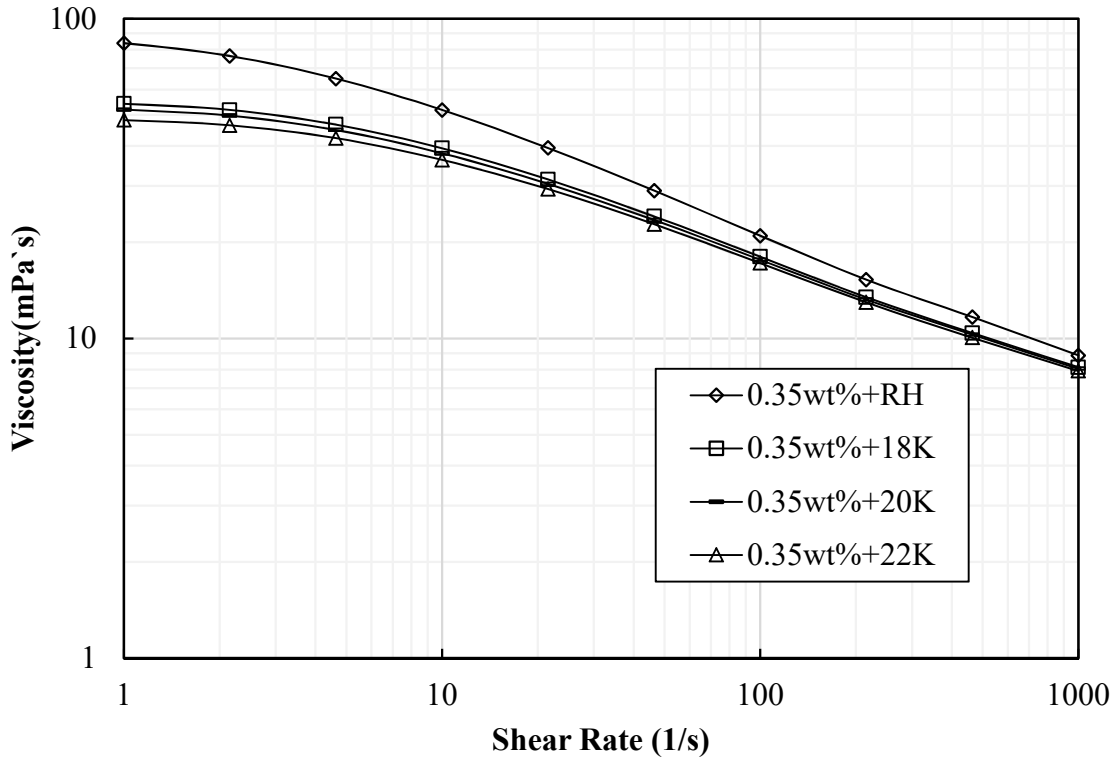

Figure 2.15 Effect of salinity on the viscosity of 0.35wt%3330S at 24°C

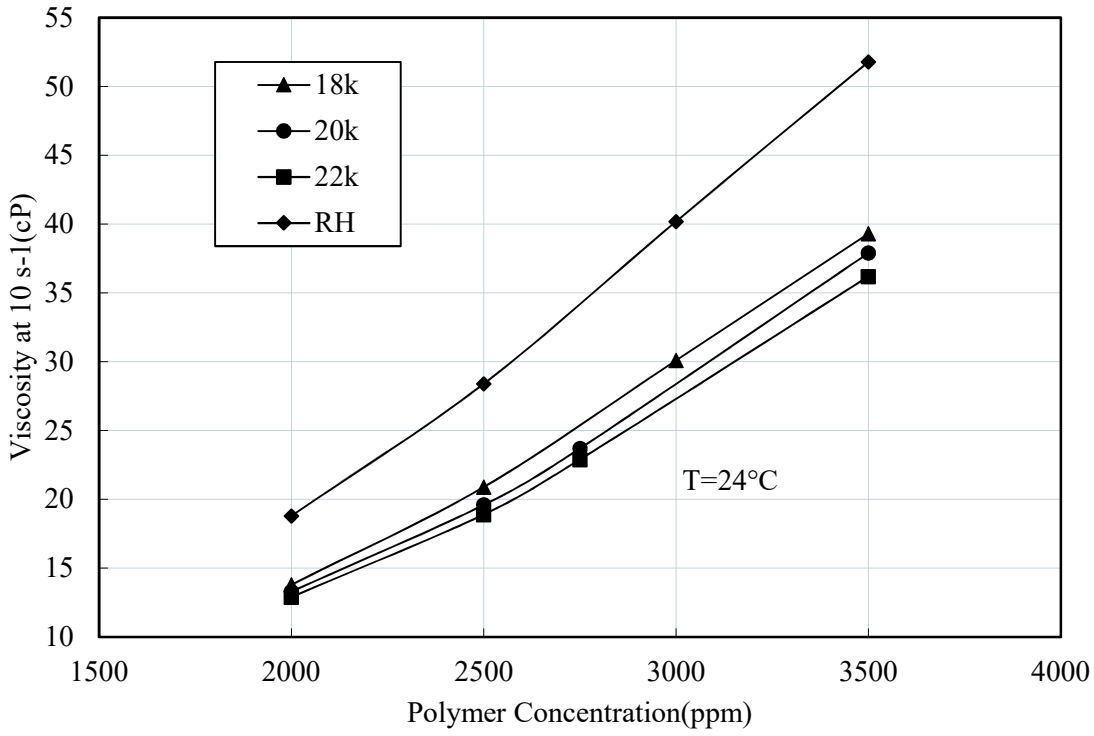

Figure 2.16 Effect of salinity on the viscosity of Flopaam 3330S solutions

Figure 2.16 summarizes the viscosity data obtained from constant shear rate tests of Flopaam 3330S solutions at different salinities as a function of polymer concentration at the reference shear rate of 10 s^{-1}. It is seen that adjusting the solution salinity from RH salinity (9400ppm) to 22k causes a reduction in viscosity greater than 30%. In practice in the cEOR process, salinity values higher than RH salinity (9400ppm) may be chosen for the chemical slug to achieve low/ultra-low IFT in the presence of the surfactant. The results presented above indicate, however, that for these higher salinity condition, higher polymer concentration will be required to meet the desired mobility ratio (for the conditions examined in Figure 2.16 the increase in polymer concentration required to achieve the same viscosity at 10 s^{-1} is in the 15-25% range). This will necessarily impact the cost of the formulation.

As part of the investigation of the effects of the salinity of the solution, viscosity measurements were conducted also on polymer solutions prepared in 'original' RH brine as well as in deionized water (DI). 'Original' RH brine refers to the filtered reservoir water sampled from wells in BRETZ SHELTON facility (see Figure 2.17). The primary motivation for the tests on solutions prepared with 'original' RH brine, was to establish to what degree the results obtained from the extensive testing program conducted using the synthetic brine could predict the behavior that would be observed in the field.

The data for the solutions prepared in deionized water provide instead a baseline against which the behavior of all other solutions can be evaluated.

Table 2.4 presents the results of viscosity of 0.5% solutions of Flopaam 3330S prepared using both 'original' and synthetic RH brine. The data, which were obtained from shear rate ramp tests conducted at both 18 and 24°C show a less than 10% difference between the solutions in the two brines over the shear rate range of 0.1 to 1000 s^{-1}. Note that this might not be the case if the iron ions in the 'original' brine had been well preserved, as the presence of these ions even at very low concentrations in reduced brines is known to significantly impact the viscosity of polymer solutions when exposed to air [12]. In the Rock Hill reservoir, which is under reducing condition, iron ions are present in the form of Fe^{2+}. However, during the filtration of the 'original' brine, exposure to air

causes Fe^{2+} to precipitate. As a result, the effect of ion ions on the rheology of the polymer solutions examined in this research remains unexplored.

(a) Reservoir water samples capped with crude oil

(b) Filtered sample

Figure 2.17 Rock Hill reservoir water

Table 2.4 Viscosity of 0.5wt% Flopaam 3330S solutions in original and synthetic Rock Hill brine

SR(1/s)	18°C			24°C		
	Original	Synthetic	Difference	Original	Synthetic	Difference
0.1	348.5	380.2	**8%**	303	328.5	**8%**
1	270.2	287.4	**6%**	241	256.1	**6%**
10	118.9	122.5	**3%**	110	113.5	**3%**
100	38.42	39.07	**2%**	35.85	36.49	**2%**
1,000	14.34	14.68	**2%**	13.2	13.48	**2%**

Similar deviations between the data for the original and synthetic RH brine were observed also for the other polymer concentrations examined (0.2wt%,0.25wt%, 0.3wt%, 0.35wt%, 0.4wt%).

Figure 2.18 shows the rheology of 0.2-0.5wt% Flopaam 3330S solutions in DI water tested at 24°C. For reference also a curve for the 0.5% solution prepared in synthetic RH brine is included (see also Figure 2.13). For shear thinning fluids like polymer solutions, Newtonian behavior can be observed at low and high shear rates, with a transition to shear thinning behavior in between where viscosity decreases with

increasing shear rate. The two regions, characterized by constant viscosity, are referred to as lower and upper Newtonian region, respectively[15]. Viscosity values in DI water are much higher than in brines due to the charge shielding mechanism discussed earlier. Solutions show shear thinning behavior between 0.2 and 1000 s^{-1} with the lower-Newtonian region at low shear rate (<0.2 s^{-1}). At the reference shear rate of 10 s^{-1}, the viscosity of the 0.5wt% 3330S solution in DI water is 676 cP which is about 6 times of that in RH brine (113.5 cP). Viscosities get closer to each other at high shear rates (e.g. at 1000 s^{-1}, the viscosity of the 0.5wt% 3330S solution in DI water is only twice that of the solution in RH brine). This implies that shear thinning is reduced with increased salinity. The increase in salinity also leads to an extension of the lower-Newtonian region with shear thinning behavior starting closer to 1 s^{-1}.

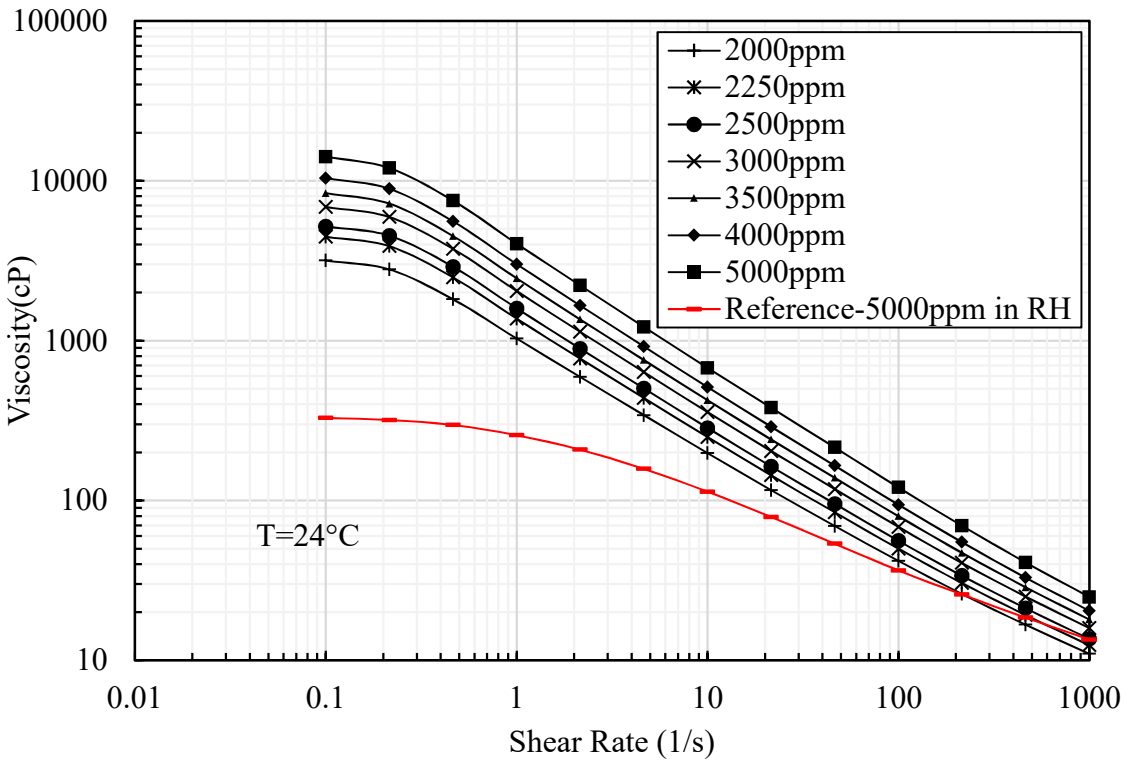

Figure 2.18 Viscosity of Flopaam 3330S in DI water

The viscosity of polymer solutions in DI water at shear rates in the 0.2-1000 s^{-1} range (shear thinning region) can be fitted using the power-law model [14]:

$$\mu = k\dot{\gamma}^{n-1} \tag{2.1}$$

where k and n are power law parameters. For Newtonian fluids, n=1 and k is the fluid viscosity. The power-law parameters obtained fitting the data for the polymer solutions in DI water are summarized in Table 2.5.

Table 2.5 Power-law parameters of Flopaam 3330S in DI water (T=24°C)

Polymer Concentration (ppm)	k (cP)	n	R^2
2000	985.28	0.329	0.9986
2250	1316.4	0.304	0.9986
2500	1525.6	0.296	0.9987
3000	1965	0.284	0.9989
3500	2361.5	0.276	0.9991
4000	2904.4	0.266	0.9993
5000	3903.3	0.255	0.9995

Table 2.6 summarizes the power-law parameters derived from measurements on 0.35wt% Flopaam 3330S solutions prepared at different salinities. The shear thinning region for solutions with salts is 10-1000 s^{-1} (see Figure 2.15). Compared to solutions containing salts, the solution in DI water has a lower n value which indicates stronger shear thinning behavior.

Table 2.6 Power-law parameters of 0.35wt% Flopaam 3330S at different salinities (T=24°C)

Salinity (ppm)	k (cP)	n	R^2
0 (Deionized water)	2276.6	0.284	0.9989
9400 (Rock Hill salinity)	127.99	0.610	0.9991
18k (RH + NaCl)	90.232	0.650	0.9989
20k (RH + NaCl)	85.88	0.656	0.9989
22k (RH + NaCl)	81.113	0.662	0.9987

2.3.3.4 Effect of Time on Polymer Viscosity

In a field cEOR operation, the injected chemicals remain in the reservoir for an extended period of time (several months to years). Therefore, it becomes of interest to evaluate the effect of time on polymer viscosity and assess the possible degree of polymer degradation. For this purpose, a 0.35wt% 3330S solution prepared in RH brine was preserved, and was measured 7 months later. The results of this test are presented in Figure 2.19 alongside data obtained on the fresh polymer solution. The deviation in the measured values of the viscosity is insignificant, indicating excellent stability of the solution.

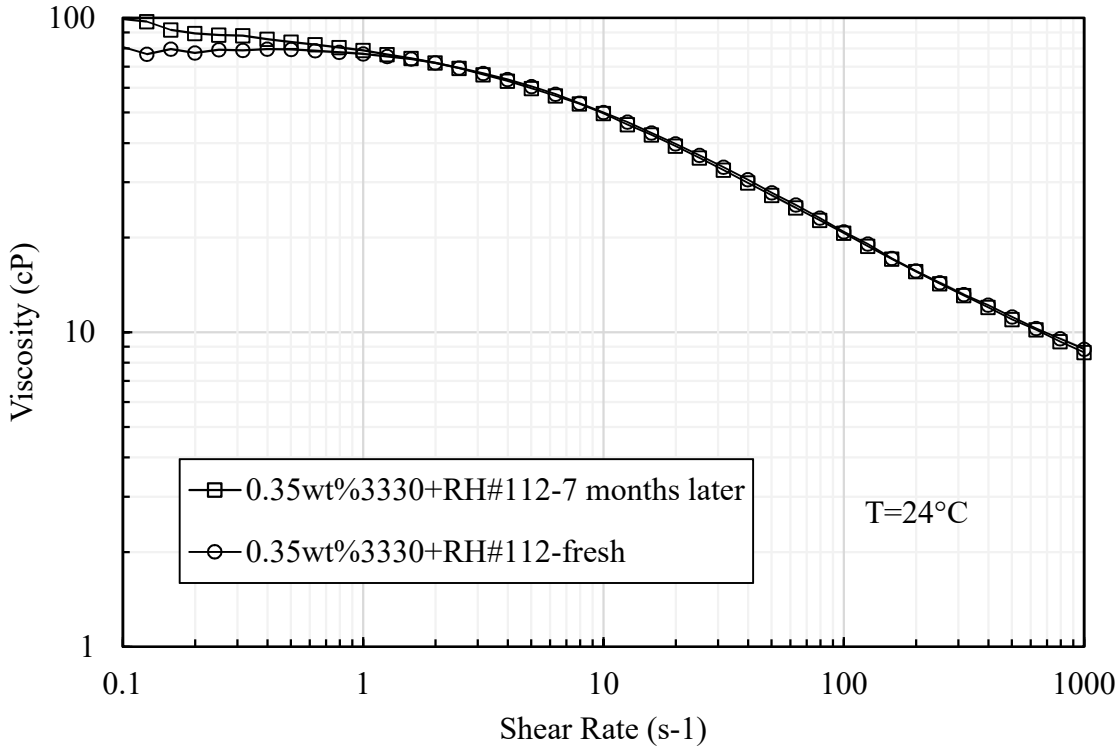

Figure 2.19 Effect of time on the viscosity of a 0.35% 3330S solution

2.3.4 Viscosity of Surfactant-Polymer Solutions

In a chemical flooding EOR process, a surfactant-polymer solution is injected in the formation. The role of the surfactant is to lower the interfacial tension (IFT) and help mobilize the oil. The rheological behavior of the surfactant-polymer solution is also very important, and thus the effect of the surfactant on polymer viscosity was examined and is discussed here. Note that both the surfactants (S13D, A6) and the polymers (3330S, 3230S) used here are all anionic. All tests on surfactant-polymer solutions were conducted at 24°C.

2.3.4.1 Effect of S13D-HA on Polymer Solutions in RH Brine

Four surfactant concentrations - 0.4, 1.0, 2.0, and 3.0wt% - were evaluated in combination with 0.3wt% 3230S and 3330S solutions at RH brine salinity. The results of shear rate ramps conducted on these solutions are presented in Figure 2.20**.** The figure shows a decrease in solution viscosity with increasing S13D concentration. This observation is consistent with the reported effect of anionic surfactant on the viscosity of HPAM polymers [11][15][16]. Equation (2.2) was used to calculate viscosity reduction and the results are plotted in Figure 2.21. For low surfactant concentrations (0.4wt% - 1.0wt%), the effect is insignificant. The reduction in viscosity grows more severe in the lower shear rate region as the surfactant concentration increases. A more marked decrease in viscosity is observed with the 3230S polymer (see Figure 2.21). For example, when adding 3wt% S13D, at the reference shear rate of 10 s^{-1}, the viscosity reduction increases from about 7% for 3330S to 15% for 3320S.

A possible explanation for this effect is the contribution of the anionic surfactant to an increased ionic strength of the polymer solutions [16]. As shown above (2.3.3.3)**,** the Flopaam polymers evaluated in this study are quite sensitive to the ionic strength of the solutions.

$$\text{Viscosity reduction}=\frac{\eta(\text{Polymer solution})-\eta(\text{SP solution})}{\eta(\text{Polymer solution})}\times 100\% \qquad (2.2)$$

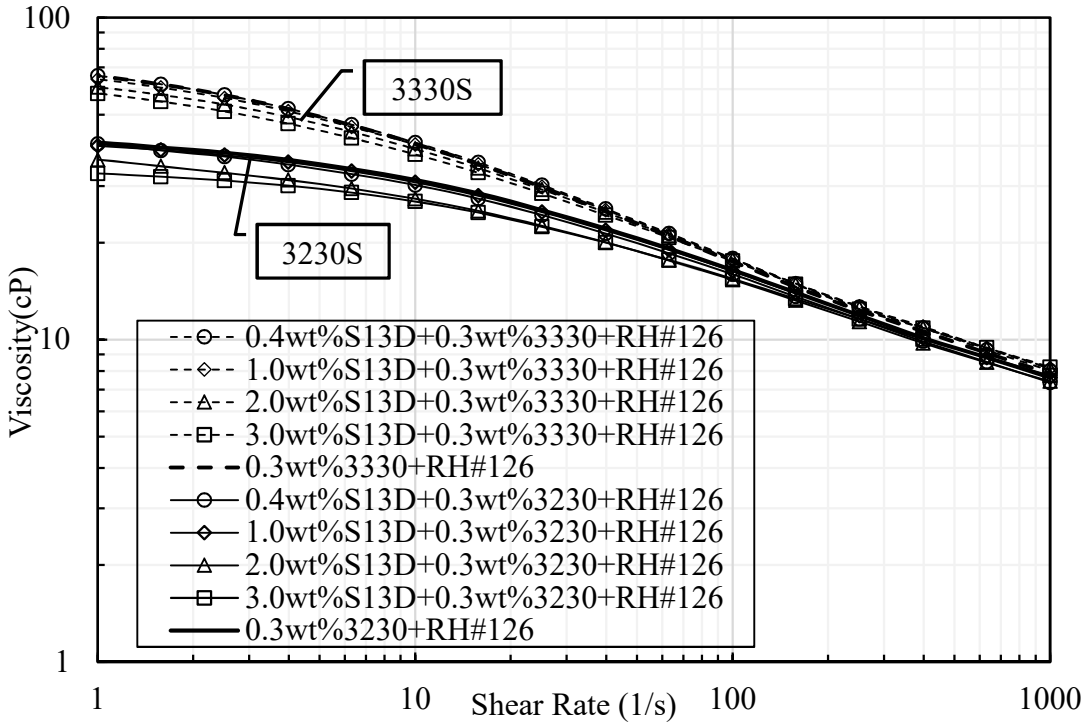

Figure 2.20 Effect of S13D on the viscosity of 0.3% polymer solutions

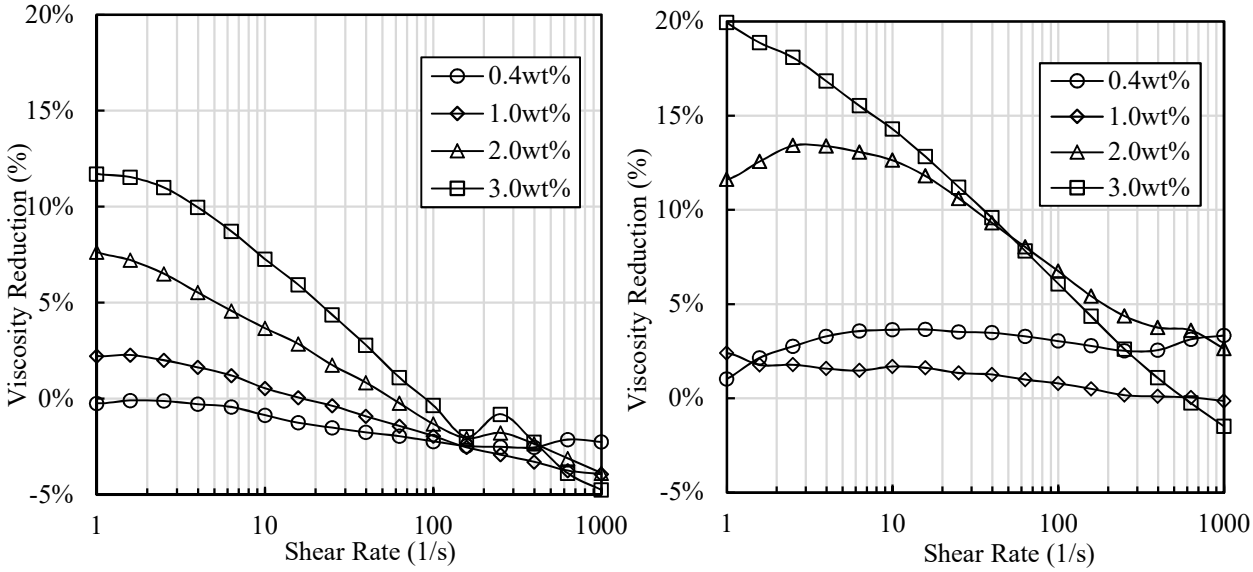

Figure 2.21 Viscosity reduction of S13D on polymer solutions (Left:3330S Right:3230S)

2.3.4.2 Effect of Surfactant Mixture on Polymer Solutions in RH Brine

Different concentrations of the surfactant mixture-S13D+A6+L4-2(7:2:1) were also added into 0.3wt% polymer (both 3330S and 3230S) solutions in RH brine to examine the effect on polymer viscosity. Figure 2.22 summarizes the results from shear rate ramps conducted on these solutions.

Overall, the effect of the addition of the surfactant mixture is both qualitatively and quantitively similar to that described above for the single surfactant. Values of the viscosity reduction are presented in Figure 2.23. At the reference shear rate of 10 s^{-1}, the viscosity reduction for 3330S is about 9% and for 3230S is about 12% when adding 3wt% surfactant mixture.

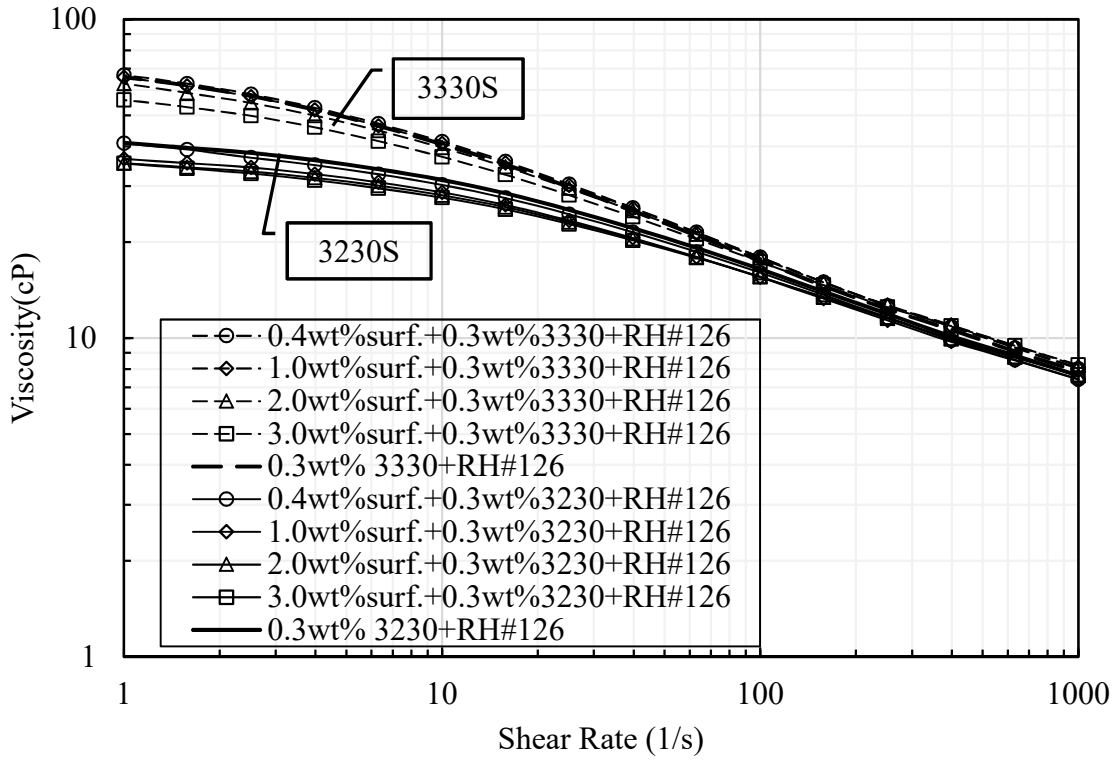

Figure 2.22 Effect of surfactant mixture on polymer viscosity

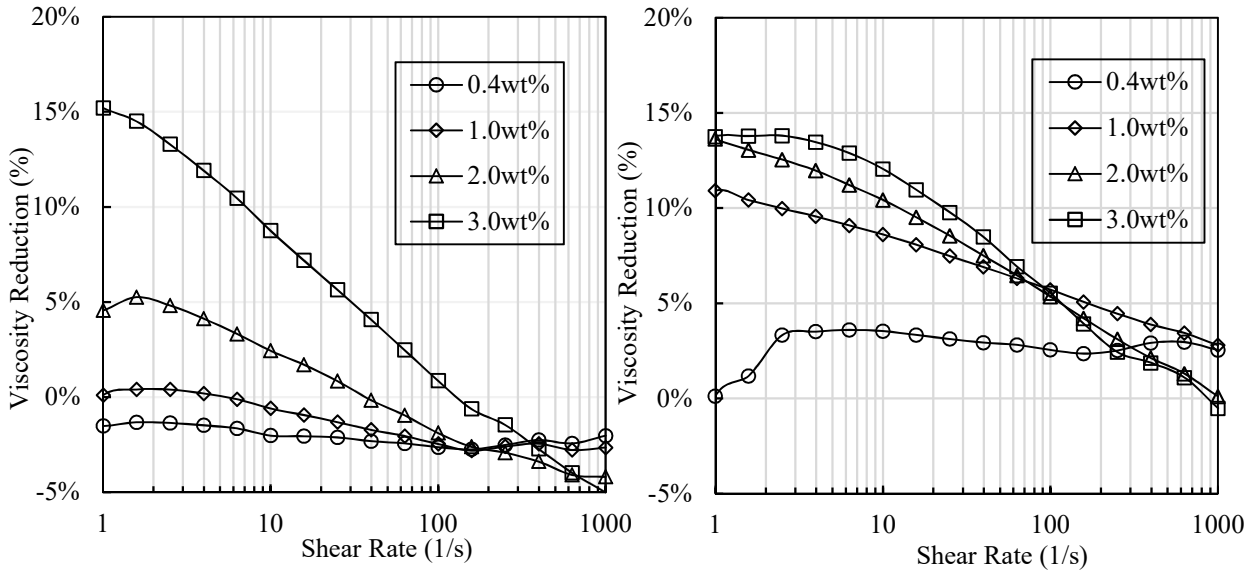

Figure 2.23 Viscosity reduction of surfactant mixture on polymer solutions (Left:3330S Right:3230S)

2.3.4.3 Viscosity of Surfactant-polymer Solutions Prepared in High Salinity

Phase behavior experiments performed in Purdue's EOR lab, indicate that to achieve low/ultra-low IFT of the SP slug, the salinity of the SP solution to be used in the field will need to be adjusted adding NaCl. To evaluate the effect of high salinity on the viscosity of SP solutions, 0.3wt% Flopaam 3330S solutions with S13D concentration ranging from 0 to 3wt%A at 18k, 20k, 22k were prepared and tested.

Viscosity values of 0.3wt%3330S solutions at different salinities from constant shear rate tests at 11.5 s^{-1} are plotted in Figure 2.24, as a function of S13D concentration. For reference, the viscosity of 0.3wt%3330S in RH brine is also shown. As discussed in 2.3.4.1, the viscosity decreases when S13D is added at high concentrations into the polymer solution at RH salinity. On the other hand, for polymer-only solutions, the increase in salinity causes the viscosity to reduce (e.g. see Figure 14). This can also be observed in Figure 2.24 when the S13D concentration is zero. Essentially the same results are obtained in high salinity (18k, 20k, 22k) SP solutions with 0.4wt%A S13D, indicating that the addition of this concentration of S13D has no significant impact on the viscosity of the solution. A different trend is instead observed when the concentration of S13D goes up to 1wt%A or higher, as an increase in viscosity is observed with increase in salinity. For each salinity, the higher the S13D concentration,

the higher the solution viscosity. At 3wt%A, the viscosity of the high salinity solutions all exceed the viscosity of solution in RH salinity. In particular, for 22k salinity, the viscosity reaches 136cP which is 3 times greater than the value measured in RH brine (36.6cP). This phenomenon can be better observed in Figure 2.25 where the viscosity is plotted as a function of salinity. Note that this effect is also shear rate related (see Figure 2.26).

While, further research is required to understand the mechanism, it appears to be due to the different structures/phases of surfactant formed in these solutions thus changing the rheological behavior (see Chapter 0 for relevant information).

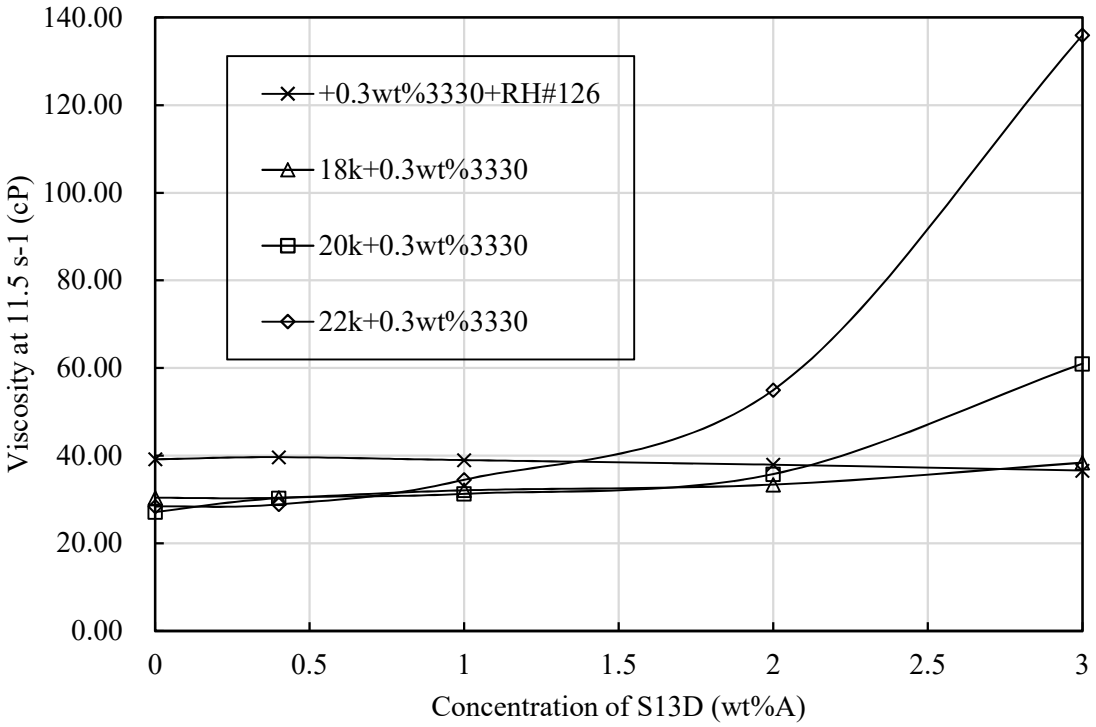

Figure 2.24 Effect of S13D on 0.3wt% 3330S at 18k, 20k, 22k

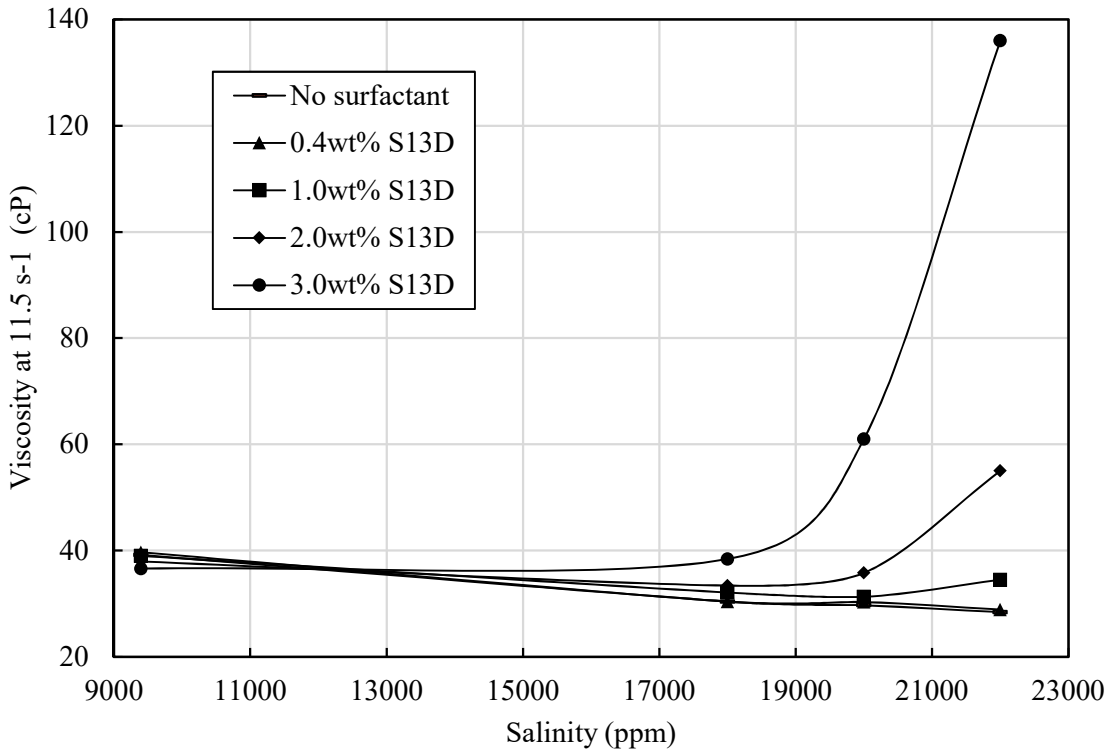

Figure 2.25 Viscosity of SP solutions as a function of salinity at 11.5 s-1

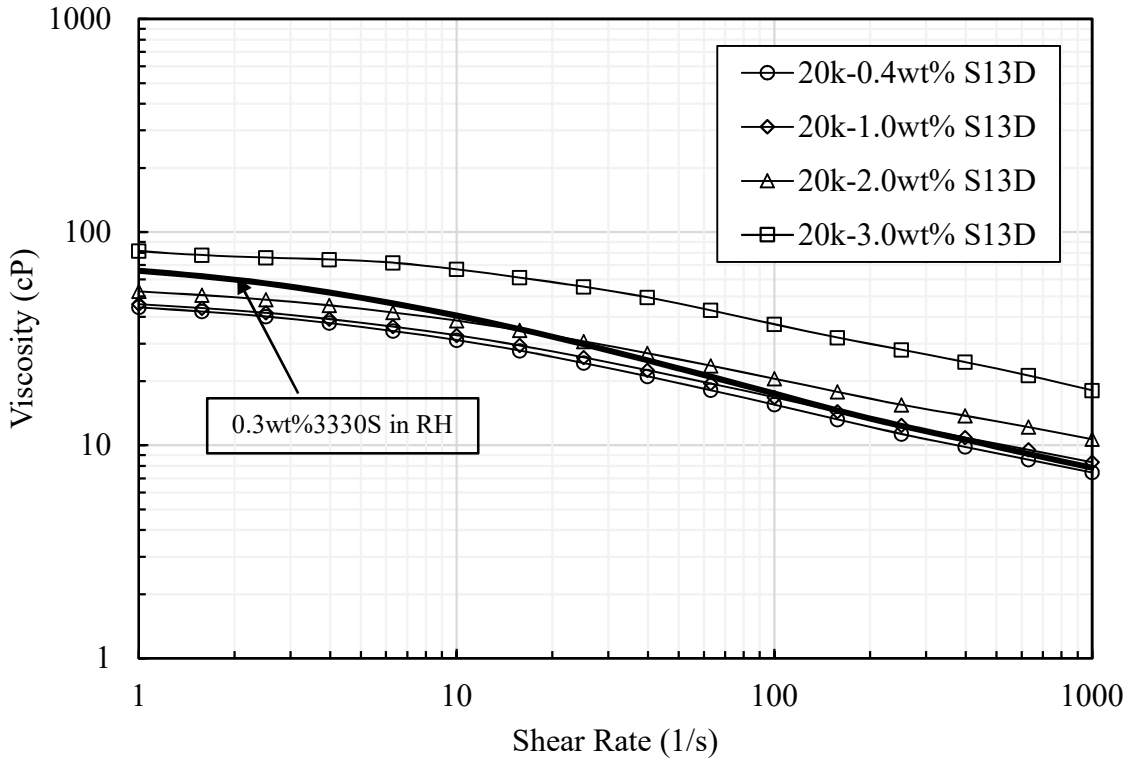

Figure 2.26 Viscosity of 0.3wt% 3330S + (0.4-3.0wt%A) S13D at 20k

2.3.4.4 Viscosity of Optimal Formulations

Following extensive research in Purdue's EOR lab, a 0.8wt%A solution of S13D+A6+L4-2(7:2:2) at 17.5k was chosen as the formulation for the most recent Purdue core flood tests and the pilot test in the field. As a result, additional viscosity measurements were conducted on this formulation, with the primary objective of selecting an appropriate polymer concentration to achieve the required slug viscosity for mobility control. Different concentrations (0.15-0.5wt%) of polymer solutions (3330S and 3230S) adding 0.8wt%A S13D+A6+L4-2(7:2:2) at 17.5k were tested at a constant shear rate of 11.5 s^{-1} over the temperature range of 4 to 35°C (see Figure 2.27 for 3230S, Figure 2.28 for 3330S). Shear rate ramp tests were also conducted at 4°C, 18°C and 24 °C.

Figure 2.29 presents the results of shear rate ramp tests for 0.15-0.5wt% 3330S with 0.8wt%A S13D+A6+L4-2(7:2:2) performed at 24°C.

As discussed earlier for polymer-only solutions, polymer concentration and testing temperature have similar effects on the polymer-surfactant solutions tested in this section. Viscosity increases with increasing polymer concentration, and higher viscosity values are measured at a lower testing temperature.

As shown in Figure 2.27, at 24°C, the viscosity at 11.5s^{-1} of 0.35wt%3330S with 0.8wt%A S13D+A6+L4-2(7:2:2) at 17.5k is 43cP. This value is very close to the viscosity (39.3cP) of a similar polymer only solution (0.35wt%3330S at 18k) measured at 10s^{-1} (see Figure 2.16). This indicates that concentrations of surfactants combined with alcohol as high as 0.8wt%A have little effect on polymer viscosity at 17.5k. This finding is consistent with the discussion presented in 2.3.4.3.

Similar behavior with higher viscosity values are obtained for other temperatures. The 3230S solutions exhibit similar results, and in general lower viscosity values due to the polymer's lower molecular weight.

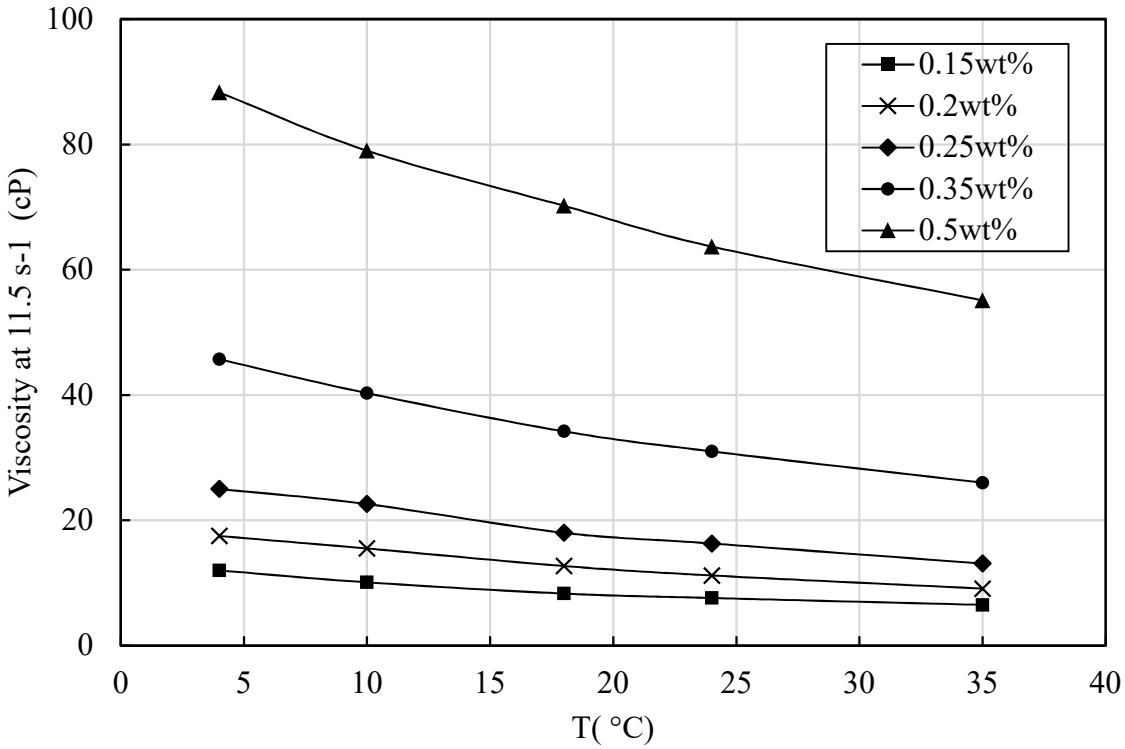

Figure 2.27 Viscosity of 0.15-0.5wt% 3230S with 0.8wt%A S13D+A6+L4-2(7:2:2) at 17.5k

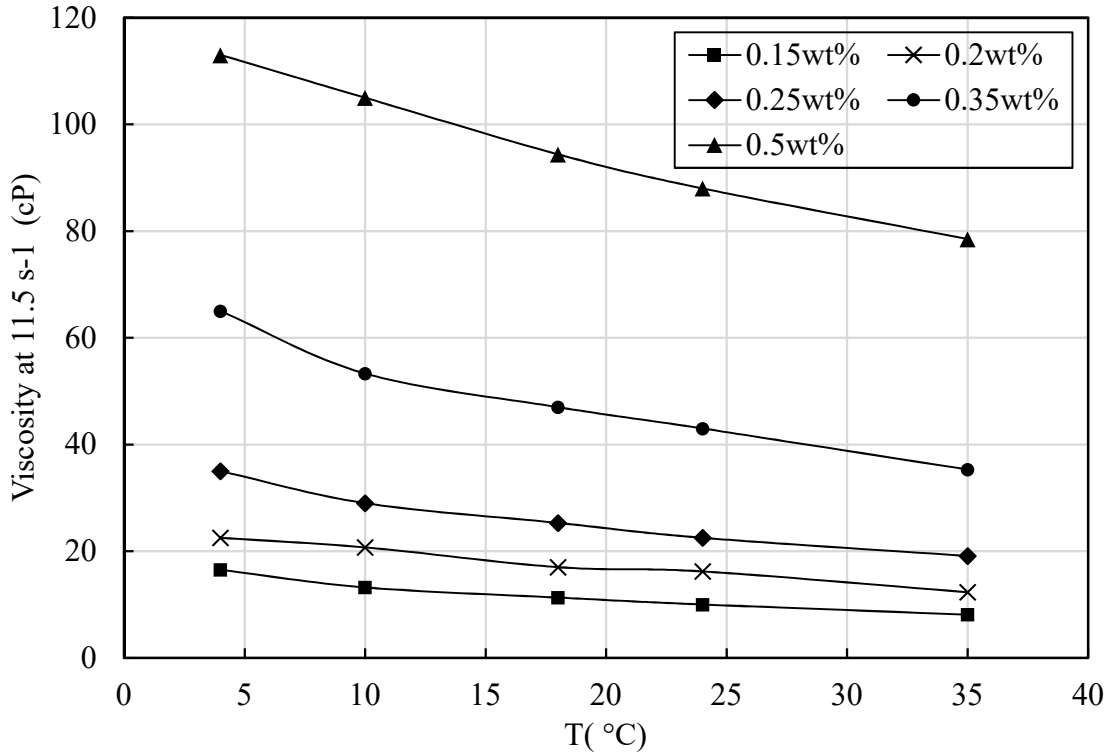

Figure 2.28 Viscosity of 0.15-0.5wt% 3330S with 0.8wt%A S13D+A6+L4-2 at 17.5k

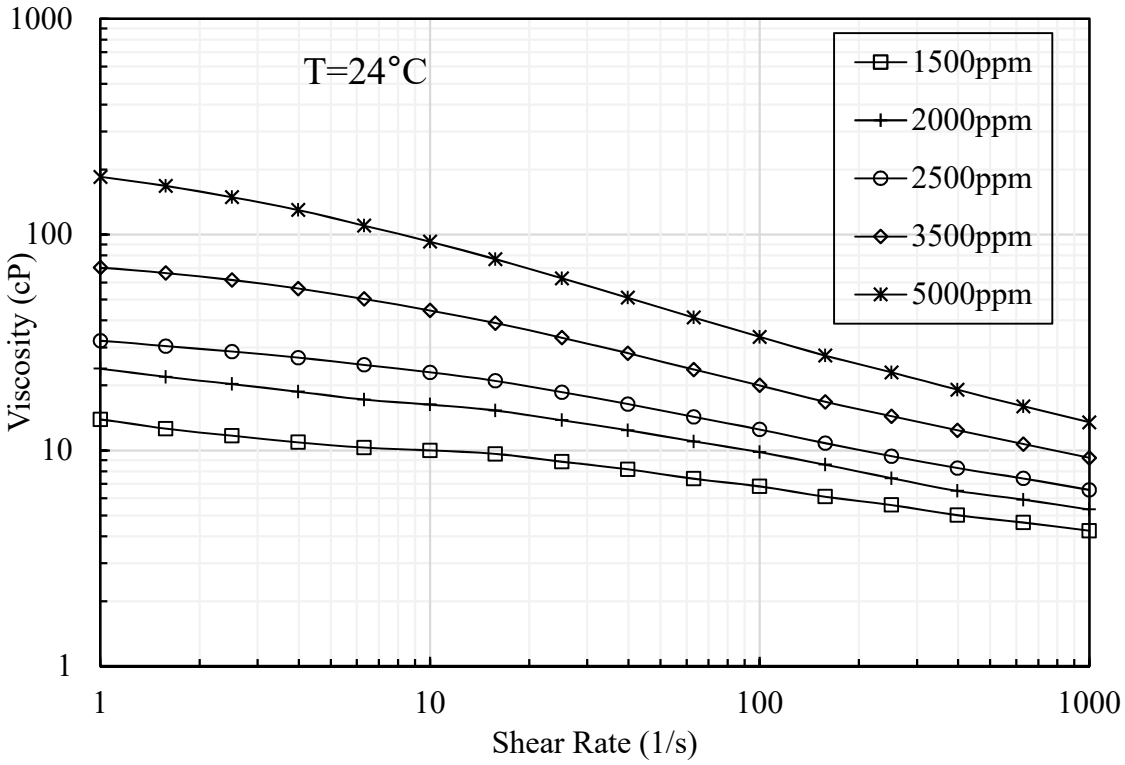

Figure 2.29 Viscosity of 0.15-0.5wt% 3330S with 0.8wt%A S13D+A6+L4-2(7:2:2) at 17.5k under 24°C

3. CORE FLOOD DATA ANALYSIS

3.1 Introduction

This chapter summarizes and analyzes select data obtained from 14 core flood tests performed in Purdue's Chemical Enhanced Oil Recovery Laboratory as part of a research effort funded by Pioneer Oil to develop a solution for cEOR at their Rock Hill site in southern Indiana.

As detailed in the following section, core flood tests involve the injection of one or more chemical slugs into a rock core while monitoring flow rate and pore pressure development across the length of the core, and extracting effluents produced during the various stages of the injection process. Core flood tests are performed to examine the oil recovery performance in a porous medium of a given formulation under conditions (temperature, confining stress, salinity) that mimic the oil recovery process in the field. Core flood tests are rather complex and lengthy tests, and, therefore, are generally conducted after identifying candidate optimal formulations suitable for the particular reservoir conditions and crude oil properties. As illustrated in Figure 3.1, this preliminary stage of testing centers around a phase behavior study, through which a large number of combinations of chemicals at different concentrations and salinities can be rapidly and cost-effectively screened. Rheological tests (see previous chapter) and IFT measurements support this stage of the formulation design.

A critical component of core flood tests is the analysis, after the completion of the test, of the effluents produced by the injection process. These analyses produce oil recovery results and relevant chemical parameters (chemical sorption, conductivity, pH etc.), which, in conjunction with mobility and pressure data also obtained from the core flood tests, are used to further optimize the formulation prior to field implementation. When possible, forensic tests can also be conducted on the cores to gain complementary information, for example on residual oil distribution.

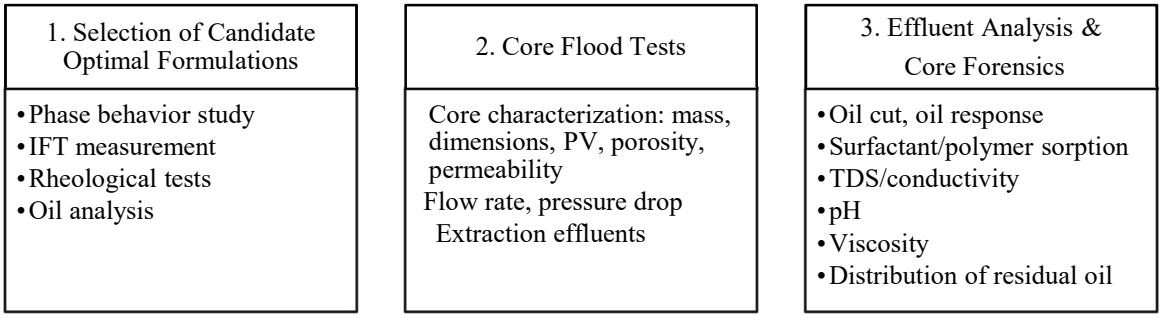

Figure 3.1 Approach followed in Purdue's cEOR laboratory for the design of a formulation for the Pioneer Oil Rock Hill site

This chapter focuses on the analysis and interpretation of data from core flood tests and effluent analysis of 14 core flood tests conducted in Purdue's EOR laboratory between November 2015 and March 2017. 13 of these tests were performed utilizing Berea sandstone cores, with the fourteenth providing the first data for Rock Hill core. Berea sandstone is a rock material obtained from Ohio which has been extensively used for EOR research as it well represents a typical reservoir rock. Core flood testing was overseen by Dr. Borgohain, manager of the Purdue EOR lab, and effluent analyses were performed in various laboratories associated with the Purdue EOR project. The author of this thesis was not involved in performing the core flood tests or analyzing the effluents, but was tasked with organizing and analyzing some of the data collected as part of this process. The outcome of this effort is presented in this chapter.

The chapter is organized in three main sections beyond this introduction. Section 3.2 summarizes the apparatus and procedures used to conduct core flood tests in Purdue's EOR laboratory. The following section (Section 3.3) outlines the data that are collected from each core flood test, including those pertaining to core and oil properties and to slug characteristics, and discusses the parameters derived from the measured quantities that are used to describe the injection process during the different stages of the test and to assess the effectiveness of a given injectant and compare the outcome of the different tests. These data are then analyzed in Section 3.4, starting with those pertaining to the pre-chemical flood conditions (Section 3.4.1), and the breakthrough curves derived from single core flood tests (Section 3.4.2). Finally, Section 3.4.3 presents an analysis of the performance date of the 14 coreflood tests, discussing the role of the various

testing parameters examined. The section concludes with a comparison to literature data for select core flood tests performed under conditions (temperature and salinity) similar to those examined in this testing program.

3.2 Core Flood Test Description

3.2.1 Core Flood Setup

Figure 3.2 shows the core flood setup in Purdue's EOR lab. The apparatus, which was constructed and assembled by SRC Inc., is comprised of the following major components:

a. Blue™ 1406 Series oven with heating/cooling function. Temperature range: 5ºC to 350 ºC;
b. core holder, which can house core stack of variable diameter (1'', 1.5'' and 2'') and stack length (3'' to 18''), and can withstand maximum working confining pressure of 5,800 psi;
c. 3 fluid transfer cylinders, with1,000 mL capacity/cylinder and 6,000 psi rating;
d. Teledyne ISCO™ Model 260D continuous flow dual syringe pump (flow rate range:0.001-107 mL/min; capacity:260mL; maximum pressure: 7500 psi);
e. Foxy™ 200 fraction collector;
f. data acquisition and automatic control system with LabView®-based program installed on a Dell computer.

All valves, core holder, tubing, BP regulators, DP pressure transducers used are SS-316 stainless steel.

Figure 3.2 Core flood setup in Purdue's EOR lab

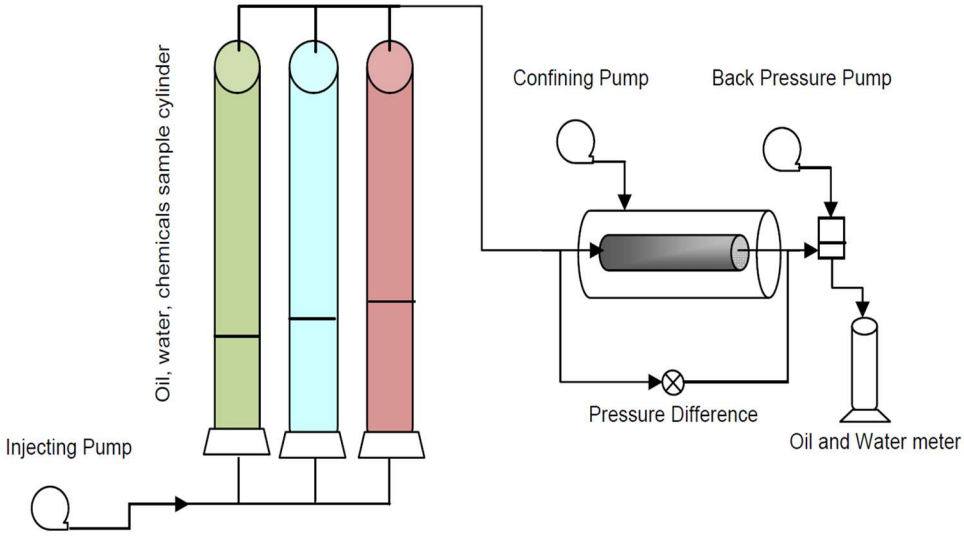

Figure 3.3 Schematic diagram of core flood experiment apparatus [17]

Figure 3.3 presents the schematic diagram of the core flood apparatus [17]. Oil, water (brine), chemicals stored separately in the transfer cylinders are injected into the core using an injecting syringe pump during different stages of the core flood test. Confining stress is applied to simulate the stress condition of the field. A differential pressure transducer is installed to monitor pressure across the core. A fraction collector is used to collect effluent samples.

3.2.2 Core Flood Procedure

A general procedure was followed to conduct all core flood experiments (see Figure 3.4). These tests were carried out at the reservoir temperature (24 ºC), monitoring the pressure across the core from brine saturation to the final water flood.

Core Preparation. Berea core used in core flood tests was approximately 1 foot long and 2 inches in diameter. Dimensions and mass of the core were measured and recorded. Vacuum was applied to the dry clean core in the core holder to ensure no air was left trapped in the pore space.

Brine Saturation. The core was saturated with synthetic Rock Hill brine and the pore volume was measured, based on which porosity of the core was calculated. Then the core was aged overnight under Rock Hill reservoir temperature and overburden pressure. Absolute brine permeability k_{brine} of the rock was measured averaging steady state measurements obtained at flow rates of 0.25, 0.5, 1.0, 1.25, 1.5 mL/min during this stage.

Oil Saturation. The core was then flushed with crude oil. The oil was filtered before injection to avoid particulate matter blocking the pores. The volume of the brine produced from the core during the oil flood is assumed equal to the amount of oil injected into the core, and is used for calculation of oil saturation. The oil flood was terminated when the pressure reached a steady state. Relative permeability of oil was calculated using the pressure data at steady state. Aging time for the core under reservoir conditions was at least 2 weeks. Then 1-2 PV oil were injected to displace the oxygenated oil, and changes in oil saturation, if any, were recorded.

Initial Water Flood (IWF) and HTDS Water Flood. During the IWF synthetic Rock Hill brine was injected until no more oil was displaced from the core. Residual oil saturation after initial water flood was estimated from the volume of collected oil. End-point relative permeability to water was calculated after the pressure reached steady state.

Given the low salinity of the formation brine, after the initial water flood, about 1 PV of adjusted high TDS brine was injected in most of the core flood tests to bring the core

salinity to optimal salinity (OS) conditions and maximize the efficiency of the chemicals injected.

Chemical Flood. The surfactant-polymer (SP) slug at the desired salinity was injected, followed by a 1 PV polymer drive at RH brine salinity. Viscosities of the two slugs were adjusted to be consistent based on the minimum requirement of mobility ratio. This is the ratio of the displacing fluid mobility to the displaced fluid mobility, which is taken as 1 to back calculate the required viscosity of the displacing fluids. Mobility of a fluid is defined as the effective permeability divided by its viscosity.

Final Water Flood. 1.5-2.0 PV of synthetic Rock Hill brine were injected after the chemical flood.

During all testing stages, the effluents were collected. The flow rate adopted for all floods was 0.09 mL/min which, for the 2-inch diameter cores used in this study, corresponds to a frontal advance rate of 1 ft./day. According to [18], a displacement rate of 1 ft./day or a pressure drop of 1 psi/ft is a good simulation of actual field conditions.

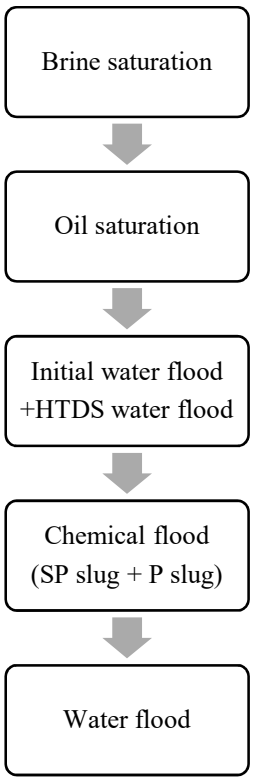

Figure 3.4 Core flood procedure

3.2.3 Effluent Analysis

Effluent samples obtained from the core flood were centrifuged as needed in 15 mL centrifuge tubes. Figure 3.5 shows a typical series of effluent samples for a core flood test from SP flood to final water flood at room temperature (close to 24 ºC). These samples were labeled based on the time of collection. For instance, the first tube from the left in Figure 3.5 marked as 'SP1' indicates that this sample was the first collected at the outlet at the start of the chemical flood.

Oil cut (the ratio of produced oil volume to the total volume of liquids produced) against pore volume injected can be easily observed and accurately determined from these samples. Values of viscosity, pH and conductivity were measured in the EOR lab at 24 ºC, and chemical sorption of surfactants and polymers was calculated from analyses of chemical concentrations of these effluent samples conducted in the Clay Chemistry Lab of the Department of Agronomy. These measured parameters can help understand the changes of the displacing fluids during the different injection stages.

Figure 3.5 BCF#15 effluents (SP1 to EWF2)

3.3 Purdue Core Flood Data

3.3.1 Excel Template

To better organize and analyze core flood data, an excel template was developed and used to synthesize data for each of the core flood tests performed between November 2015 and March 2017, on both Berea core (tests identified by letters BCF and progressive numbers from 5 to 18) and Rock Hill core (test RCF#1). The excel template consists of three sheets – pressure data, fraction information and summary plots. An

example of the sheet containing fraction information is shown in Figure 3.6. It includes at its top information on core properties including the volume of oil present in the rock pore space after saturation (and termed original oil in place, OOIP); slug characteristics (pore volumes and concentration of polymer-surfactant and polymer slugs); and chemicals injected and recovered (based on which the amounts sorbed onto the core rock material are calculated). Below, the sheet summarizes a series of parameters as a function of the injected pore volumes during the stages that go from to the initial (IWF) to the final (EWF) water floods. These are quantities obtained from measurements on the effluents that include viscosity (column AE), amounts of oil and water (columns E and F), concentration of surfactant (column S) and polymer (column Y), total dissolved solids (column AG) measured in the effluent. Based on these quantities some key parameters are derived, also as a function of the injected pore volumes. The most significant are: the oil cut for each sample (column H), the percentage of the OOIP recovered from both each sample (column I) and cumulatively (column J), the percentage of the residual oil (that remains after waterflooding) recovered following injection of the slug (column N), the residual oil saturation (column P).

Summary plots (see an example for BCF#5 in Figure 3.7) of pressure differential across the core, oil cut, oil recovery in terms of cumulative OOIP% and ROIP%, residual oil saturation of the core, TDS, pH, viscosity and chemical concentrations as a function of cumulative PV of water and chemical injected, are drawn for each test based on these data. These plots will be discussed in more detail later in this chapter.

Finally, end of test values of the key parameters are used to compare the outcome of the different tests, as discussed in Section 3.3.4.

3.3.2 Formulations used in Purdue Core Flood Tests

Figure 3.8 summarizes the formulations adopted in the 14 core flood tests examined in this thesis. Data for preliminary tests conducted before BCF#5 are not shown here. The data presented in Figure 3.8 include: chemicals used, viscosity of SP and P slugs, size (expressed in pore volumes), surfactant concentration, polymer concentration and salinity of the SP slug. More detailed information and other parameters such as core and oil properties are summarized in Table 3.1. In general, the Purdue core flood testing

program used five different surfactants or surfactant mixtures: S13D+A6(9:1), S13D, J13131, S13D+A6+L4-2(7:2:1), S13D+A6+L4-2(7:2:2), in which the last two involved the use of a co-solvent. These formulations were selected from phase behavior studies so as to generate favorable oil-water interactions with Rock Hill oil under reservoir temperature (18-24 ºC). No alkali was added in these formulations due to the low acid number (0.15 mg KOH/g) of the RH oil.

A typical SP slug solution consists of a primary surfactant, a co-surfactant, a co-solvent (alcohol), polymer and salts. The selected primary surfactant was Petrostep® S13D (J13131 was used for BCF#9); Petrostep® A6 acted as co-surfactant to help improve the performance in 12 of the 14 tests. The presence of a co-solvent (Surfonic® L4-2) in some tests was aimed at reducing the equilibration time, lower the viscosity of the micro-emulsion formed and increase the compatibility between surfactant and polymer [19][20]. Two HPAM polymers with different molecular weight, Flopaam 3230S and 3330S, were used.

As summarized in Figure 3.8, all core flood tests involved the injection of a 0.25-0.75 PV SP slug, with surfactant concentrations in the 0.4-1% range. Detailed information on the polymer (P) slug is summarized in Table 3.1**.** Note that P slugs for BCF#11, BCF#12 and BCF#16 were slightly different from the others, as 0.25-0.3 PV of polymer at the same salinity of the SP slug were first injected to prevent dilution in salinity of the SP slug (in all other tests the P slug was injected at RH salinity). BCF#15 used RH salinity for the SP slug, and in BCF#16 the surfactant and polymer were injected separately (i.e. no polymer in the SP slug). For BCF#18, the slug size for both SP slug and P slug was reduced to half.

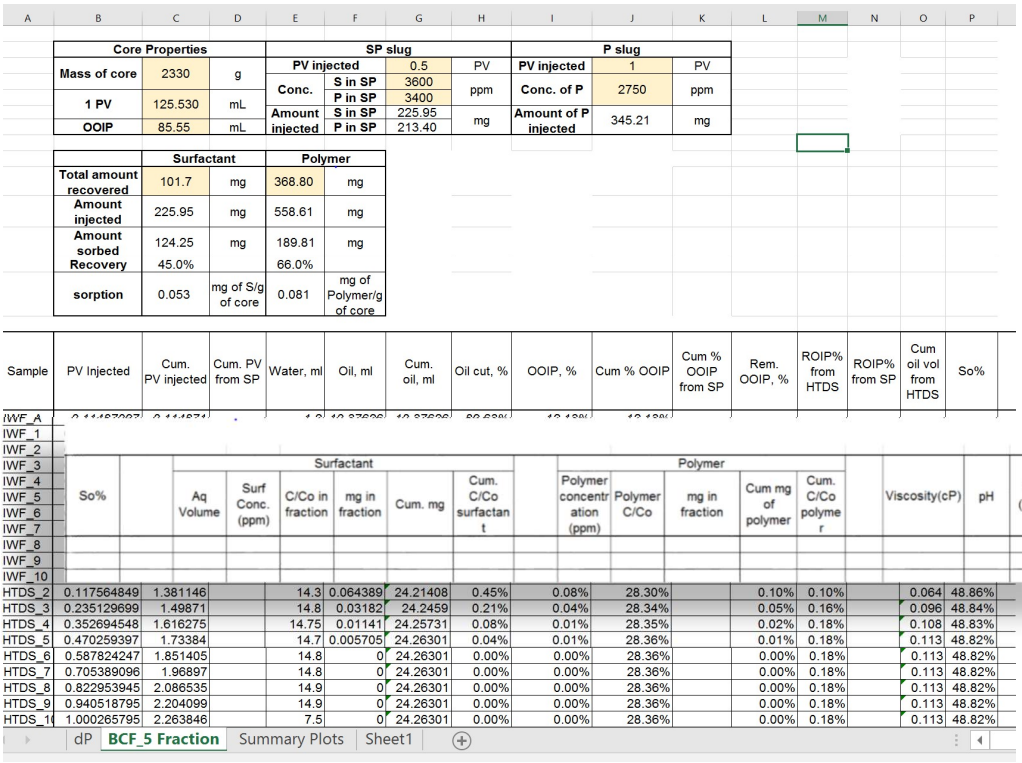

Core Properties		
Mass of core	2330	g
1 PV	125.530	mL
OOIP	85.55	mL

SP slug			
PV injected		0.5	PV
Conc.	S in SP	3600	ppm
	P in SP	3400	
Amount injected	S in SP	225.95	mg
	P in SP	213.40	

P slug		
PV injected	1	PV
Conc. of P	2750	ppm
Amount of P injected	345.21	mg

	Surfactant		Polymer	
Total amount recovered	101.7	mg	368.80	mg
Amount injected	225.95	mg	558.61	mg
Amount sorbed	124.25	mg	189.81	mg
Recovery	45.0%		66.0%	
sorption	0.053	mg of S/g of core	0.081	mg of Polymer/g of core

Sample	PV Injected	Cum. PV injected	Cum. PV from SP	Water, ml	Oil, ml	Cum. oil, ml	Oil cut, %	OOIP, %	Cum % OOIP	Cum % OOIP from SP	Rem. OOIP, %	ROIP% from HTDS	ROIP% from SP	Cum oil vol from HTDS	So%
IWF_A															
IWF_1															
IWF_2															
IWF_3															
IWF_4															
IWF_5															
IWF_6															
IWF_7															
IWF_8															
IWF_9															
IWF_10															
HTDS_2	0.117564849	1.381146		14.3	0.064389	24.21408	0.45%	0.08%	28.30%		0.10%	0.10%		0.064	48.86%
HTDS_3	0.235129699	1.49871		14.8	0.03182	24.2459	0.21%	0.04%	28.34%		0.05%	0.16%		0.096	48.84%
HTDS_4	0.352694548	1.616275		14.75	0.01141	24.25731	0.08%	0.01%	28.35%		0.02%	0.18%		0.108	48.83%
HTDS_5	0.470259397	1.73384		14.7	0.005705	24.26301	0.04%	0.01%	28.36%		0.01%	0.18%		0.113	48.82%
HTDS_6	0.587824247	1.851405		14.8	0	24.26301	0.00%	0.00%	28.36%		0.00%	0.18%		0.113	48.82%
HTDS_7	0.705389096	1.96897		14.8	0	24.26301	0.00%	0.00%	28.36%		0.00%	0.18%		0.113	48.82%
HTDS_8	0.822953945	2.086535		14.9	0	24.26301	0.00%	0.00%	28.36%		0.00%	0.18%		0.113	48.82%
HTDS_9	0.940518795	2.204099		14.9	0	24.26301	0.00%	0.00%	28.36%		0.00%	0.18%		0.113	48.82%
HTDS_10	1.000265795	2.263846		7.5	0	24.26301	0.00%	0.00%	28.36%		0.00%	0.18%		0.113	48.82%

		Surfactant							Polymer							
Sample	So%		Aq Volume	Surf Conc. (ppm)	C/Co in fraction	mg in fraction	Cum. mg	Cum. C/Co surfactant		Polymer concentration (ppm)	Polymer C/Co	mg in fraction	Cum mg of polymer	Cum. C/Co polymer		Viscosity(cP)	pH	TDS (mg/L)

dP | BCF_5 Fraction | Summary Plots | Sheet1

Figure 3.6 Excel template for core flood tests (BCF#5)

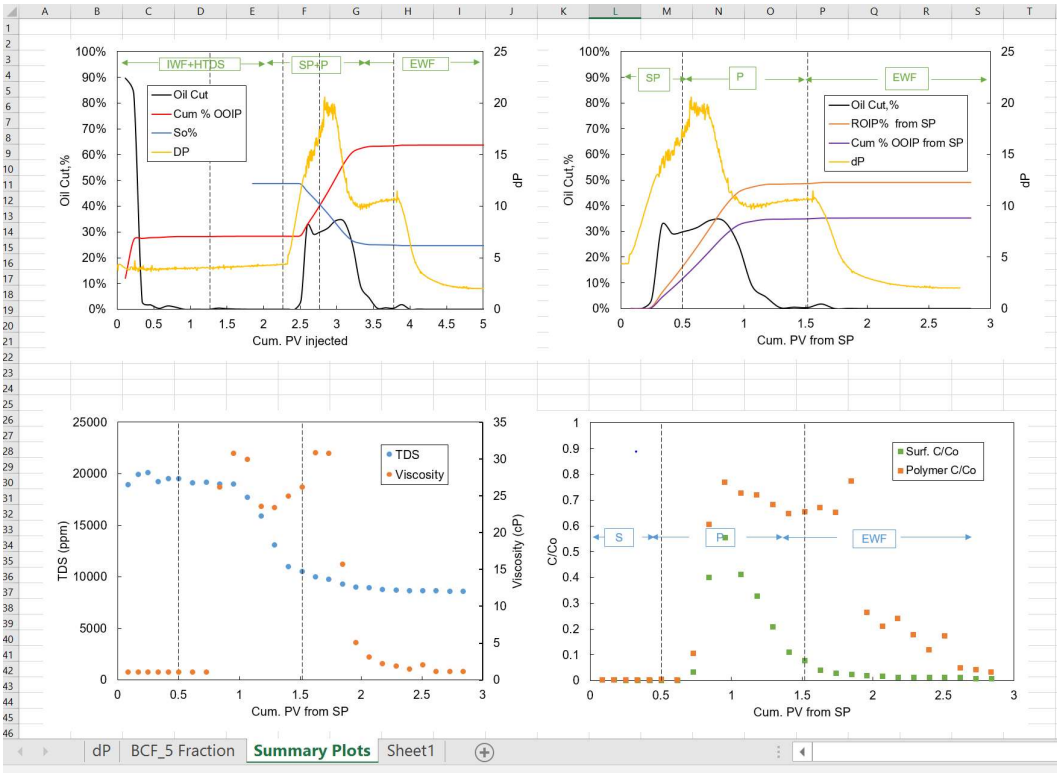

Figure 3.7 Summary plots (BCF#5)

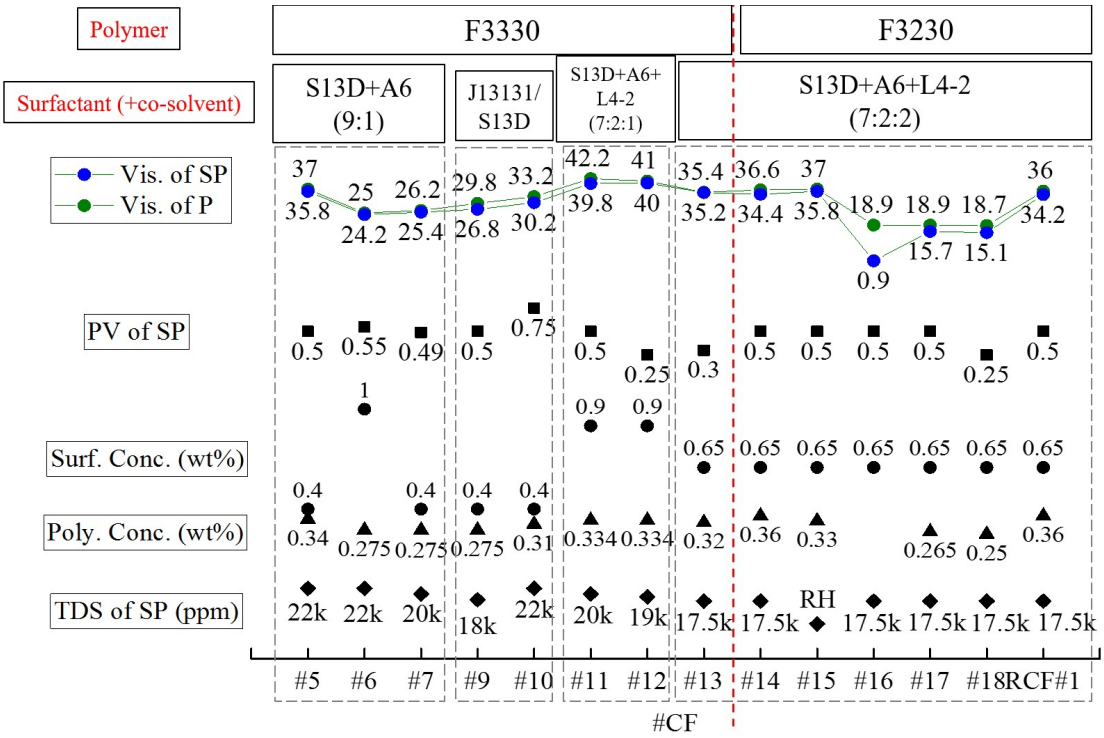

Figure 3.8 SP slug formulations used in Purdue core flood tests

Table 3.1 Core and formulation parameters of Purdue core flood tests

Coreflood ID	BCF#5	BCF#6	BCF#7	BCF#9	BCF#10
Core Properties					
Pore volume (mL)	125.53	126.12	124.56	144.80	141.73
Mass of core (g)	1318.4	1318.4	1318.4	1227.16	1242.63
Abs. brine perm (mD)	270.7	232.7	201.9	714.2	817.2
Flow rate (cc/min)	0.09	0.09	0.09	0.09	0.09
Oil Properties					
Batch	V	V	VI	VII	VII
Viscosity (cP)	23.172	23.172	12.6	14.2	14.2
IWF (9400 ppm RH Brine)					
PV	1.26	1.72	1.72	1.47	1.45
HTDS + Sacrificial agent (1 PV)					
Formulation	--	22000 ppm + 0.275wt% 3330	20000 ppm, Na poly Acrylate	--	--
PV	1	1.14	1	1	1
TDS	22000	22000	20000	18000	22000
SP slug					
PV	0.5	0.55	0.49	0.5	0.75
TDS (ppm)	22000	22000	20000	18000	22000
Formulation	S13D + L4-2 (9:1), 0.4wt%A + 0.34wt% 3330	S13D + L4-2 (9:1), 1.0wt%A + 0.275wt% 3330	S13D + L4-2 (9:1), 0.4wt%A + 0.275wt% 3330	J13131, 0.4wt%A + 0.275wt% 3330	S13DHA, 0.4wt%A + 0.31wt% 3330
Viscosity (cp)	35.8	24.2	25.4	26.8	30.2
P slug (1PV)					
Formulation	0.275wt% 3330 @RH (9400 ppm)	0.18wt% 3330 @RH (9400 ppm)	0.2wt% 3330 @RH (9400 ppm)	0.25wt% 3330 @RH (9400 ppm)	0.276wt% 3330 @RH (9400 ppm)
Viscosity (cp)	37	25	26.2	29.8	33.2
EWF (9400 ppm RH Brine)					
PV	1.32	1.13	0.5	1.17	1.41

Table 3.1 Core and formulation parameters for Purdue core flood tests (continued)

Coreflood ID	BCF#11	BCF#12	BCF#13	BCF#14	BCF#15
Core Properties					
Pore volume (mL)	141.73	134.54	116.20	136.09	132.73
Mass of core (g)	1242.29	1150.3	1023.3	1275.4	1274.3
Abs. brine perm (mD)	669.7	581.5	572.9	420.4	452.3
Flow rate (cc/min)	0.09	0.09	0.09	0.09	0.09
Oil Properties					
Batch	VII	VII	VII	VII	VII
Viscosity (cP)	14.2	14.2	14.2	14.2	14.2
IWF (9400 ppm RH Brine)					
PV	1.45	1.79	2	1.6	1.45
HTDS + Sacrificial agent (1 PV)					
Formulation	--	--	--	--	--
PV	1	1.01	1	1	0
TDS	20000	19000	17500	17500	9400
SP slug					
PV	0.5	0.25	0.3	0.5	0.5
TDS (ppm)	20000	19000	17500	17500	9400
Formulation	S13DHA +A6 +L4-2 (7:2:1),1.0wt%A +0.334wt% 3330	S13DHA +A6 +L4-2 (7:2:1),1.0wt%A +0.334wt% 3330	S13DHA+A6+ L4-2(7:2:2),0.8wt %A +0.32wt% 3330	S13DHA +A6 +L4-2 (7:2:2),0.8 wt%A +0.36wt% 3230	S13DHA +A6 +L4-2 (7:2:2),0.8wt %A +0.33wt% 3230
Viscosity (cp)	39.8	40	35.2	34.4	35.8
P slug (1PV)					
Formulation	0.3 PV @ 20000 ppm 3330, 0.334wt% followed by 0.7 PV @ RH (9400 ppm), 3330, 0.3wt%	0.3 PV @ 19000 ppm 3330, 0.33wt% followed by 0.7 PV @ RH (9400 ppm), 3330, 0.3wt%	0.273wt% 3330 @RH (9400 ppm)	0.33wt% 3230 @RH (9400 ppm)	0.33wt% 3230 @RH (9400 ppm)
Viscosity (cp)	42.2	41	35.4	36.6	37
EWF (9400 ppm RH Brine)					
PV	1.41	1.62	1.9	1.36	1.27

Table 3.1 Core and formulation parameters for Purdue core flood tests (continued)

Coreflood ID	BCF#16	BCF#17	BCF#18		RCF#1
Core Properties					
Pore volume (mL)	126.90	133.55	133.23		126.00
Mass of core (g)	1237.9	1275.4	1278.15		1316.94
Abs. brine perm (mD)	409.1	225.3	411.5		--
Flow rate (cc/min)	0.09	0.09	0.09		0.09
Oil Properties					
Batch	VIII	VIII	IX		VII
Viscosity (cP)	14.7	14.7	13.8		14.7
IWF (9400 ppm RH Brine)					
PV	1.58	1.58	1.73		1.4
HTDS + Sacrificial agent (1 PV)					
Formulation	--	--	--		--
PV	1	1	1.01		0.99
TDS	17500	17500	17500		17500
SP slug					
PV	0.5	0.5	**0.25**		0.52
TDS (ppm)	17500	17500	17500		17500
Formulation	S13DHA +A6 +L4-2 (7:2:2),0.8wt%A **No polymer**	S13DHA +A6 +L4-2 (7:2:2),0.8wt%A + 0.1wt% Na-isoascorbate +0.265wt% 3230	S13DHA +A6 +L4-2 (7:2:2),0.8wt%A +0.25wt% 3230		S13DHA +A6 +L4-2 (7:2:2),0.8wt%A +0.36wt% 3230
Viscosity (cp)	0.9	15.7	15.1		34.2
P slug (1PV)					
Formulation	0.25 PV @ 17500 ppm 3230, 0.25wt%, +L4-2,1455 ppm followed by 0.75 PV @ RH (9400 ppm), 3230, 0.25wt%	0.265wt% 3230 @RH (9400 ppm) + 0.1wt% Na-isoascorbate	**0.5 PV** 0.25wt% 3230 @RH (9400 ppm)		0.33wt% 3230 @RH (9400 ppm)
Viscosity (cp)	18.9	18.9	18.7		36
EWF (9400 ppm RH Brine)					
PV	1.41	1.58	1.66		2

3.4 Analysis of Core Flood Test Data

3.4.1 Initial Conditions for Chemical Flooding

Absolute brine permeability of the core (k_{brine}), crude oil viscosity, initial oil saturation (S_{oi}) and residual oil saturation after water flooding (S_{orw}) are plotted for each test in Figure 3.10 to show the starting conditions for the chemical flood.

Despite the relatively broad range of the Berea core permeability (202 – 817 mD), which is due to the heterogeneity of the sandstone reservoir, the two oil saturation values (S_{oi} and S_{orw} defined as the initial and post water flooding fractions of the pore space occupied by oil) remain fairly consistent, with average values of 64% for S_{oi} and 43% for S_{orw}. Similar starting conditions allow more straightforward comparison of the efficiency of the different chemical floods.

8 pieces of reservoir cores with air permeability ranging from 722 to 1575 mD were stacked in RCF#1 (see Figure 3.9). S_{oi} for RCF#1 was relatively close to the values for Berea core, while S_{orw} (25.7%) was much lower. This value is close to S_{orw} estimates (~ 25%) for the Rock Hill reservoir derived from field surveys, indicating that the laboratory reservoir core flood test well mimics the field conditions. On the other hand, the fact that it is much lower than the values obtained for Berea core suggests the more challenging conditions for oil recovery existing in the reservoir cores.

Figure 3.9 Arrangement of reservoir cores for RCF#1

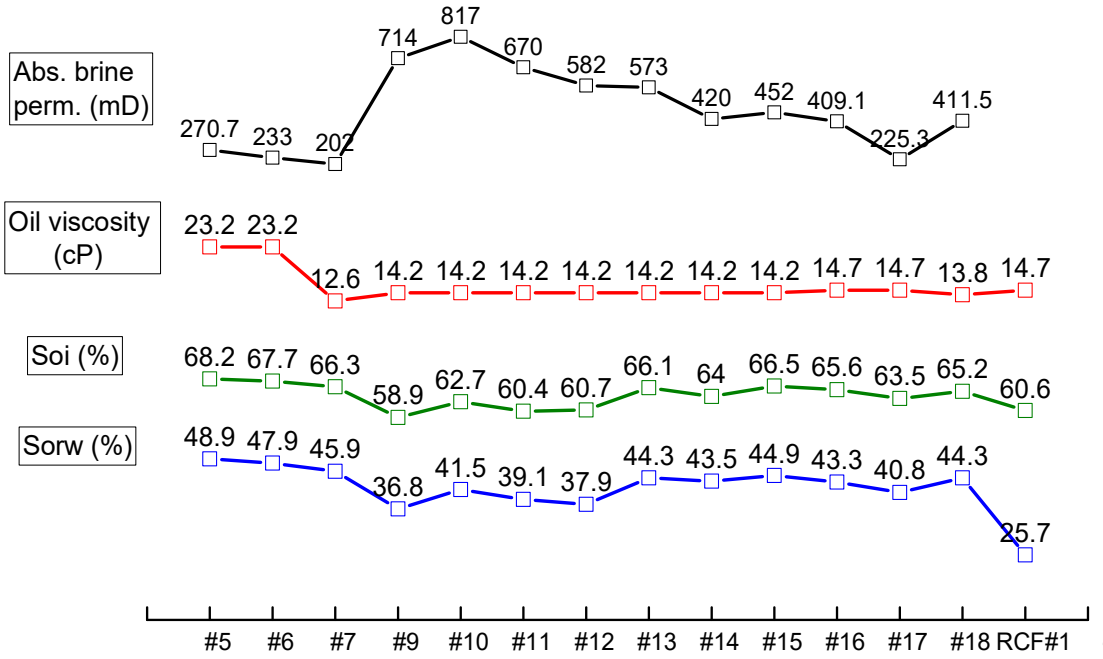

Figure 3.10 Initial conditions for chemical flood

3.4.2 Breakthrough Curves

Figure 3.11 to Figure 3.14 present breakthrough curves extracted from the excel file for BCF#5 that can be considered representative, at least on a qualitative basis, of the results of all core flood tests performed on Berea core. Pressure data, shown with a continuous line, were derived from readings of the differential pressure transducer placed between the ends of the core, while individual data points shown in the plots are results of analyses conducted on the on effluent fractions. Breakthrough curves for all other tests are presented in Appendix A. Some summary parameters derived from the breakthrough curves are shown in Table 3.4.

Figure 3.11 shows oil cut, cumulative oil recovery in terms of %OOIP, residual oil saturation and pressure across the core versus cumulative injected pore volume over the entire duration of the test. The data shown in the figure illustrate how in this test the initial water flood recovered 28.3% OOIP, with an overall oil recovery of 63.6% OOIP and a residual oil saturation of 24.8% resulting from the chemical flood. A pore

pressure drop is necessarily generated during all flooding stages, with higher values developed as a result of the injection of the higher viscosity chemical slug.

The same data are plotted in Figure 3.12**,** in this case as a function of the cumulative pore volumes injected since the start of the SP slug. The figure highlights how the injection of the SP slug mobilizes oil trapped by capillary forces and an oil bank, a region where oil saturation increases, is formed at the front and pushed forward to the production outlet [21]. As shown in Figure 3.12**,** in BCF#5 the first oil response (arrival of the oil bank) occurred ~ 0.2PV from the start of the chemical flood. Values of the first oil response for all core flood tests, summarized in Table 3.2, are observed to be relatively consistent (Ave=0.24$\pm$0.09), a reflection of the consistent pore structure characteristics of the Berea cores. Values of the pore volumes corresponding to the first emulsion response are reported in the second column of Table 3.2. First emulsion response refers to the time when the aqueous phases of the produced effluents become unclear (see Figure 3.5). The difference between the PV of the first oil and first emulsion response gives the PV of neat oil. For reference, the slug size of SP slug is also included in Table 3.2. In general, all oil production produced by chemical flooding occurs between ~ 0.25PV and 1.25PV from the start of the chemical flood. For all tests, a sharp increase in the pressure differential across the core is observed with the start of the chemical flood, with a peak (in this case of ~20 psi) reached when the oil cut approaches its highest value. A sharp drop in pressure is observed as the oil cut decreases, and a steady state value is reached as the polymer drive is completed. The pressure is further reduced with the start of the final water flood. Note that this value falls below that measured during the IWF, reflecting the final higher permeability of the core.

As shown in Figure 3.13 and Figure 3.14, the water phase of the effluent first produced is HTDS brine with surfactant/polymer breakthrough occurring approximately 0.65PV after arrival of the oil bank. The TDS of the effluent decreases reflecting the difference in salinity between SP slug (OS) and P slug (RH salinity). Concurrent with the surfactant/polymer breakthrough is the increase in the viscosity of the effluent, which reaches a maximum in correspondence to the maximum polymer concentration.

In BCF#14, in addition to measuring the overall pressure drop across the core, measurements of pore pressure were made at ports located along the core using standard (gage) pressure transducers. The difference between the values measured at two consecutive ports was used to calculate the pressure drop across a given core section. The resulting data were plotted as shown in Figure 3.15. During the chemical flood, pressure drops of these sections peaked in sequence which indicates the mobilization of the oil bank across the core. The pressure drop then reached a plateau after the oil bank had passed through as a result of the relative permeability in this section attaining a steady state value [18].

Table 3.2 Results of oil response

Coreflood ID	First oil response (Cum. PV from SP)	First emulsion response (Cum. PV from SP)	PV of neat oil	PV of SP
#5	0.17	0.61	0.45	0.5
#6	0	0.15	0.15	0.55
#7	0.21	0.72	0.51	0.49
#9	0.43	0.78	0.35	0.5
#10	0.29	0.78	0.49	0.5+0.25
#11	0.22	1.33	1.11	0.5
#12	0.25	0.95	0.7	0.25
#13	0.3	0.72	0.42	0.3
#14	0.17	0.84	0.68	0.5
#15	0.25	0.76	0.51	0.5
#16	0.25	0.67	0.42	0.5
#17	0.26	0.8	0.54	0.5
#18	0.25	0.67	0.42	0.25
RCF#1	0.49	0.94	0.45	0.5

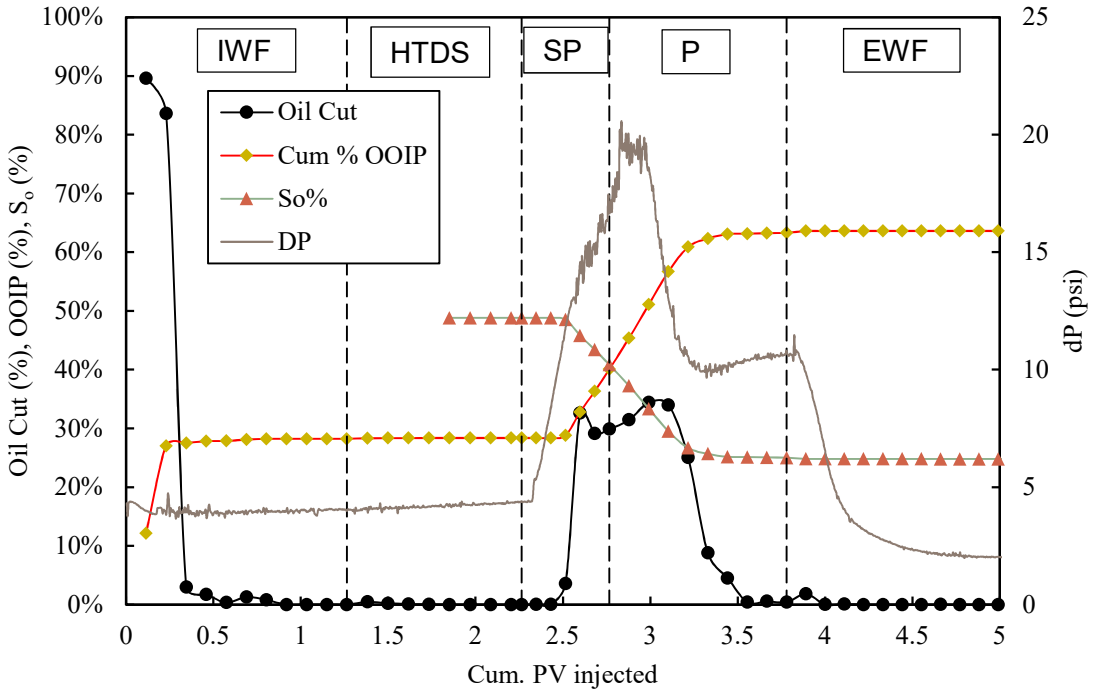

Figure 3.11 Oil cut, oil recovery and pressure data for BCF#5 as a function of cumulative pore volumes injected over entire duration of test

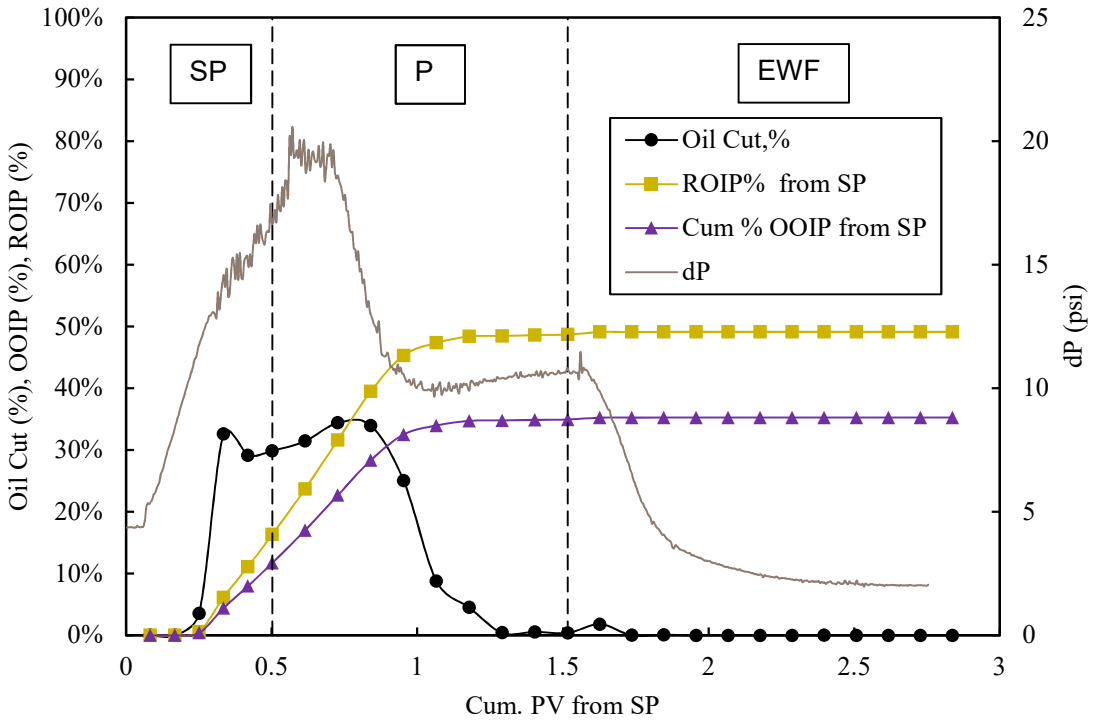

Figure 3.12 Oil cut, oil recovery and pressure data for BCF#5 as a function of cumulative pore volumes injected from start of chemical flood

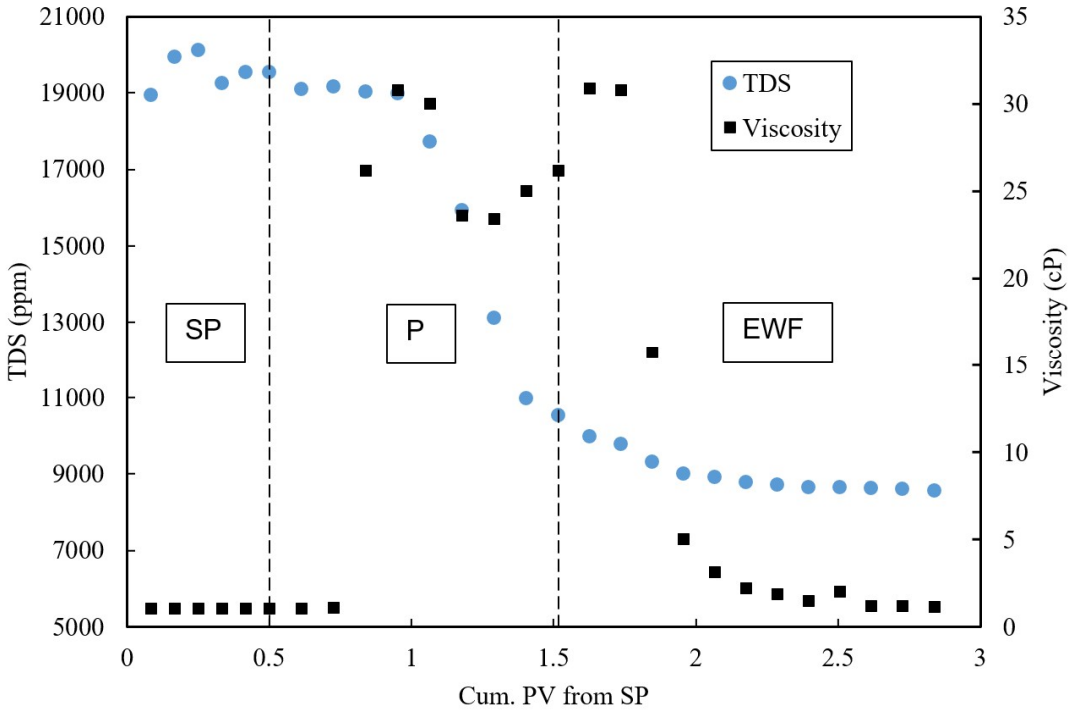

Figure 3.13 TDS and viscosity data for BCF#5 as a function of cumulative pore volumes injected from start of chemical flood

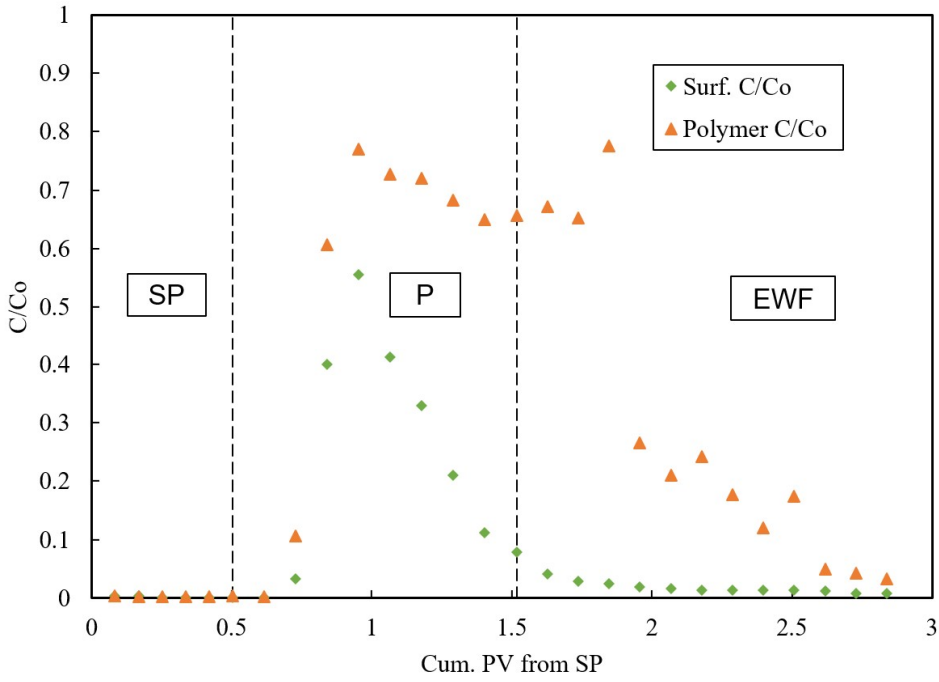

Figure 3.14 Surfactant and polymer concentrations for BCF#5 as a function of cumulative pore volumes injected from start of chemical flood

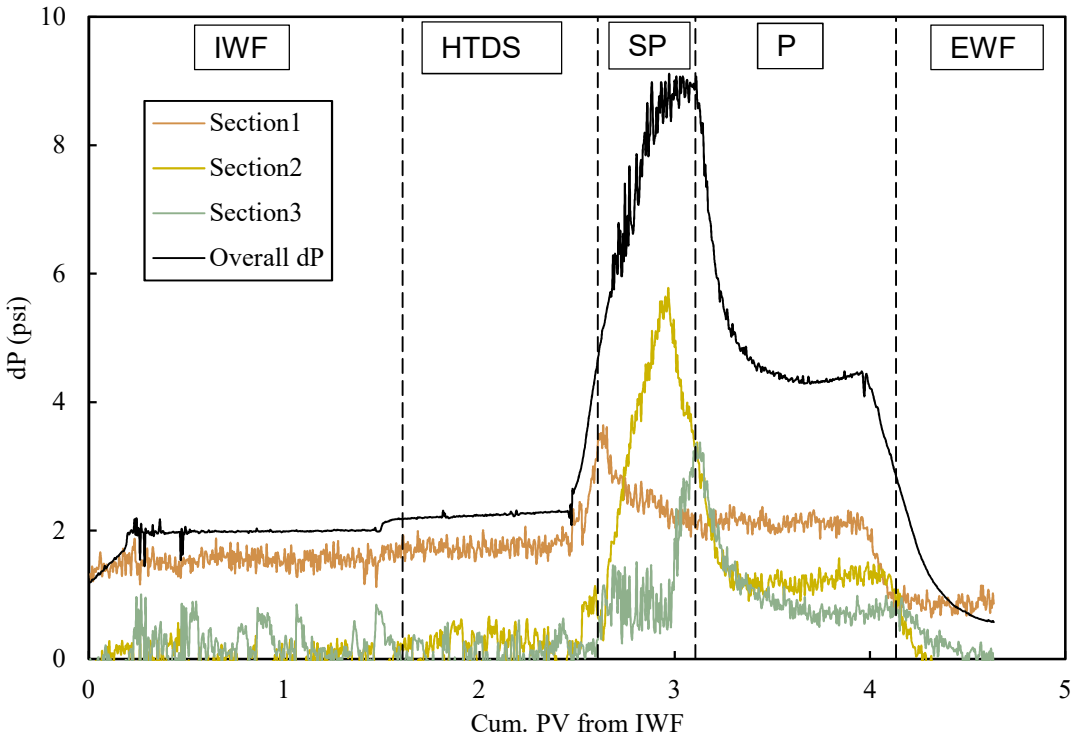

Figure 3.15 Pore pressure data for BCF#14

Pore pressure measurements along the core were made also in RCF#1. This test highlighted some issues in obtaining dP from the difference of two measurements rather than from a differential measurement. Particularly when the pressures are very small, this can lead to calculating negative values of dP.

3.4.3 Performance Analysis

3.4.3.1 Performance Parameters

Based on technical and economic feasibility, five parameters were selected to assess test efficiency: recovery factor in terms of %ROIP, oil saturation after chemical flooding (S_{orc}), maximum injection pressure drop during chemical flooding, surfactant sorption and total injectant cost per barrel. Note that this last value is calculated considering exclusively the cost of surfactant, polymer and salts in the chemical slug.

See Table 3.3 for target values for these parameters, which were defined based on conversations with Pioneer Oil, and are considered minimum requirements for technical and economic feasibility of cEOR in the field. These parameters define a zone of unacceptable performance on the spider plot (see Figure 3.16) created to illustrate the core flood results. For a formulation to be considered viable in the field, measured/calculated values of all these parameters need to fall outside this zone.

Table 3.3 Target values of performance parameters

Performance Parameters	Expected Values
Recovery factor %ROIP	>75%
S_{orc}	<10%
Total injection cost ($/B)	<$15
Surfactant sorption	<0.2mg/g
Max dP	<1.5psi

$$\text{Recovery Factor (\%ROIP)} = \frac{\text{oil recovered during chemical flood}}{\text{residual oil after water flood}} \times 100\% \quad (3.1)$$

$$S_{orc} = \frac{\text{residual oil after chemical flood}}{\text{pore volume}} \times 100\% \quad (3.2)$$

$$\text{Total injectant cost} = \frac{\text{total cost of surfactant, polymer, alcohol and salt}}{\text{volume of oil recovered during chemical flood}} \quad (3.3)$$

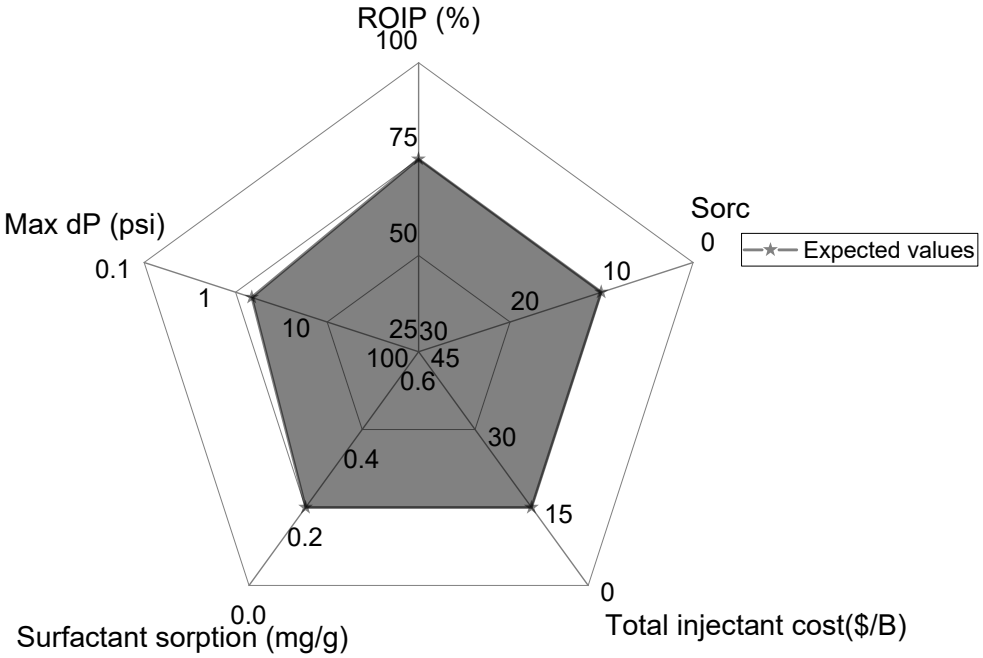

Figure 3.16 Spider plot with target performance parameter values

3.4.3.2 Results and Discussion

Values of performance parameters for all core flood tests are summarized in Table 3.4, while the subsequent figures present spider plots of these same data. Each plot shows data for tests conducted using the same surfactant formulation.

Tests BCF#5, #6, and #7 presented in Figure 3.17 all used a SP slug with approximately 0.5 PV of S13D+A6(9:1). As summarized in Table 3.1, the main difference between the three core floods is the surfactant concentration (1wt% in BCF#6 versus 0.4wt% in BCF#5 and #7). Additionally, the chemical slug of BCF#5 had higher polymer concentration (0.34% versus 0.275%) compared to the other two. Given the consistent permeability of these three cores (202-270 mD) the variation in the performance parameters can be thought to reflect for the most part the impact of the different characteristics of the formulation. The higher recovery measured in BCF#5 relative to BCF#7 highlights for example, the role of the viscosity of the slug (note also the difference in oil viscosity between these two tests). As expected, oil recovery increases with surfactant concentration (see BCF#6 versus BCF#7). For the conditions examined

in these three tests this does not, however, translate into an improvement in the cost per barrel. Moreover, higher surfactant sorption is also observed with higher surfactant concentration. Overall, as summarized in Figure 3.17, the three formulations based on S13D+A6(9:1) investigated in BCF#5, #6 and #7 show generally unfavorable performance.

Figure 3.18 shows the results for BCF#9 and #10, the only two core flood tests performed using a single surfactant: 0.4wt% of J13131 for #9 and 0.4wt% of S13D for #10. The data from these two tests indicate the better performance on all dimensions of S13D relative to J13131. Additionally, comparison of the performance of BCF#10 relative to BCF#5 shows that a 50% increase in surfactant (0.75 PV versus 0.5 PV) is needed to obtain similar recovery when using a single surfactant, this despite the more favorable testing conditions (higher permeability and lower oil viscosity) in BCF#10. These results were the basis for not further considering single surfactant formulations.

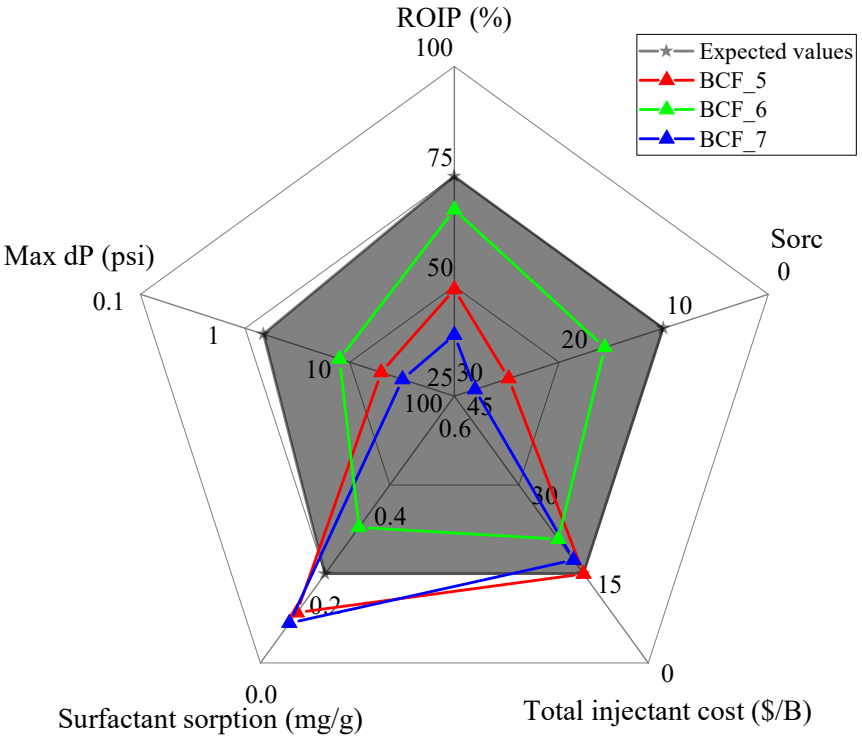

Figure 3.17 Spider plot for BCF#5, #6, #7 (formulation: S13D+A6(9:1))

Table 3.4 Performance parameters

Coreflood ID	Recovery factor (% ROIP)	S_{orc} (%)	Total injectant Cost ($/B)	Surfactant sorption (mg/g)	Max dP (psi)
#5	49.3%	24.8%	$15.00	0.113	20
#6	67.4%	15.6%	$20.90	0.305	8
#7	38.9%	28.0%	$17.40	0.090	32
#9	31.7%	25.1%	$27.50	0.107	9.7
#10	52.3%	19.8%	$21.40	0.046	8.9
#11	84.7%	6.0%	$17.30	0.444	4.4
#12	75.2%	9.4%	$12.60	0.174	8.6
#13	64.4%	15.8%	$11.40	0.134	5.8
#14	82.8%	7.5%	$13.60	0.260	9.6
#15	60.1%	17.9%	$16.30	0.127	5.4
#16	54.7%	19.6%	$17.00	0.170	3.2
#17	75.2%	10.1%	$14.60	0.214	7.8
#18	70.24%	13.2%	$7.50	0.111	6
RCF#1	60.1%	10.2%	$32.2	0.170	22

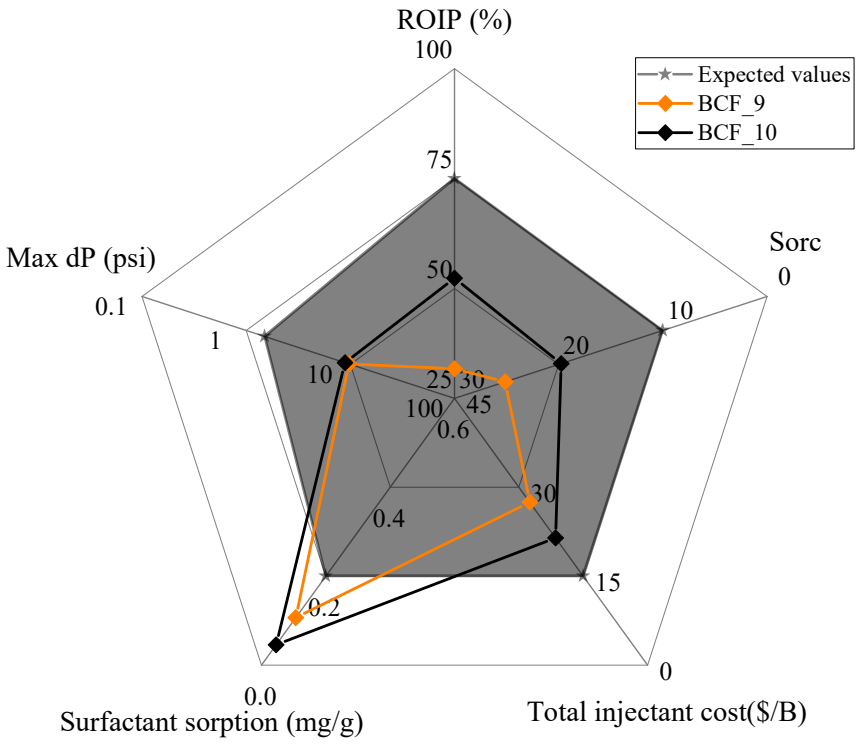

Figure 3.18 Spider plot for BCF#9, #10 (single surfactant formulations)

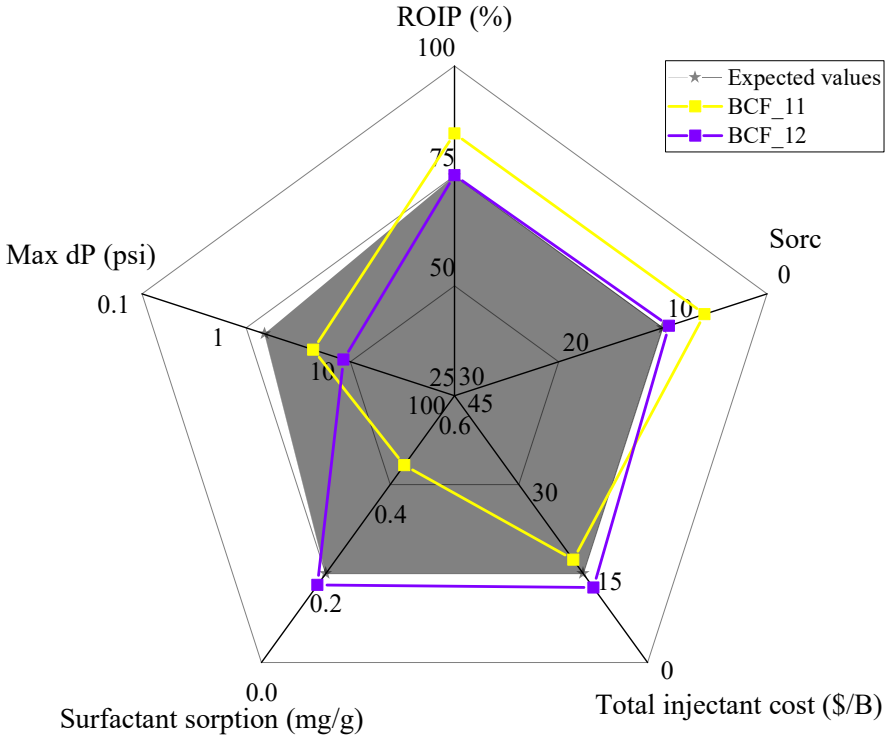

Figure 3.19 Spider plot for BCF#11, #12 (formulation: S13D+A6+L4-2 (7:2:1))

Tests (BCF#11 and #12) presented in Figure 3.19 first explored the use of a co-solvent (L4-2) in the formulation. Concentration of surfactant mixture combined with the co-solvent increased to 1wt% (note that the 0.9% value of the surfactant concentration shown in Figure 3.8 refers to surfactant and co-surfactant alone). For both tests the viscosity of the chemical slug remained at about 40cP, higher than previous tests. The major difference between the two tests is in the 0.25PV size of the SP slug injected for BCF#12, half of the value (0.5 PV) used in BCF#11 (as well as in the majority of the previous tests) (see also the slight difference - 20k versus 19k – in the salinity of the slug). As expected, the higher amount of surfactant translates into higher oil recovery in BCF#11. In both tests the recovery parameters are found to greatly improve relative to all previous core floods, with ROIP values of 85% and 75%, and S_{orc} values of 6 and 9%, in BCF #11 and #12, respectively. Of particular significance are the results for BCF#12, in which four of the five performance parameters meet or exceed the target requirements. The single requirement not met is this test is the limitation on the maximum pressure developed across the core.

The ratio of surfactants and co-solvent was adjusted to 7:2:2 starting with BCF#13, with the concentration of S13D+A6+L4-2 (7:2:2) fixed at 0.8wt% (corresponding to a 0.65% concentration of the surfactants).

Viscosities of the chemical slugs remained at about 35cP for BCF#13, #14, #15, all performed on cores with permeability around 400-450 mD. Less surfactant (0.3PV) was injected in #13 compared to #14 and #15 (0.5PV), and starting with BCF#14 a shift was made to a lower molecular weight polymer (F3230 instead of F3300). Comparison of the results of BCF#13 and BCF#14 confirms previous observations of improved recovery and increased surfactant sorption associated with increases in the amount of surfactant injected (the different polymer likely plays a lesser role, as, due to the different amount of polymer present in the SP slug, the slug viscosity does not change). BCF#15 used RH salinity for the SP slug rather than the optimal salinity of 17.5k derived from the phase behavior studies. As expected, salinity adjustment is found to be essential to maximize the effectiveness of the injected chemicals. This is clearly shown by the results of BCF#14 and #15, as the same surfactant mixture recovered 82.8% of the residual oil at 17.5k (BCF#14) compared to 60% residual oil at RH

salinity (BCF#14). BCF#14 also shows lower S_{orc}, and injectant cost per barrel. The surfactant sorbed and the maximum pressure measured across the core are instead higher. Despite this, as illustrated in Figure 3.20, the formulation investigated in BCF#14 appears to be the most promising of the three.

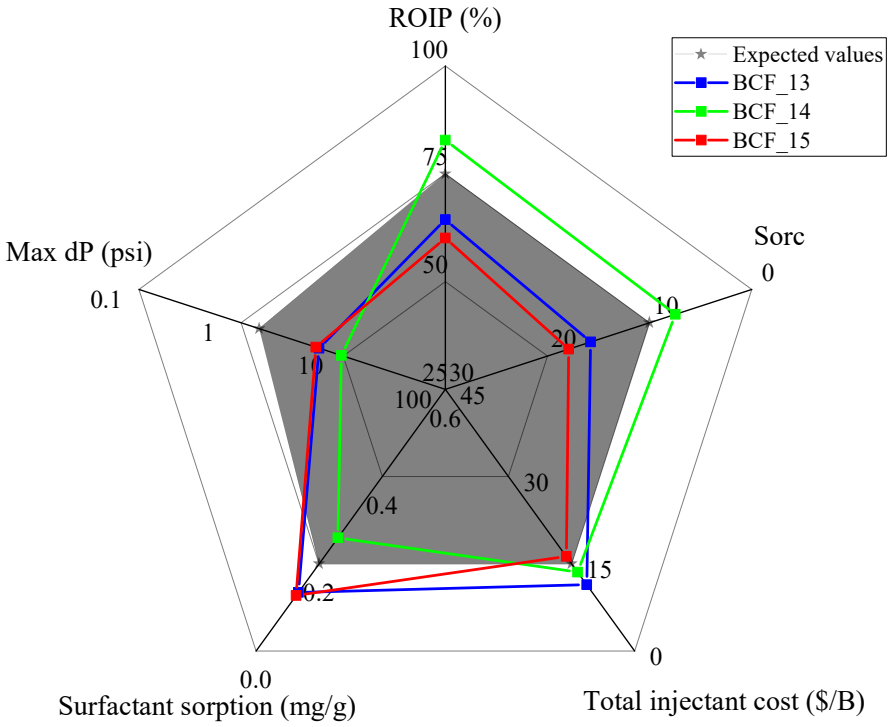

Figure 3.20 Spider plot for BCF#13, #14, #15 (formulation: S13D+A6+L4-2 (7:2:2))

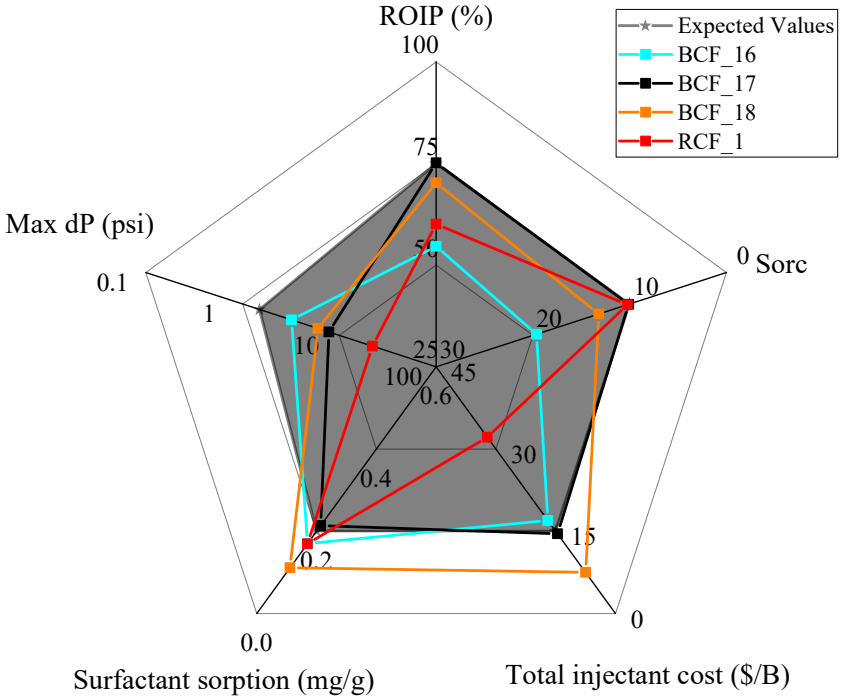

Figure 3.21 Spider plot for BCF#16, #17, #18, RCF#1 (formulation: S13D+A6+L4-2 (7:2:2) – no polymer in SP slug)

As shown in Figure 3.21, lower polymer concentrations (0.25-0.27%), chosen to target SP viscosities in the 15-19cP range, were used in BCF#17, #18. For BCF#16, no polymer was included in the 0.5PV surfactant slug. This was done in an attempt to isolate the factors responsible for the high maximum dP values measured in the previous core flood tests. As the dP measured in BCF#16 was the lowest of the values measured in any of the tests, the high dP values were attributed to the effects of polymer viscosity and oil saturation and not to the viscosity of the middle phase. Despite identical viscosity of the subsequent P slug, oil recovery was much smaller in BCF#16 compared to BCF#17 (ROIP = 55% versus 75%; S_{orc}=19.6% versus 10.1%) due to the reduced sweep efficiency of the SP slug (note also the higher permeability of the core used for BCF#16 that should have facilitated recovery relative to #17). Additional insight into the role played by the viscosity of the SP (and P) slug is obtained comparing the results of BCF#17 to those of #14. These two tests employed identical sizes and salinity of both SP and P slug, and the same surfactant mixture and concentration, the only difference being the concentration of the F3230 polymer, 0.27% in BCF#17 versus

0.36% in BCF#14. The decrease in the slug viscosities due to the reduction in polymer concentration leads to some reduction in oil recovery, with ROIP going from 82.8% to 75.2% and S_{orc} going from 7.5% to 10.1%. No significant difference is observed in the amount of surfactant sorbed, in both cases close to the target value, and in the injectant cost per barrel, which for both tests satisfies the target requirement (the reduction in cost due to the lower amount of polymer used is compensated by the smaller volume of oil recovered). Consistent with the lower viscosity of the slug is the smaller value of the pressure differential measured across the core. In fact, of all the tests performed, the smallest pressure differential is measured in test BCF#16 that did not utilize polymer in the SP slug.

Finally, BCF#18 was conducted using a formulation very close to that of BCF#17, except that in #18 the size of the SP slug was reduced from 0.5PV to 0.25PV and that of the P slug from 1 PV to 0.5PV. As a result, the recovery factor is slightly reduced in #18 compared to #17, with the ROIP decreasing to 70%, and the S_{orc} increasing to 13.2%, in both cases following just outside the zone of acceptable performance. Improvements are instead observed in the other these parameters, with the surfactant sorption reaching 0.111mg/g, and the total injectant cost reaching $7.50/barrel, the lowest value among all the tests.

In RCF#1 (which was conducted between BCF#15 and #16), a 0.5PV slug of 0.8wt% S13D+A6+L4-2 (7:2:2) with 0.36% F3230 at 17.5k was injected in the stacked reservoir cores. This formulation, which is identical to that which yielded the best results for Berea core in BCF#14, was not found to be equally successful in the reservoir cores. Only 60% of the residual oil was recovered in RCF#1, under the conditions of low S_{orw}. Additionally, although surfactant sorption was low, the total injectant cost of $32.2 per barrel of recovered oil was the highest of any of the tests performed and well outside the acceptable range, and the maximum pressure drop across the stack was also amongst the highest measured.

In conclusion, as shown in the spider plots, none of the core flood tests performed to date as part of the cEOR Pioneer initiative yielded favorable values of the maximum

pressure differential across the core, and reduction of this parameter remains a challenge. Minimizing surfactant sorption appears to be attainable reducing the amount of surfactant injected, i.e. lowering the concentration and/or decreasing the size of the SP slug. However, as oil recovery is closely correlated to the amount of surfactant injected, balance should be maintained between these two parameters.

3.5 Comparison with Data from Literature

To place the Purdue core flood data in context, a literature review on core flood tests was performed. Given the specific conditions of the Rock Hill reservoir, this review emphasized core flood tests with relatively low total dissolved solids (TDS) and low testing temperature. Tests with comparable testing conditions were summarized to develop a database consisting of formulations (chemicals, concentrations), core characteristics, oil data, and recovery results. This database was used to evaluate the current recovery efficiency of Purdue BCF tests. Several controlling parameters were examined and key conclusions from specific references were extracted to gain a better understanding of the core flood process.

3.5.1 Core Flood Test Database

54 core flood tests in total from 5 references were selected after careful review. Table 3.5 summarizes the basic information of oil, core, chemicals, salinity and temperature. Note that tests from [18] were ASP flooding and several kinds of crude oils from different fields were used. The reason for including these tests, despite the fact that no alkali was employed in any of the Purdue core floods, is that the same primary surfactant (S13D) and polymer (FLOPAAM 3330S) as those used in the Purdue CF tests were adopted in this study. For easy reference, the relevant parameters for the Purdue BCF tests are also listed in Table 3.5**.**

Figure 3.22 summarizes the core material used in the 54 core flood tests. 27 out of the 54 tests were performed on Berea sandstone core, one of the rocks most commonly used in the petroleum industry for laboratory core flood experiments. The remaining were reservoir cores from different sources. In [23], two parallel layers of consolidated

sandstone cores (without crossflow between layers and with a permeability contrast ratio of two) were used to simulate a heterogeneous formation. Reservoir cores used in [25] were natural sandstone cores selected from the targeted oilfield. Note that the types of core permeability reported are not the same. Air permeability is always greater than absolute brine permeability due to the Klinkenberg effect [22].

Table 3.5 Basic information of selected references

No.		1	2	3	4	5					Purdue Berea Core Flood Tests
Reference		[23]	[24]	[17]	[25]	[18]					
Type		SP				ASP					SP
Oil Name		Kerosene	Bradford Crude Oil	Dehydrated crude oil from Xinjiang Karamay oilfield	Crude oil from Huabei Oilfield Jing-11 block reservoir	Muddy Creek	Tobias	Chester Unit	Woodhead-Vinland		RH crude oil
Oil Viscosity (cP)		2.15	4	27	11.97	3.61-3.83	4.8	-	-		13.8-23.172
Core Permeability	**Type**	Not reported	Not reported	Air	Air	Brine-SFB					Brine-SFB
	Value (mD)	1333.3 (K_{eq})	203	340-406	288.6,208.3	226-282	265	152	166.5-204		201.9-817.2
Surfactant		PS + DEA	PS (TRS-16+PRL-15)	PS + HABS	PS-2	S13D + (1-2) cosurfactant					S13D + cosurfactant
Polymer		HPAM	Xanthan gum (follows surfactant slug)	KYPAM	KYPAM	FLOPAAM 3330S			FLOPAAM 3330S/3530S		FLOPAAM 3230S/3330S
T (°C)		30	-	40	53	40.6	40.6	48.9	27.9		24
TDS (ppm) of SP slug		20,000 (NaCl)	10,000,20,000 (NaCl)	5,448.7 synthetic field brine (SFB)	10,790 SFB	~ 40,000	34,900	44,300	23,000-62,500		17500-22000

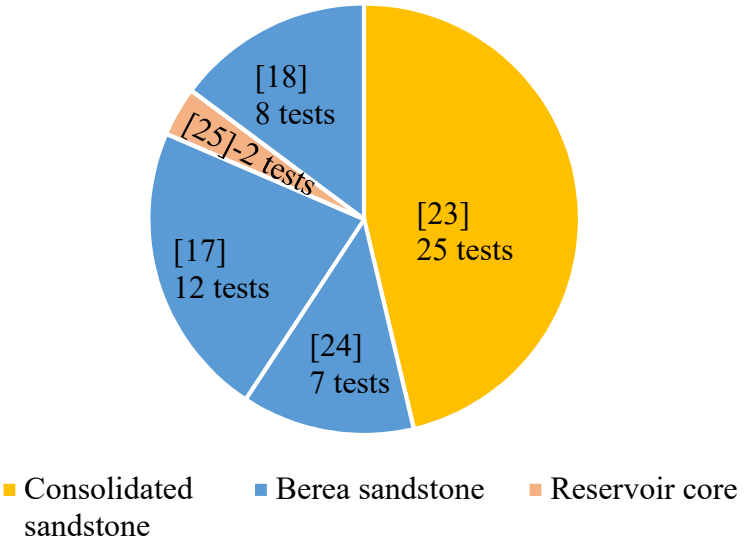

Figure 3.22 Core materials of the selected tests

Source	Oil			T/°C	Core Sample					Waterflood		
	Name	Density/(g/cm3)	Viscosity (mPa·s)		Source	Diameter	Length	Porosity/%	Permeability/md	salinity/ppm	PV injected	Recovrery (%OOIP)
1	Kerosene	0.00796	2.15	30	Two parallel layers of Consolidated sandstone cores (without crossflow between layers and with a	2.5cm	10cm	-	2000 and 1000, respectively Keq=1333.3 mD	20000	until 98% water cut	28.43 27.51 28.33 29.03 28.05 28.13 28.98 28.66 28.56 27.87 27.99 28.65 29.12 27.97 28.43

SP slug													P slug			Additional recovery by SP flooding (% OOIP)	Additional recovery by SP flooding (% ROIP)
	Surfactant				Polymer												
Salt/ppm	Name	Conc./ppm	Name	Conc./ppm	Name	Conc./ppm	IFT/(mN/m)	Visc./cp	Tot. Conc.(%)	PV injected	Capillary number	Flow rate	Name	Conc./ppm	PV injected		
20000	PS	200	-	-	HPAM	500	4.3000	5.1	0.02	0.3	1.71E-05	0.2 mL/min	Waterflood until the water cut of efflux reached 98% again			12.5	17.4
	PS	1,000	-	-		500	0.1842	5.1	0.10		4.21E-04					13.0	18.0
	DEA	3,000	-	-		500	0.0202	5.1	0.30		3.86E-03					14.9	20.8
	PS	1,000	DEA	2000		500	0.0035	5.1	0.30		2.32E-02					16.4	23.1
	PS	4,000	DEA	4000		500	0.0005	5.1	0.80		1.59E-01					16.5	22.9
	PS	200	-	-		750	4.4000	8.3	0.02		2.77E-05					17.4	24.1
	PS	1,000	-	-		750	0.2012	8.3	0.10		6.10E-04					19.2	27.1
	DEA	3,000	-	-		750	0.0187	8.3	0.30		6.59E-03					21.3	29.9
	PS	1,000	DEA	2000		750	0.0032	8.3	0.30		3.87E-02					23.8	33.4
	PS	4,000	DEA	4000		750	0.0006	8.3	0.80		2.23E-01					24.0	33.2
	PS	200	-	-		1000	4.4000	12.0	0.02		4.02E-05					22.6	31.4
	PS	1,000	-	-		1000	0.2217	12.0	0.10		8.18E-04					27.1	38.0
	DEA	3,000	-	-		1000	0.0151	12.0	0.30		1.17E-02					32.6	46.0
	PS	1,000	DEA	2000		1000	0.0037	12.0	0.30		4.68E-02					27.8	38.6
	PS	4,000	DEA	4000		1000	0.0006	12.0	0.80		3.17E-01					27.3	38.2
	PS	200	-	-		1250	4.4000	16.0	0.02		5.58E-05					23.6	32.9
	PS	1,000	-	-		1250	0.2067	16.0	0.10		1.19E-03					27.6	38.3
	DEA	3,000	-	-		1250	0.0188	16.0	0.30		1.32E-02					33.0	46.1
	PS	1,000	DEA	2000		1250	0.0036	16.0	0.30		6.80E-02					28.3	39.0
	PS	4,000	DEA	4000		1250	0.0006	16.0	0.80		4.26E-01					29.0	40.8
	PS	200	-	-		1500	4.5000	21.0	0.02		6.92E-05					24.1	33.6
	PS	1,000	-	-		1500	0.1792	21.0	0.10		1.79E-03					28.1	38.7
	DEA	3,000	-	-		1500	0.0140	21.0	0.30		2.27E-02					33.0	46.2
	PS	1,000	DEA	2000		1500	0.0047	21.0	0.30		6.81E-02					29.5	40.7
	PS	4,000	DEA	4000		1500	0.0006	21.0	0.80		5.43E-01					29.0	40.8
20000	TRS-16/PRL-15 (1.3 : 1.0)	5000	-	-	-		0.00353	1.02	0.55	0.4		1ft/d	Kelzan+ 200ppm NaCl	500	0.7 PV	--	11.0
20000									0.55	0.5				500	1.0 PV		30.0
20000									0.55	0.5				1000	0.7 PV		33.0
20000									0.55	0.4				1000	1.2 PV		19.0
20000									0.55	0.9				1000	0.8 PV		44.0
20000									0.55	0.5				500	0.5 PV		29.0
10000									0.55	0.57				500	0.7 PV		11.0

Figure 3.23 Database of core flood tests

All the selected core flood tests followed the same basic testing procedure. Chemical flooding (SP slug) was conducted after initial water flooding except that in tests from [24] the surfactant and the polymer slugs were injected separately.

An excel file was developed to summarize the key parameters of the 54 tests (see Figure 3.23). Table 3.6 shows the framework of the database which is comprised of source, oil and core characteristics, temperature, slug design and recovery results.

Table 3.6 Key parameters collected

Source	Oil Properties	Core Properties	T(°C)	Water flood	Chemical flood	Tertiary recovery (% OOIP)
	Name Density Viscosity	Material K Dimensions Porosity		Salinity PV Injected	Formulation IFT Viscosity PV Injected	

3.5.2 Reservoir Conditions

Figure 3.24 presents a plot of oil viscosity plotted versus core permeability for all core flood tests, including those performed at Purdue. In this representation, the top quadrant, which corresponds to the higher values of oil viscosity and lower values of core permeability, represents the most challenging conditions for oil recovery. A few of the Purdue BCF data fall in this part of the plot. Note that while core permeabilities were quite consistent for tests from the same source, the Purdue BCF tests explored a wide range of core permeabilities. While this variation in permeability was not expected (all tests used Berea core), it may ultimately prove insightful, due to the nature of high heterogeneity of the Rock Hill reservoir.

Colors of the markers represent core materials which are the same as in Figure 3.22.

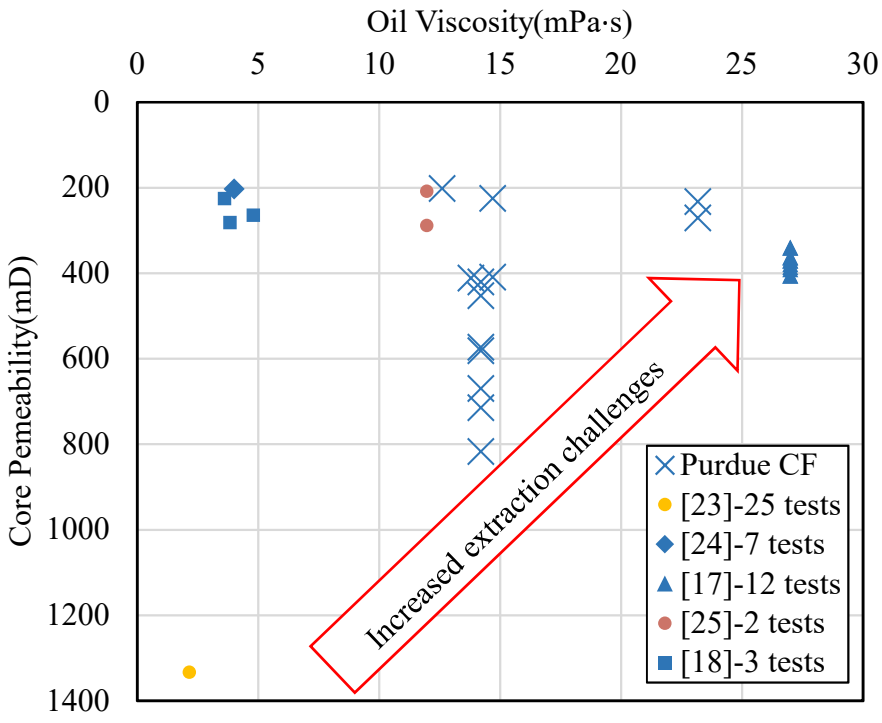

Figure 3.24 Oil and core characteristics

Figure 3.25 presents a plot of testing temperature versus SP slug salinity, and highlights the low-temperature and low-salinity conditions of the Purdue BCF tests. Data points representing the Purdue BCF tests fall in the left bottom part of the plot, and the 24°C temperature of all the Purdue BCF tests falls below the data for all other tests (this value was selected for consistency with measurements in the Rock Hill reservoir). Note that temperature data were not reported for the tests in [24].

Values of the SP slug salinity also fall at the low end of the range of the literature data.

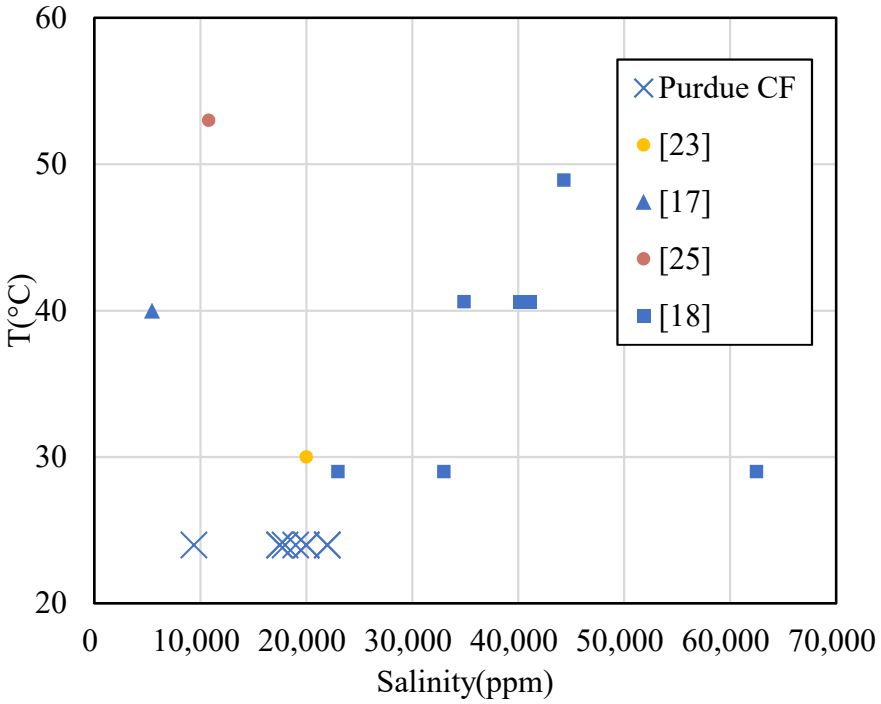

Figure 3.25 Temperature and SP salinity conditions

3.5.3 Parameters Controlling Recovery

3.5.3.1 Surfactant concentration and total amount of injected chemicals

Table 3.7 presents the optimal formulations with the highest tertiary recoveries.

As discussed earlier in this chapter, many factors related to core, oil and properties control oil recovery. With regard to SP slug properties, while IFT and viscosity play a critical role, they are impacted by a very large number of variables including type and concentration of surfactant(s) and polymer. To compare the Purdue BCF recovery data to those obtained in the studies chosen for the database, given the range of core materials, of surfactant types and concentrations, and given also the incomplete information (e.g. regarding IFT values) available in some of the studies, the following two "summary" parameters for describing the SP slug were selected after careful review: surfactant concentration and total amount of injected chemicals.

Table 3.7 Optimal slug compositions

NO.	Chemical Slug Formulation		TDS	Surfactant Conc. (wt%)	Alcohol	PV injected	Tertiary recovery (% ROIP)
	Surfactant	Polymer					
1	0.3% DEA	0.15% HPAM	2% NaCl	0.30	-	0.3	46.2
2	0.5% TRS-16/PRL-15 (1.3: 1.0) +0.05% cosurfactant oxy C_6	0.1% Kelzan	2% NaCl	0.55	-	0.9	44.0
3	0.3% PS	0.26% KYPAM	0.54487% SFB	0.3	-	0.5	57.4
4	0.3% PS-2	0.14% KYPAM	15.5% SFB	0.3	-	0.5	43
5-1	0.67% S13D +0.33%S2	0.3% F3330s	1% Na2CO3 + 3.11% NaCl	1	1.5% SBA	0.6	99
5-2	0.75% S13D +0.25% S2	0.3% F3330s	1% Na2CO3 + 2.49% NaCl	1	1.5% EGBE	0.6	98
5-3	0.07% S13D +0.07% S2 +0.36% S3	0.2% F3330s	1% Na2CO3 + 3.43% NaCl	0.5	0.25% BD	0.6	54
5-4	0.45% S13D+ 0.13% TDA6 + 0.68% S3	0.1% F3530s	Synthetic formation brine (SFB)	1.26	-	0.45	82

Figure 3.26 shows a plot of tertiary oil recovery versus surfactant concentration. The data collected pertain to tests with a wide range of surfactant concentrations, from 0.02wt% to 1.25wt%, with the Purdue BCF data falling in the middle region. Overall, the data indicate the expected trend of increasing recovery with increasing surfactant concentration. The large band in which the data fall reflect the effects of different cores (and oils), surfactant type and slug size. In general, the Purdue BCF tests show average to good performance compared to tests in the literature, with some of the results (e.g. those corresponding to BCF#14 and #17) falling at the very high end of the range.

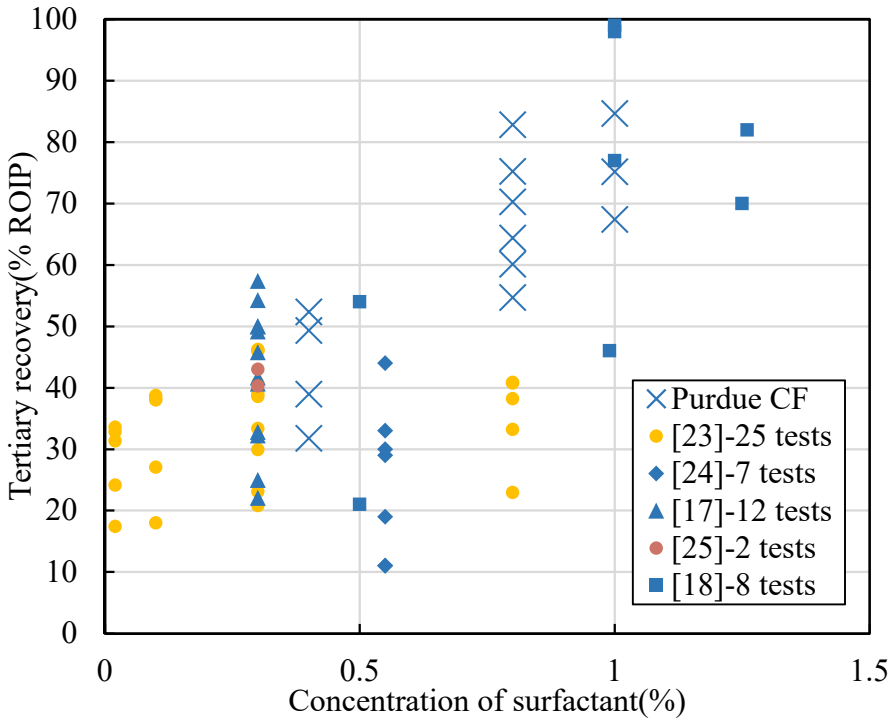

Figure 3.26 Effect of surfactant concentration

In [18], it was reported that tertiary oil recovery correlated well with the amount of chemical injected in the SP slug, which is calculated multiplying the chemical slug size (in pore volume) by the total weight percent of surfactant, alcohol and polymers contained in it. Based on this possible relationship, tertiary oil recovery is plotted in Figure 3.27 as a function of the amount of chemical injected in the SP slug.

As shown in Figure 3.27, the data display a general trend of increasing recovery with increasing amount of chemical injected, which therefore represents a good indicator to estimate the general economic feasibility of a cEOR process.

Again, the Purdue BCF tests fall at the middle to high range of the data, with the results for BCF#14 and #17 amongst the highest recovery of all the tests examined.

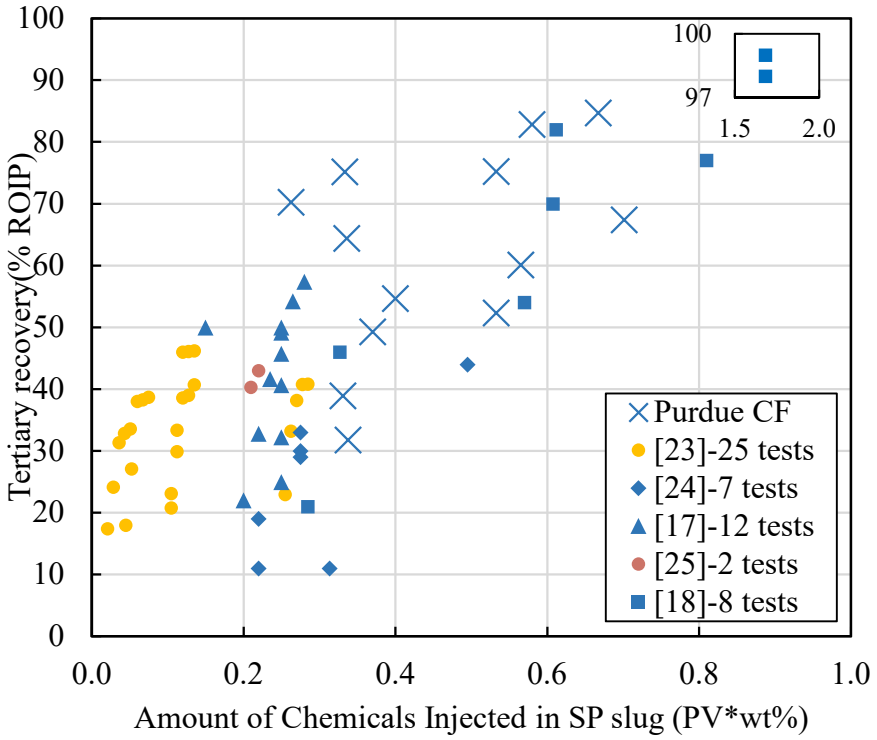

Figure 3.27 Effect of amount of chemical injected in SP slug

3.5.3.2 Insight into the Effect of Heterogeneous Core Conditions

Tertiary oil recovery is known to be controlled by the capillary number. When viscous forces applied on the trapped oil blobs by the displacing fluid exceed the capillary retaining forces, the residual oil can be mobilized and recovered [26]. The definition of capillary number is shown in Equation 3.4 [23]:

$$N_c = \frac{\mu V}{\sigma} \tag{3.4}$$

where μ is viscosity in cP, σ is IFT in mN/m and V is average displacement velocity in m/s.

The capillary number describes the combined influence of viscosity and IFT of the chemical slug on tertiary recovery. It can be concluded from typical capillary desaturation curves (CDC) that lower residual oil saturation can be achieved with larger capillary number. Residual oil saturation could even drop to zero when certain critical capillary number is reached (Guo et al., 2015).

Only tests from [23] and [17] provided values of the capillary number, and these data are plotted against tertiary recovery in Figure 3.29 and Figure 3.28, respectively. Different IFT or viscosity values were achieved in these studies by adjusting the concentrations of surfactant and polymer in the SP slug, thus obtaining a range of capillary number values.

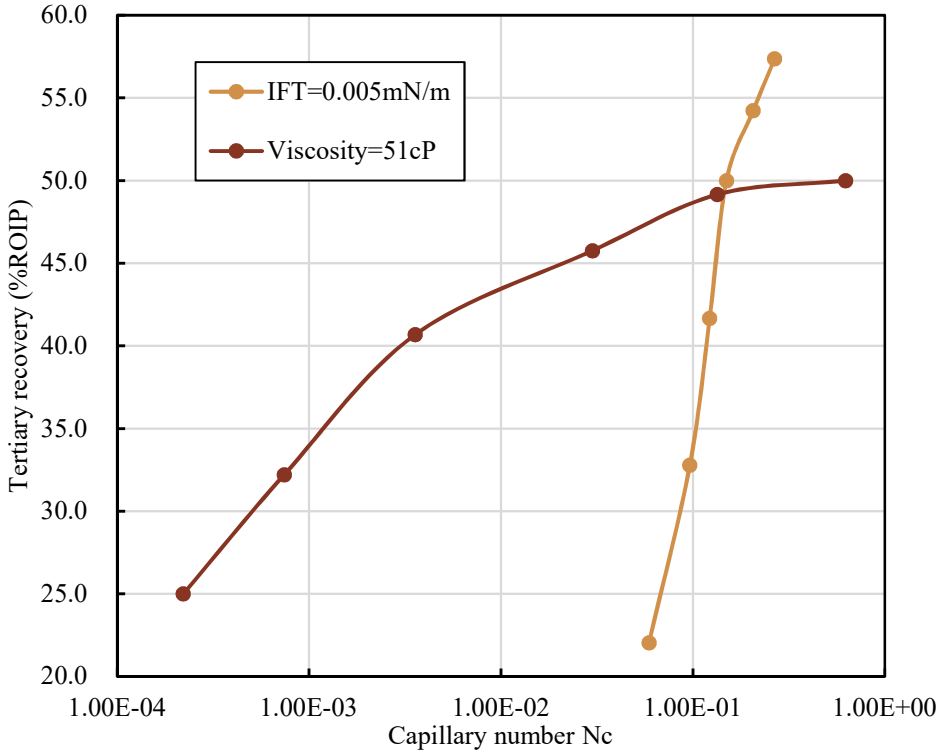

Figure 3.28 Effect of capillary numbers [17]

As shown in Figure 3.28, when the viscosity of the SP system was fixed at 51 cP, the lower IFT values, corresponding to the higher capillary numbers, led to higher tertiary oil recovery. Also, when the ultra-low IFT value was fixed as 0.005 mN/m, a favorable viscosity was the key to obtain a satisfactory tertiary recovery.

Tests from [23] were performed on two-layer heterogeneous core models. These tests provide a good reference for the Purdue cEOR project, given the high heterogeneity

conditions of the Rock Hill core material, on which testing is expected to focus moving forward.

Figure 3.29 shows plots obtained from [23] of tertiary oil recovery versus capillary number for slugs of different viscosity. It is seen that, for a given capillary number, the tertiary oil recovery increases with the viscosity of the SP slug until the viscosity reaches 12 cP. [23] terms this value the critical viscosity, which is the minimum viscosity of the displacing fluid with the same IFT that achieves the highest or close to the highest possible tertiary recovery. Above this critical viscosity, the ultra-low IFT values may not guarantee the highest recovery among formulations with the same viscosity. Instead, in contrast to what is observed in tests on homogeneous cores, the highest recovery is observed in correspondence to an optimum capillary number rather than the maximum one.

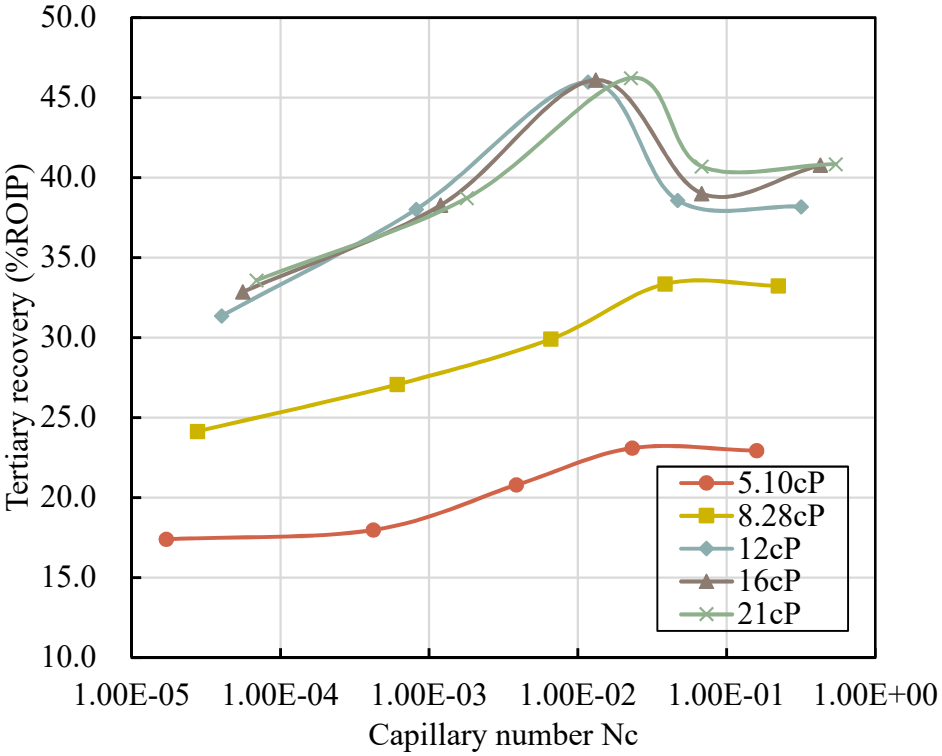

Figure 3.29 Tertiary recovery with different capillary numbers [23]

These observations are supported by the results of model experiments reported in the same paper and single core flood tests with monitoring of the pore pressure along the core, which show that formulations with "low" IFT values had higher sweep efficiency than those with "ultra-low" IFT. These data suggest that in a heterogeneous reservoir the highest recovery

is achieved when sweep efficiency and displacement efficiency are balanced with each other. An explanation for this observation is that, due to emulsification between mobilized oil and injected surfactant, sweep efficiency can be improved by low IFT flooding and the formation of larger emulsified oil droplets. In contrast, ultra-low IFT flooding may cause the entrapment of these droplets, that leads to diversion of the displacing fluid [17].

4. RHEOLOGY OF S13D SOLUTIONS

4.1 Introduction

This chapter presents data on the rheological behavior of S13D solutions in water and two different brines (RH brine with 9.4 TDS and 17.5k brine) as a function of surfactant concentration. These data were collected to support SAXS (Small-angle X-ray scattering) observations performed by the chemical engineering group of the Purdue EOR research team led by Professors Franses and Boudouris. The SAXS observations indicate the formation of different structures, including two types of liquid crystals, depending on the concentration of the surfactant.

In combination with the SAXS results, the rheological study presented here is aimed at understanding the phase diagram of S13D, the primary surfactant used in this research. Such an understanding is critical to several aspects of chemical EOR including development of slug formulations, preparation of surfactant flooding solutions, and interpretation of the behavior of phases that may form after injection of the slug in the rock formation.

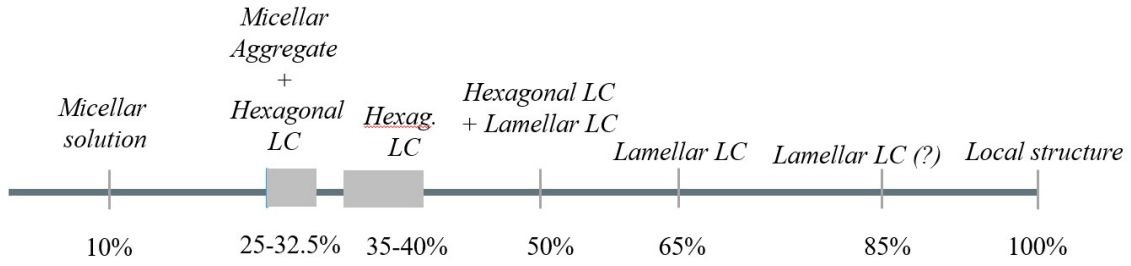

(a) S13D in water

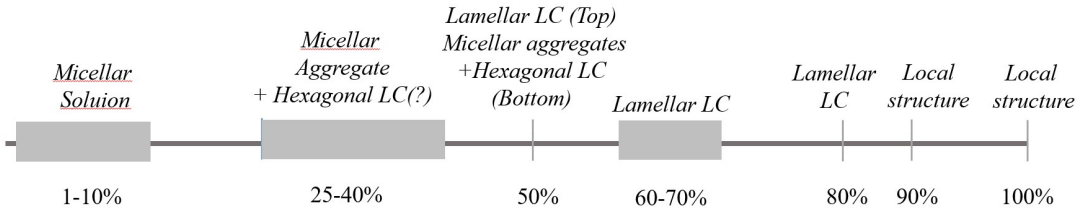

(b) S13D in RH brine

Figure 4.1 SAXS results of S13D in water and in RH brine [27]

Figure 4.1 summarizes the SAXS results for S13D in water and in RH brine over a broad range of concentrations, up to neat solution. Note that all concentrations of S13D in this chapter refer to total concentration (i.e. inactive components are included).

The SAXS results summarized in Figure 4.1 indicate the transitions in structures/phases that occur in both in water and in RH brine with increasing S13D concentration, starting from the micellar solutions formed in both cases at low concentrations. For water samples a single hexagonal liquid crystal (LC) phase is formed in the neighborhood of 40wt% and a lamellar LC around 65wt%. Schematic illustrations of these structures are shown in Figure 4.2. Two phase systems are formed at intermediate concentrations. In RH brine, a single hexagonal LC phase is not observed at any of the S13D concentrations explored, while a single lamellar LC phase is observed at 60-70wt%. At 50wt%, for both salinities, a two-phase system is formed, which separates in the vials, with the lamellar LC at the top and hexagonal LC at the bottom.

(a) Micelle

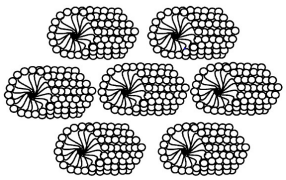

(b) Hexagonal phase

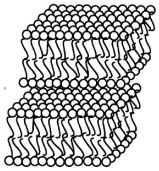

(c) Lamellar phase

Figure 4.2 Schematic illustration of observed structures [28][29]

The chapter is organized in two main sections beyond this introduction. Section 4.2 summarizes the experimental methods employed to conduct the rheological measurements. The following section (Section 4.3) presents the rheological data obtained at different concentrations, highlighting the relationship between structure and rheology.

4.2 Experimental Methods

4.2.1 Materials

The same batch of S13D samples prepared for the SAXS tests were used to obtain rheological data so as to eliminate differences caused by sample preparation. Table 4.1 summarizes the S13D solutions tested and discussed in this chapter.

Table 4.1 S13D solutions characterized using rheological tests

(a) S13D in water

Conc.(wt% total)	1	5	10	15	20	25	30	37.5	40	50	60	65	70	90	100

(b) S13D in RH brine

Conc. (wt% total)	5	10	15	20	25	30	40	50	100

(c) S13D in 17.5k

Conc. (wt% total)	1	5	10	25	30	90	100

4.2.2 Rheometer and Tests Performed

The same apparatus (Physica MCR301 rotational rheometer) and geometries (double gap coaxial cylinders and cone and plate) used to perform the tests presented in Chapter 2 was used here. Refer to that chapter for details on the apparatus. Also in this case the double gap geometry was adopted only when the viscosity of the testing material was under 10 cP, while the cone-plate geometry was used for all other tests. All tests were conducted at 24°C for consistency with the SAXS measurements.

Two types of tests were performed: shear rate ramps (with shear rate range of 1-100 s^{-1}) and oscillatory tests (amplitude and frequency sweeps). Shear rate ramp tests were conducted on the fluid samples (based on visual observation) to obtain viscosity data and oscillatory tests were performed on gel samples to characterize their viscoelastic response and gain insight on their microstructure.

Figure 4.3 shows an example of shear rate ramp tests for 20wt% S13D solution in water. The same test settings as described in 2.2.2.2 were adopted here. In the test shown

measurements were also conducted while decreasing the applied shear rate after the maximum value had been reached. The figure illustrates the consistency in the data collected during the loading and unloading ramps and represents an example of the Newtonian behavior exhibited by many of the S13D solutions at both low and very high concentrations (see more on this in Section 4.3).

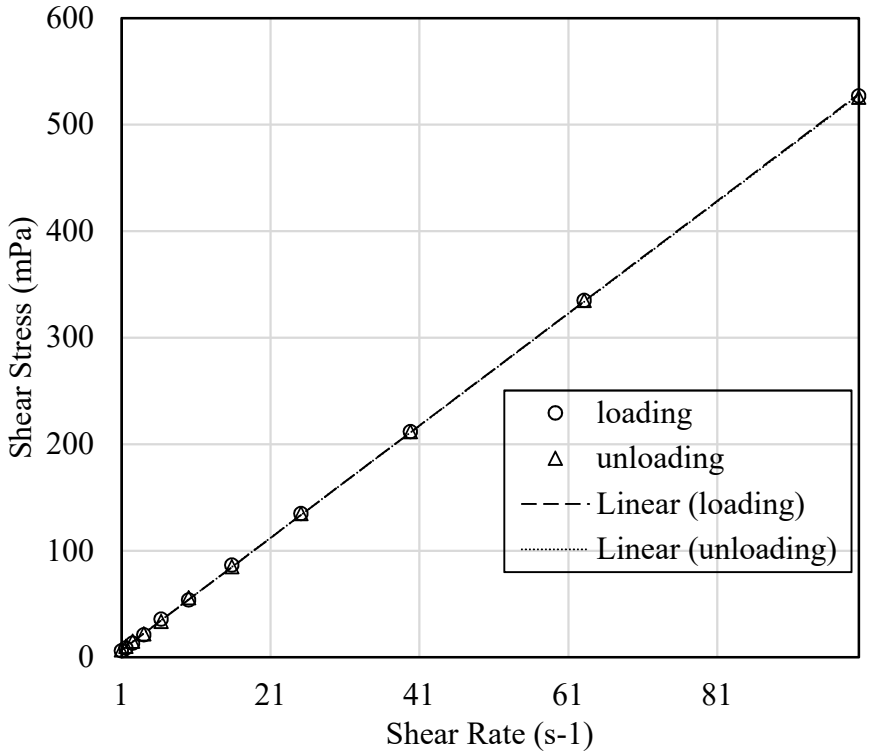

Figure 4.3 20wt% S13D in water

Oscillatory tests are conducted subjecting the specimen to a sinusoidal shear strain (or shear stress) as shown in Equation 4.1. The rheometer measures the resulting time dependent stress (or shear strain, in the case of an applies stress oscillation), which can be expressed as the sum of an elastic component in phase with the strain and a viscous component 90° out of phase with the strain (see Equation 4.2) [30].

$$\gamma = \gamma_0 \sin(\omega t) \tag{4.1}$$

where γ_0 is the maximum amplitude and ω is the angular frequency.

$$\gamma = \gamma_0 [G' \sin(\omega t) + G'' \cos(\omega t)] \tag{4.2}$$

where G' is the storage (elastic) modulus, G'' is the loss (viscous) modulus.

The loss (or damping) factor, tanδ, is defined as the ratio of the two moduli and δ, which represents the offset between the applied oscillatory strain and the measured shear stress, is termed the phase angle (see Equation 4.3). When δ equals 0° (tanδ = 0), G' >> G'', indicating purely solid/elastic behavior. When δ equals 90° (tanδ = ∞), the response is purely viscous/fluid. Phase angles of viscoelastic materials fall between 0° and 90°.

$$\tan\delta = G''/G' \quad (4.3)$$

In an amplitude sweep, the amplitude of the deformation is varied (where compatible with the torque resolution of the, a 0.01%-100% strain range was explored in all the tests presented in this chapter) while keeping the frequency constant. Storage modulus G' and loss modulus G'' are generally plotted against shear strain (or stress). See Figures 4.8 and 4.9 for examples of this representation. The presence of a region at small deformations where G' and G" are constant is indicative of linear viscoelastic response, and the application of strains within this region does not cause any disturbance the sample. This region is called linear-viscoelastic (LVE) region. Values of the shear strain to apply during frequency sweeps are chosen to fall within this region. In gels, G' is greater than G" at small shear strains, but with increasing shear strains G" eventually exceeds G'. The critical shear strain (γ_{crit}) in correspondence to which G" = G' signifies the transition to predominantly viscous behavior. The greater γ_{crit}, the greater the strain required for the solid to liquid transition to occur.

G' and G" data from amplitude sweeps can also be plotted versus applied shear stress, as shown in Figure 4.4. This representation provides an estimate of the yield stress (τ_y) as the limiting value of the LVE region, whereas the flow stress (τ_f) represents the crossover point where G' equals G'' [30].

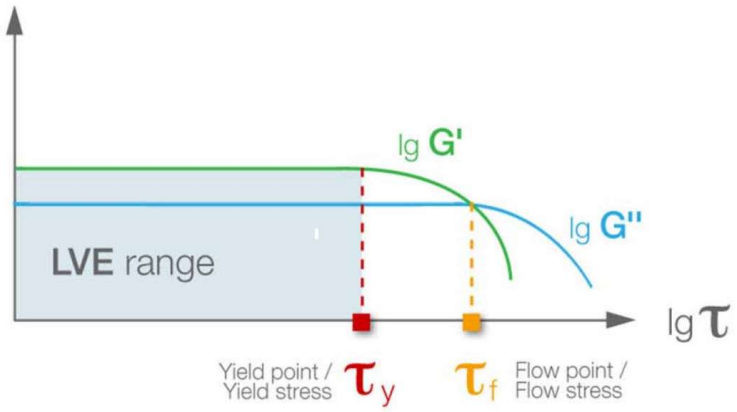

Figure 4.4 Determination of yield stress (τ_y) and flow stress (τ_f) from amplitude sweep test on a gel material (From Anton Paar)

In frequency sweeps, the frequency is varied while the amplitude of the deformation is held constant. Frequency sweeps fingerprint the viscoelastic response of a structured fluid as a function of frequency. Figure 4.5 [31] shows the general frequency dependent behavior of a structured fluid, in which five different regions, corresponding to different viscoelastic regimes, are identified. At low frequencies G”>G’ (viscous regime) and both moduli increase (transition to flow). G’ becomes greater than G” in correspondence to a material specific frequency value, ω, and the relaxation time τ corresponding to this value of ω is the longest relaxation time ($\tau_{max}=1/\omega$) of the material. It represents the characteristic time at which the material relaxes back to the equilibrium configuration after a perturbation, and is therefore a reflection of the structure of the material. As the frequency continues to increase, eventually G” once again overtakes G’ (leathery transition crossover). At very high frequencies, as the rate of increase in G” continues to exceed that of G’, the material enters the glassy regime. Depending on the material the transitions between the different regions occur at different frequencies.

tests presented in this chapter a frequency range of 0.1-100Hz was investigated where possible. As discussed in 4.3.1. with this constant range, different regions of the visco-elastic spectrum shown in Figure 4.5, are necessarily probed depending on the structure of the material.

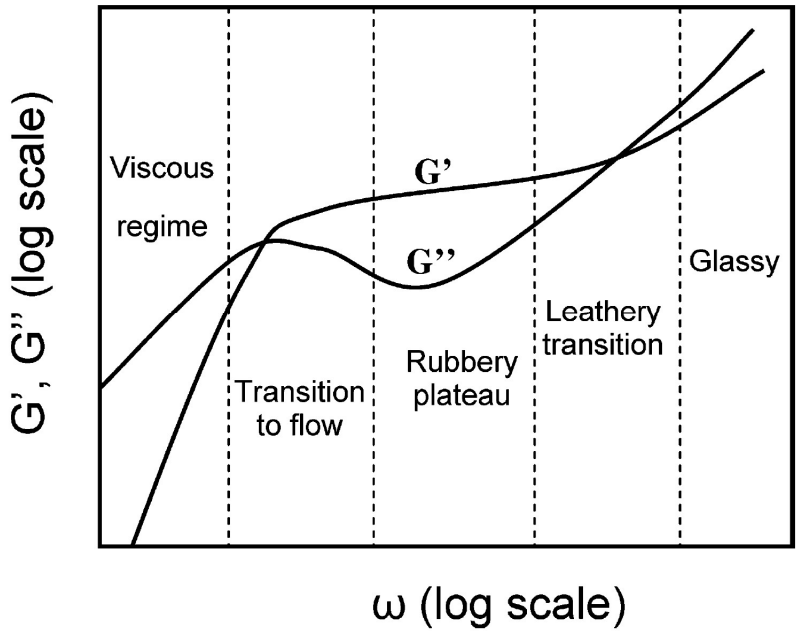

Figure 4.5 Typical viscoelastic behavior of a structured fluid [31]

4.3 Experimental Results and Discussion

Table 4.2 summarizes the testing program. In this table 'SR ramp' refers to shear rate ramp tests, while 'FS' and 'AS' are used to indicate frequency and amplitude sweep tests, respectively.

The following two subsections present the results obtained testing water and brine solutions, respectively. The presentation of the results in the following sections focuses on a subset of the tests performed. For the solutions identified by gray cells in Table 4.2, the data are not considered conclusive at this time, and are therefore not included in this thesis.

Table 4.2 Summary of rheological tests on S13D solutions (T=24°C)

S13D Conc. (wt% total)	Water	RH brine	17.5k
1	SR ramp	-	SR ramp
5	SR ramp	SR ramp	SR ramp
10	SR ramp	SR ramp	SR ramp
15	SR ramp	SR ramp	-
20	SR ramp	SR ramp	-
25	SR ramp	SR ramp	SR ramp
30	SR ramp	SR ramp	SR ramp
37.5	AS@1Hz, FS	-	-
40	AS@1Hz, FS	AS@1,10Hz	-
50	SR ramp, Top[a]-AS@1Hz, FS	SR ramp, Top-FS	-
60	AS@0.1,1,10Hz, FS	-	-
65	AS@1Hz, FS	-	-
70	AS@1,10Hz, FS	-	-
90	SR ramp	SR ramp	SR ramp
100	SR ramp		

[a] Top' refer to l (i.e. lamellar LC).

4.3.1 S13D in Water

As shown in Table 4.2, shear rate ramp tests were conducted at 24°C on 1-30wt% S13D solutions in water as well as at 90wt% and on neat S13D. The viscosity data obtained from these tests are plotted as a function of shear rate in Figure 4.6. S13D solutions with concentrations up to 20wt% and at and above 90wt% are very close to Newtonian while the 25wt% and 30wt% solutions show shear thinning behavior.

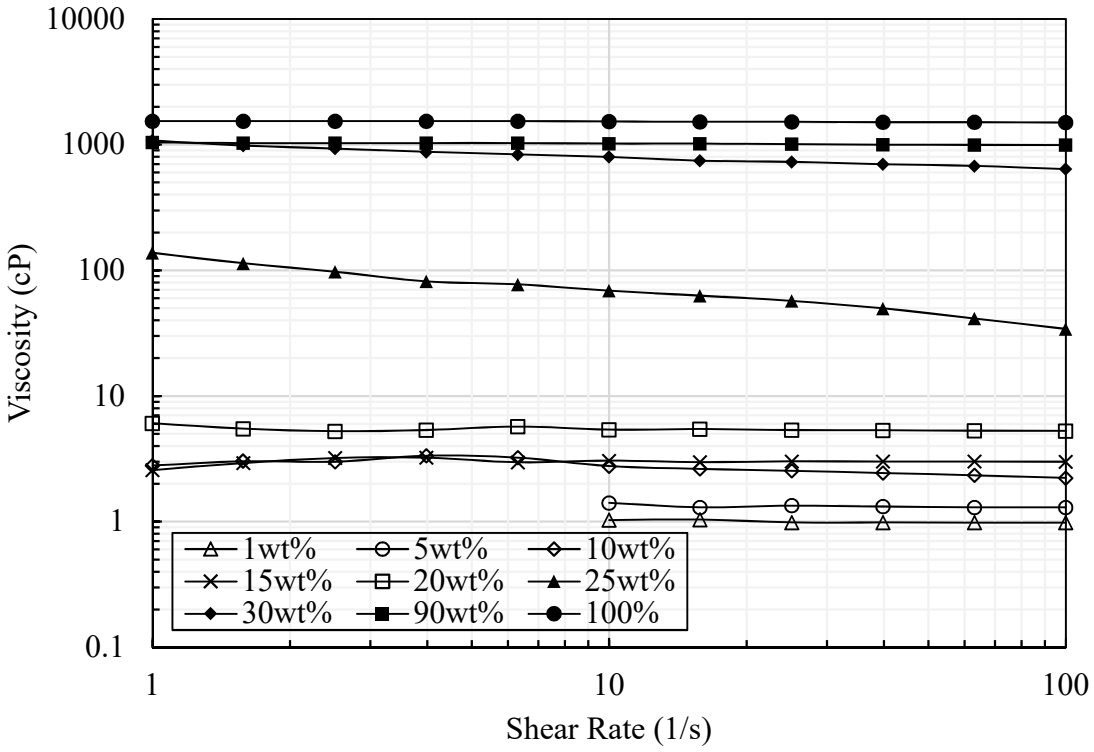

Figure 4.6 Results of shear rate ramp tests on S13D solutions in water at 24°C

To better illustrate the effect of S13D concentration, values of the viscosity measured at a shear rate of 100 s^{-1} are plotted as a function of surfactant concentration in Figure 4.8. The inset figure which focuses on the data for S13D concentrations between 1 and 25%, shows a gradual increase in viscosity up to 20% concentration. This increase reflects the increased volume fraction occupied by the micelles. Volume fraction can be estimated from the measured S13D density (1.081g/cm^3) [27] and modified using the size of S13D micelles (~3nm in diameter) [27], the hydrated radius (~0.37nm) of the hydrophilic group of S13D

(sulfate) obtained from the literature [32][33][34]. An example calculation of S13D micelles volume fraction at 10wt% (123.5mM) is as follows:

For 100g 10wt% S13D solution, volume fraction under non-hydration condition is

$$\phi_{m,non-hydration} = \frac{10g/\left(1.081g/cm^3\right)}{10g/\left(1.081g/cm^3\right)+90g/\left(0.9107g/cm^3\right)} = 0.09$$

After considering the effect of hydration, the volume fraction becomes:

$$\phi_{m,hydration} = \phi_{m,non-hydration} \times (\frac{3+0.37*2}{3})^3 = 0.17$$

As described for example by [35] the increase in viscosity can be modeled using different relationships including the generalized Einstein relation (Equation 4.4), a general empirical relationship (Equation 4.5) and the Krieger–Dougherty relation (Equation 4.6) [36].

$$\eta_r = 1+[\eta]\phi_m \tag{4.4}$$

where η_r is the relative viscosity $\eta_r = \eta/\eta_s$. η_s is taken here as viscosity of water at 24°C due to the small cmc of S13D in water; $[\eta]$ is the intrinsic viscosity which is a fitting parameter related to the particle shape, $[\eta]$=2.5 for spherical particles and $[\eta]$=3.2 for an oblate spheroid with an axial ratio of 2.0 [36].

$$\eta_r = (1-\phi_m)^{-[\eta]} \tag{4.5}$$

$$\eta_r = (1-\frac{\phi_m}{\phi_{\max}})^{-[\eta]\phi_{\max}} \tag{4.6}$$

where $\phi_{\max} = 0.64$ for a random close-packing of spheres [36].

A first attempt to model this behavior is shown in Figure 4.7 where the relative viscosity is plotted as a function of S13D concentration using the models introduced above. Lines with the same color are calculated from the same equations (i.e. Line 1,2 for Equation 4.4; Line 3,4 for Equation 4.5; Line 5,6 for Equation 4.6). $[\eta]$ is taken as 2.5 for dash lines and 3.2 for solid lines. Line 6 from Equation 4.6 with $[\eta]$=3.2 is the closest one to the measured data. At low concentrations ($\phi_m < 0.1$), only small discrepancies are observed. The

discrepancies at higher concentrations may be caused by strong interparticle hydrodynamic interactions or the effects of increasing micelle sizes [35].

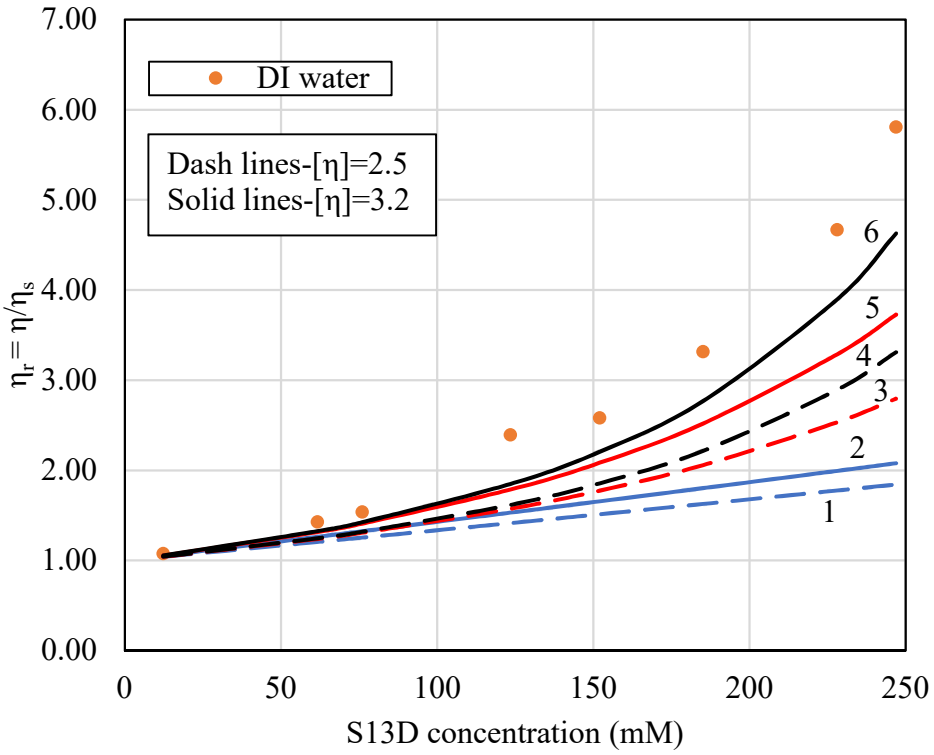

Figure 4.7 Predictions from models for S13D micelles in water

Figure 4.8 shows that beyond 20wt% there is a step increase in the viscosity, which goes from 5.29cP (20wt%) to 40cP (25wt%). This abrupt change is consistent with the SAXS results (see Figure 4.1), which indicate that at 25wt% there has been a structural transition from micellar solution to a two-phase system (micellar solution + hexagonal LC).

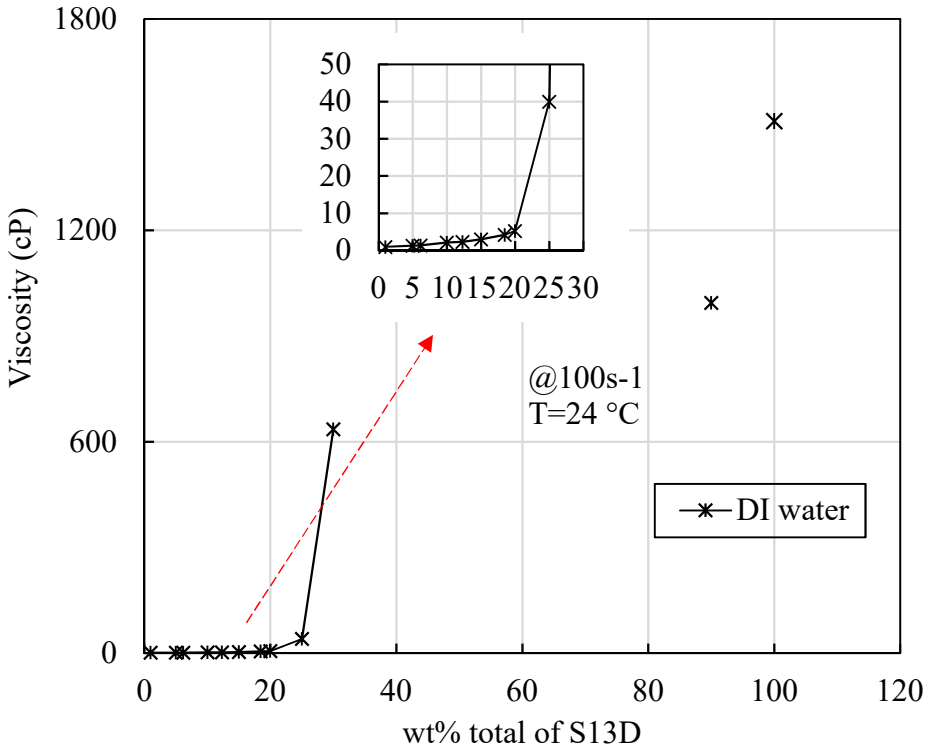

Figure 4.8 Viscosity of S13D in water at 100 s^{-1} as a function of concentration

Figure 4.9 and Figure 4.10 present results of amplitude sweep tests (performed with frequency of 1 Hz) for 40wt% S13D in water and 65wt% S13D in water, respectively. Based on the SAXS results these two solutions are considered to be representative of single phase hexagonal and single phase lamellar liquid crystals, respectively. In both cases the samples are characterized by G'>G" at small strains (viscoelastic solid); with increasing strain, G' decreases, until G'=G" (solid to fluid transition) in correspondence to a critical strain (γ_{crit}). Beyond this strain the behavior is that of a viscoelastic fluid (G'<G''). Despite these similarities, there are important differences between the 40wt% and 65wt% solutions. As summarized in Table 4.3, they pertain not only to the values of the moduli measured in the LVE region (greater for 40wt%), but more importantly to the corresponding value of the phase angle, which is ~ 6° for 65wt% (close to elastic behavior) versus ~ 36° for 40wt%. This indicates that despite being "softer," the lamellar liquid crystal exhibits more elastic behavior compared to the hexagonal liquid crystal. Figure 4.9 and Figure 4.10 also show a significant difference in the critical strain, ~ 14% for 65wt% versus ~ 1.5% for 40wt%. This indicates that the lamellar liquid crystal can sustain a larger deformation before flowing.

Figure 4.11 shows an example of the determination of yield stress (τ_y) and flow stress (τ_f) for 65wt% S13D in water. The limit of the LVE region was identified in correspondence to a 5% deviation in the value of G'. Yield stress (τ_y) and flow stress (τ_f) data for this gel are compared to those for the 40wt% solution (and other solutions) in Table 4.3. The relationship between the measured values of τ_y and τ_f are consistent with the above observations on the values of the moduli and of the critical strain.

Table 4.3 summarizes data at 1Hz for three additional solutions. Based on SAXS results, the first (37.5wt%) represents another example of hexagonal LC, while the other two (60wt% and 70wt%) are lamellar liquid crystals. In general, these data confirm the observations made above (e.g. higher G', G" and δ in LVE and lower γ_{crit} in hexagonal LC compared to lamellar LC).

For the two hexagonal liquid crystals, the data also indicate a decrease in the values of G' and G" measured in the LVE region at 1Hz, an increase in the corresponding value of δ, as well as a decrease in γ_{crit} and a reduction in the size of the LVE region, with increasing surfactant concentration. For the lamellar LC the data are less clear (sample variability appears to be an issue for some of these materials). However, the data suggest that an increase in concentration is associated with an increase in G', G" and δ in the LVE region, and a decrease in γ_{crit} (all data at 1Hz).

Finally, it should be noted that for any material, the behavior observed in an amplitude sweep is frequency dependent. As a result, before conducting a frequency sweep, amplitude sweeps should be conducted at different frequencies. An example of this is provided in Figure 4.12 and Figure 4.13 which show results of amplitude sweeps on a 70wt% S13D solution in water at 1Hz and 10Hz. Note that, despite the different values of G' and G" (which reflect the frequency dependent response of the material – see more on this below), at both 1 and 10Hz the LVE region exceeds 0.1% strain. This justifies the use of this value of strain in frequency sweeps. Similar observations were made for the other solutions and a strain of 0.1% was selected for all frequency sweep tests.

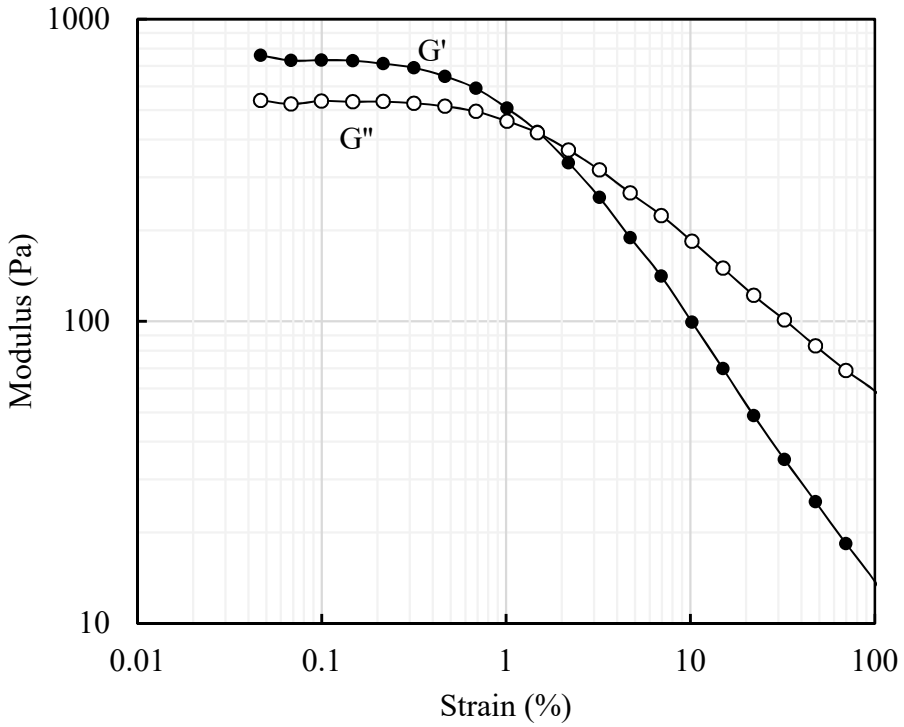

Figure 4.9 Results of amplitude sweep on 40wt% S13D in water (f=1Hz)

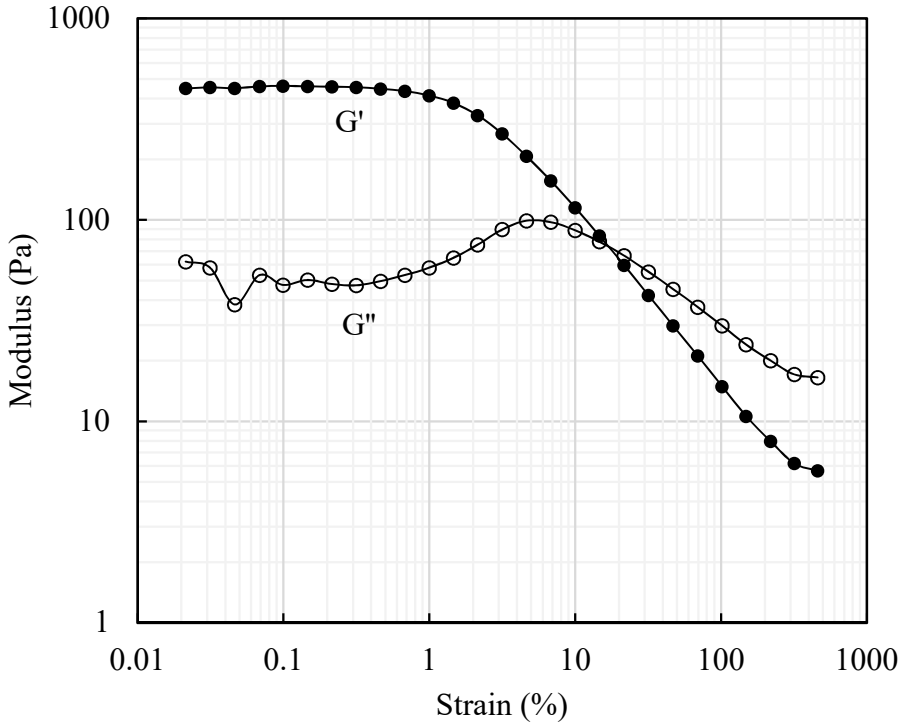

Figure 4.10 Results of amplitude sweep on 65wt% S13D in water (f=1Hz)

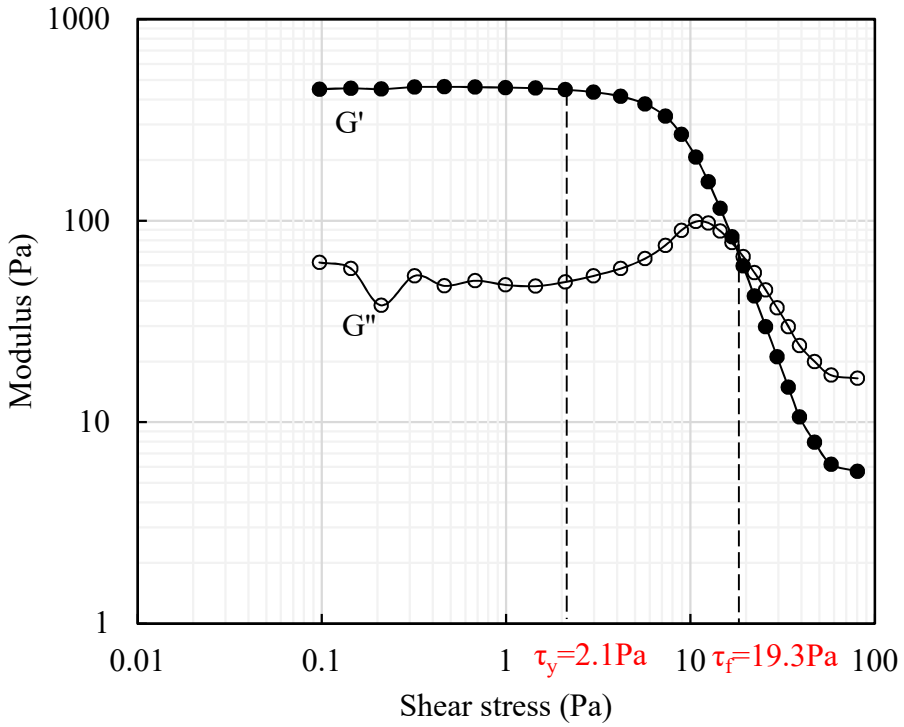

Figure 4.11 Derivation of yield stress (τ_y) and flow stress (τ_f) from results of amplitude sweep on 65wt% S13D in water (f=1Hz)

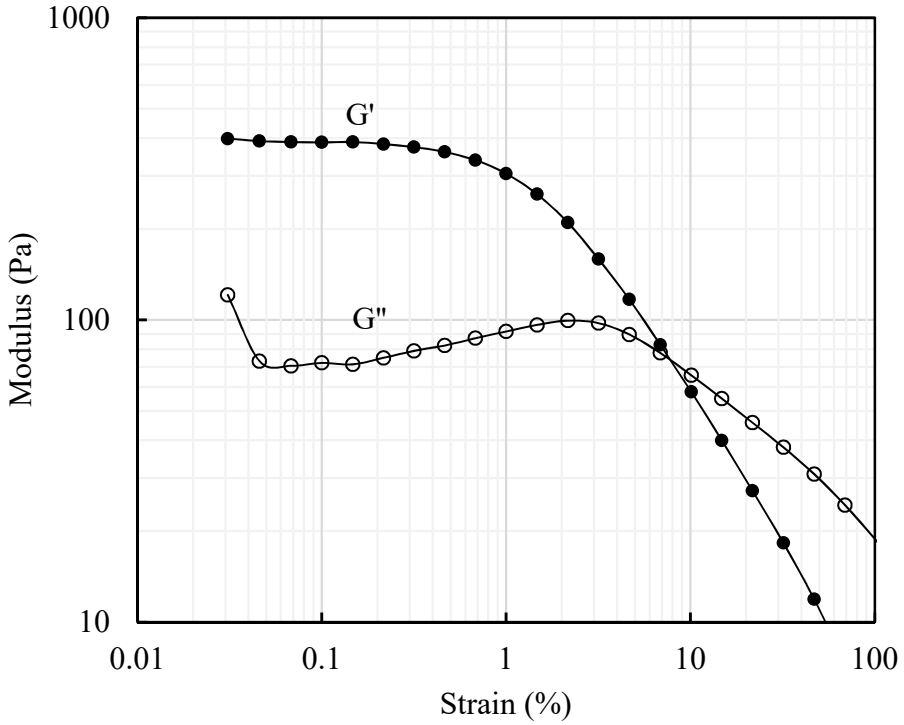

Figure 4.12 Results of amplitude sweep on 70wt% S13D in water (f=1Hz)

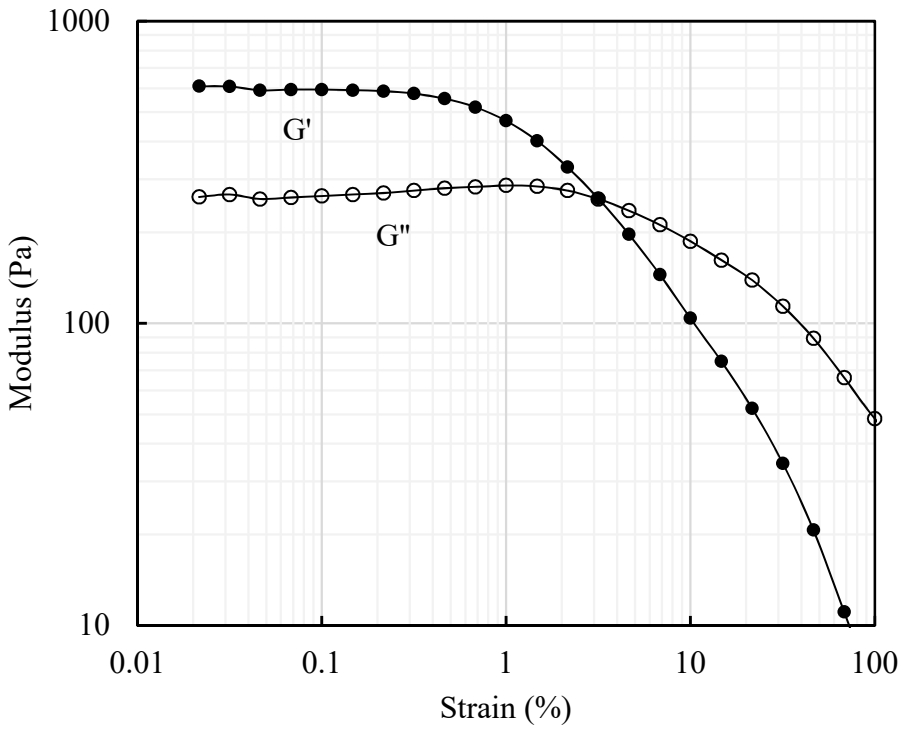

Figure 4.13 Results of amplitude sweep on 70wt% S13D in water (f=10Hz)

Table 4.3 Summary of select results from amplitude sweeps performed at 1Hz

S13D Conc.(wt%)	37.5	40	60	65	70
G' (Pa)-LVER	1600	729	231	460	390
G" (Pa)-LVER	680	533	24	48	70
δ (°)-LVER	23	36	6	6	10
τ_y (Pa)	10.7	2.8	2.2	2.1	1.2
τ_f (Pa)	32.4	8.9	12.0	19.3	8.0
γ_{crit} (%)	7	1.5	21.7	14	7.5

Figure 4.14 shows G' and G'' as a function of frequency for the hexagonal phase of 40wt% S13D in water at 24 °C. G' dominates over most of the frequency spectrum with increasingly elastic behavior as G' increases more rapidly than G'' (phase angle δ goes from 53° to 28°). The response corresponds to the transition to flow region shown in Figure 4.5. A crossover at about 0.1Hz is observed which corresponds to a relaxation time on the

order of 1.5 s. In general, the behavior is consistent with that reported in the literature for hexagonal liquid crystals (e.g. see [31]).

Distinct frequency response is observed for the 65wt% and 70wt% S13D solutions in water (see Figure 4.15 and Figure 4.16), both lamellar liquid crystals based on the SAXS results. Although G' still dominates over a large frequency spectrum, eventually G'' exceeds G'. This behavior corresponds to leathery transition regime described in Figure 4.5. For both solutions, a low-frequency crossover is not observed over the examined frequency range, indicating that it occurs at a much lower frequency (i.e. at a very long relaxation time). Again, the behavior is consistent with data reported in the literature for lamellar liquid crystals (e.g. [31]).

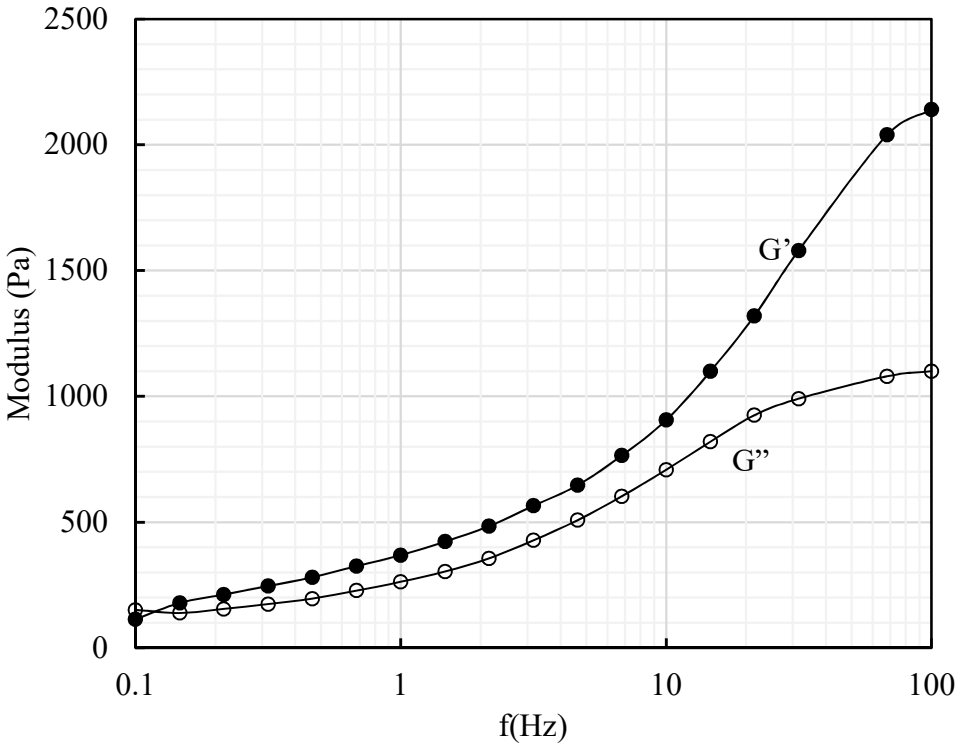

Figure 4.14 Results of frequency sweep on of 40wt% S13D in water (γ=0.1%)

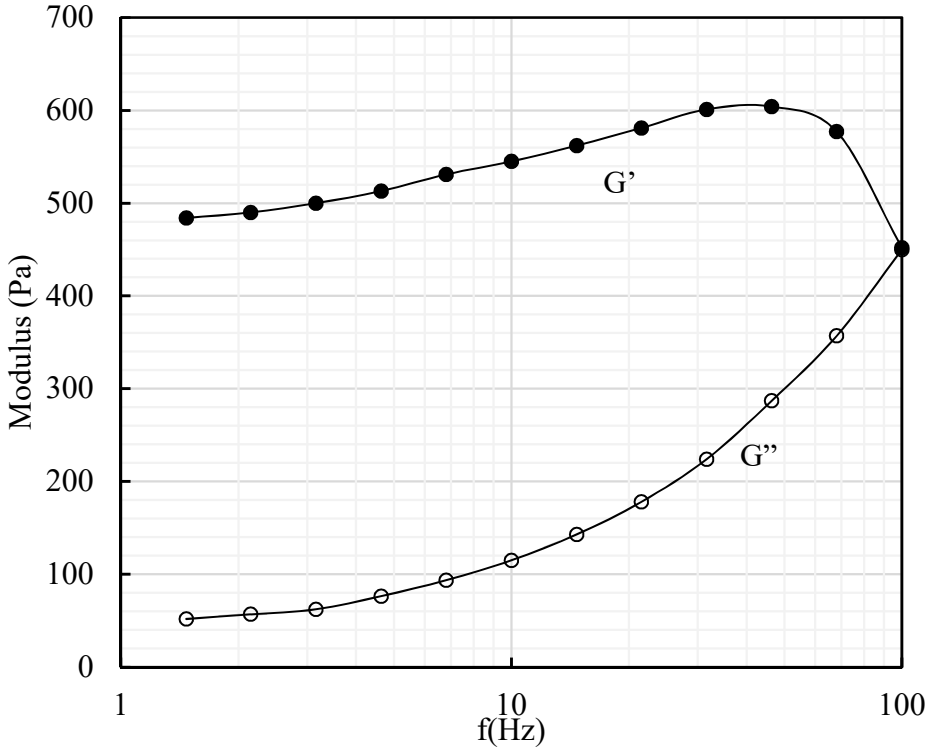

Figure 4.15 Results of frequency sweep on 65wt% S13D in water (γ=0.1%)

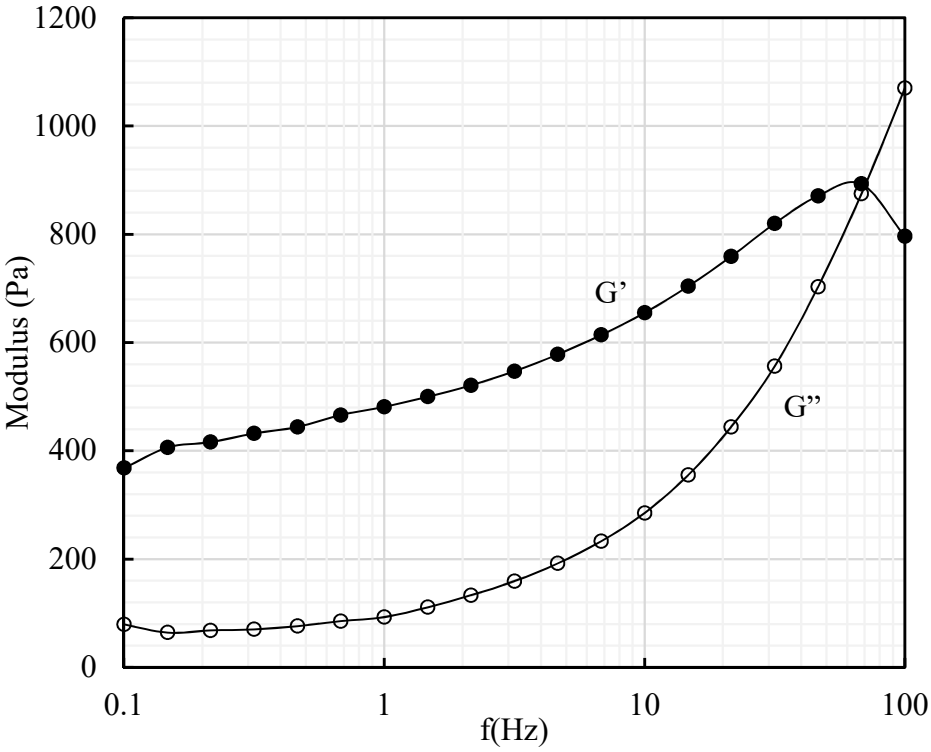

Figure 4.16 Results of frequency sweep on 70wt% S13D in water (γ=0.1%)

4.3.2 S13D in Brines

As some of the tests for brine samples are still in progress, just part of the results for S13D solutions in RH brine and 17.5k are presented here (see Table 4.2). Figure 4.17 and Figure 4.18 show the outcome of shear rate ramp tests performed on S13D solutions in RH brine and 17.5k at 24°C, respectively. For RH brine, S13D solutions with concentration up to 25wt% show Newtonian or close to Newtonian behavior (change in viscosity over the shear rate range examined <10%). Beyond 25wt%, the behavior is Non-Newtonian with the viscosity first increasing and then decreasing (for 30wt% the viscosity exceeds that of the 40wt% solution at all shear rates). No data were collected for highly concentrated solutions in RH brine.

For 17.5k brine, all tested solutions are Newtonian. Also in this case the the viscosity first increases continuously (up to 25wt%) and then decreases (compare data for 25wt% and 30wt%). For 17.5k a shear rate ramp was performed on a 90wt% S13D solution. The resulting viscosity values are close to those obtained at 25wt% (and slightly higher than the viscosity of 90wt% solution in water – see Figure 4.19).

Figure 4.19 summarizes viscosity data at a shear rate of 100 s^{-1} as a function of S13D concentration for all three salinities. As seen for the solutions in water, for each of the two brines the viscosity shows an early gradual increase with increasing surfactant concentration. As above, the rapid step increase in viscosity seen in the figure inset is thought to represent a structural transition, which occurs at 20wt% for RH brine and 10wt% for 17.5k, compared to 25wt% in water, indicating that with increasing salinity the structural/phase transition is shifter to lower surfactant concentrations.

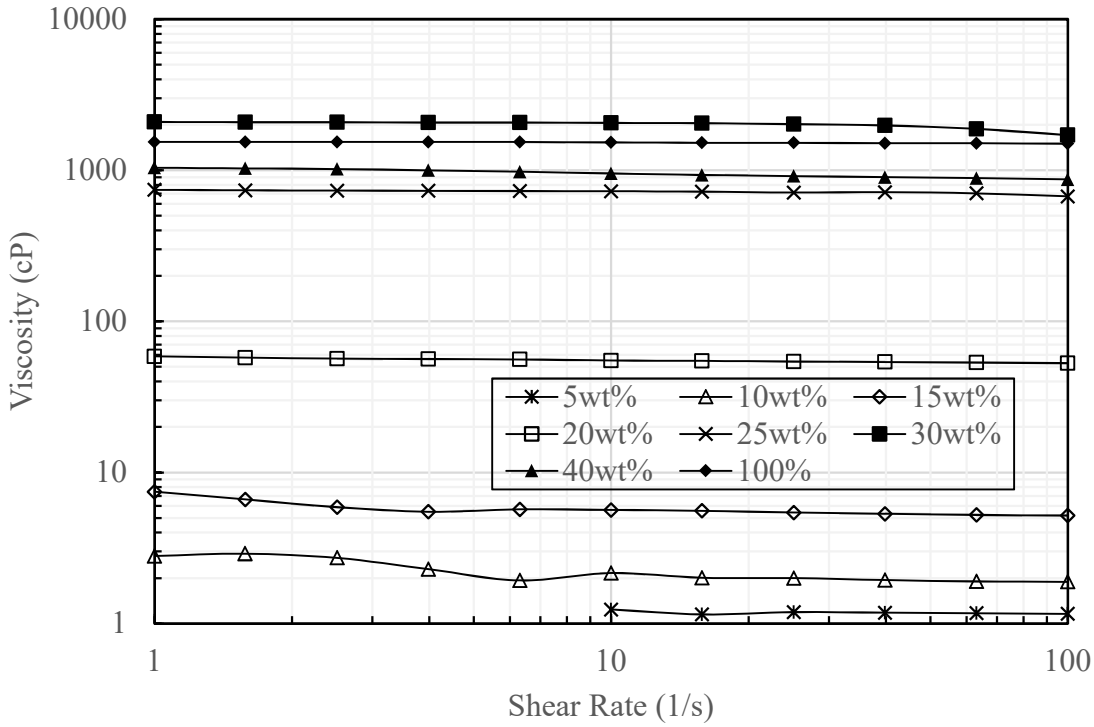

Figure 4.17 Results of shear rate ramp tests on S13D solutions in RH brine at 24°C

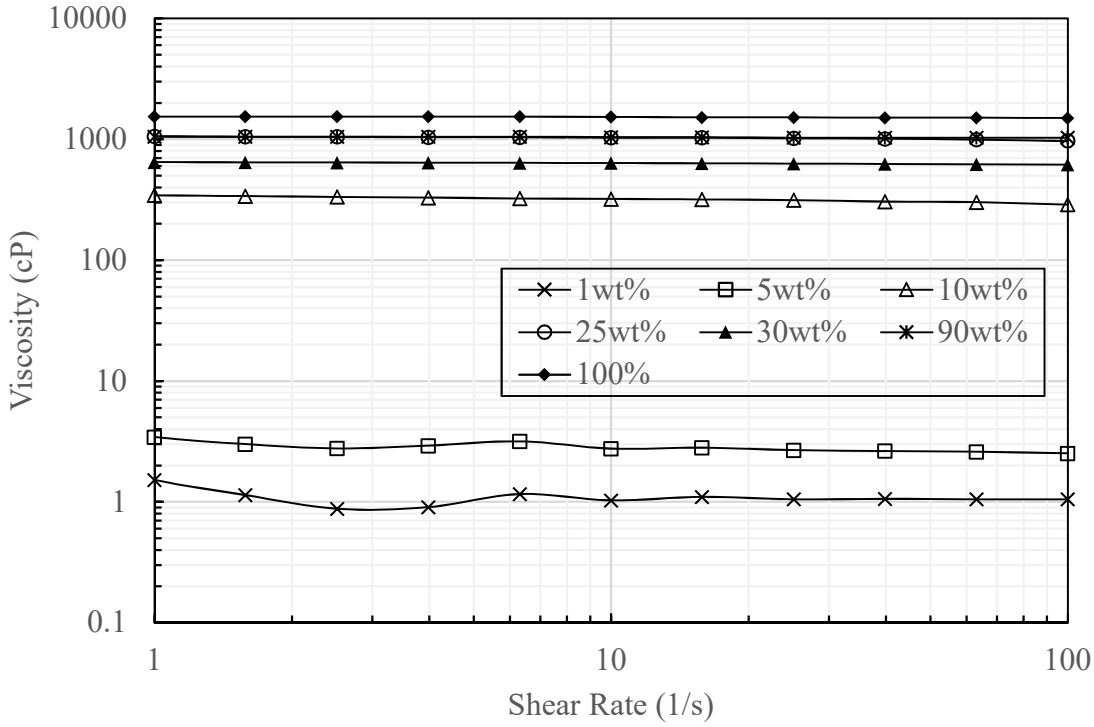

Figure 4.18 Results of shear rate ramp tests on S13D solutions in 17.5k brine at 24°C

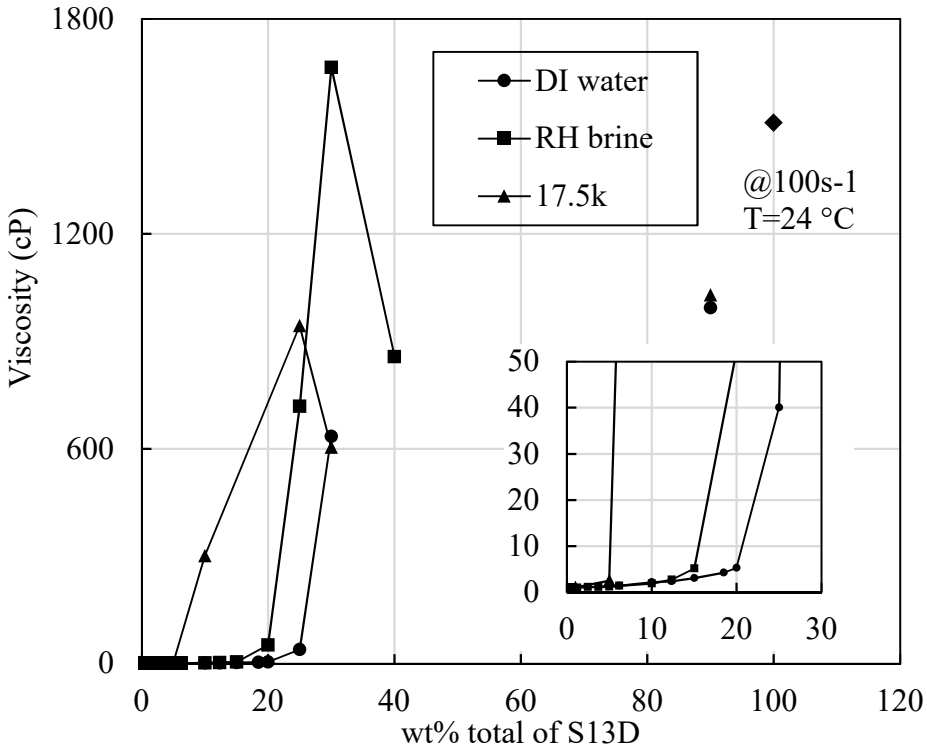

Figure 4.19 Viscosity of S13D in water, RH and 17.5k brines at 100 s^{-1}

5. CONCLUSIONS AND RECOMMENDATIONS

5.1 Introduction

This thesis presents work performed as part of a broader research effort, funded by Pioneer Oil, aimed at developing and implementing a chemical EOR solution at the Pioneer Rock Hill site in Southern Indiana. As detailed in the previous chapters, the contributions by the author of this research to this effort came in three areas: rheological measurements in support of slug design; core-flood (CF) test data analysis; and study of the rheology of water and brine solutions of the primary surfactant (S13D). Section 5.2 of this chapter provides a brief summary of the work and the conclusions drawn from the results. Recommendations for future research work are provided in Section 5.3.

5.2 Summary and Conclusions

5.2.1 Rheological Measurements in Support of Slug Design and Site Operations

This portion of the experimental program investigated the rheology of surfactant, polymer and surfactant-polymer solutions as a function of shear rate, using the Physica MCR 301 rotational rheometer available in the Rheology Lab of Purdue's Lyles School of Civil Engineering. The effects of the following variables were examined: concentration (up to 0.5wt%) and type (Flopaam 3230S and 3330S) of the HPAM polymer; concentration (up to 3wt%) and type (S13D, the primary surfactant, used alone or in combination with a co-surfactant and a co-solvent), temperature (4-35°C), water chemistry (DI water, Rock Hill [RH] original and synthetic brine), salinity (up to 22,000 ppm). The results furnish a clear picture of the role played by these factors on solution viscosity, and, in some cases provide insights that have direct relevance to the design of the formulation for the Rock Hil reservoir, and of the handling/mixing/pumping operations at the site. Specifically:

a) The behavior of all surfactant formulations examined is Newtonian, with an over 7 fold difference between the value of S13D alone (highest viscosity) and that of the 7:2:2 mixture of S13D with a co-surfactant and a co-solvent. This applies at all temperatures examined.

b) For all neat surfactants, the viscosity shows significant temperature dependence with an over threefold increase in viscosity going from 25°C to 4°C. This indicates that increased challenges in mixing and pumping the surfactants are to be expected during the winter months at the Rock Hill site. Depending on the conditions, thermal insulation of the surfactant storage and mixing tanks may be required.

c) All polymer solutions examined (500-5000 ppm) show shear thinning behavior, with viscosity controlled by the concentration. For both polymers examined, the increase in viscosity with polymer concentration is well described by a second order polynomial equation.

d) Salinity has a very significant effect on the viscosity of polymer solutions. For all polymer solutions examined, the viscosity at any shear rate is found to decrease with increasing salinity due to a charge shielding mechanism. HTDS (17.5k-22k salinity) conditions, which, based on the phase behavior studies, maximize the efficiency of the chemicals injected, can cause 20-30% decrease in viscosity of polymer solution compared to measurements at RH salinity. This indicates that higher polymer concentrations will be required for mobility control, leading to an increase in the cost of the chemical slug.

e) The viscosity of polymer solutions is also affected by temperature. For the temperature range expected in the reservoir (18°C to 24°C) the data show a 7-15% variation in viscosity for all polymer solutions over the range of shear rates (0.1-1000 s^{-1}) examined.

f) Tests performed on 0.2-0.5wt% 3330S solutions prepared using original RH brine show data consistent (<10% difference over the shear rate range of 0.1 to 1000 s^{-1}) with those of solutions prepared with the synthetic RH brine (which was used for the majority of the tests performed in this experimental program). This demonstrates that the data obtained in this study are directly relevant to field conditions and can continue to be employed in the experimentation. One issue remains unresolved, and that is the effect of the presence of iron, in the form of Fe^{2+} in the Rock Hill reservoir. Iron, which is known to affect polymer stability, was not included in the synthetic RH brine, and precipitated in the original RH brine

samples used for the tests. This issue requires further research, as discussed in the recommendations.

g) All surfactant solutions examined in this part of the research (concentrations up to 3wt%) exhibit close to Newtonian behavior with very small values of viscosity (< 1.3 cP). For surfactant concentrations relevant to cEOR formulations (≤1wt% active), the viscosity of polymer-surfactant solutions is controlled by the polymer alone at both RH salinity and HTDS (with a less than 5% reduction in the viscosity caused by the surfactant).

h) Measurements performed on a 0.35wt% polymer solution both immediately after mixing and after over 7 months of storage shown no changes in viscosity. The stability of the polymer solutions over this time scale is of practical significance as the the duration of the flow process of the slug through the reservoir is expected to last several months.

i) At high salinity (18k-22k) and surfactant (S13D) concentrations (≥ 2%wt%A), a significant increase in the viscosity of the surfactant solutions relative to RH salinity is observed. In particular, with 3wt%A S13D, the viscosity of 0.3wt% 3330S at 22k reaches a value 3 times greater than that measured in RH brine. This increase in viscosity appears to be related to structural/phase changes of the surfactant solution. This effect may play a role in determining the rheological response of the middle phase that is observed to form in the interaction between some surfactant solutions and crude oil.

5.2.2 Analysis of Purdue Core Flood Data

The second part of the research work involved the analysis of data obtained from core flood tests and effluent analysis of 14 core flood tests conducted in Purdue's EOR laboratory between November 2015 and March 2017. 13 of these tests were performed utilizing Berea sandstone cores, with the fourteenth providing the first data for Rock Hill core. The core flood tests on Berea core examined the impact of a number of aspects related to the composition of the surfactant-polymer (SP) and polymer (P) slugs, including slug chemicals used, viscosity of SP and P slugs, size, surfactant concentration, polymer

concentration and salinity of the SP slug. As stated earlier, the author of this thesis was involved exclusively in the organization and the analysis of select data. One key component of the analysis was to select, in collaboration with Pioneer, the following five parameters (and the target values that must be met for the cEOR process to be technically and economically feasible in the field) to be used for assessing the performance of any test: recovery factor in terms of %ROIP (>75%), oil saturation after chemical flooding (S_{orc}<10%), maximum injection pressure drop during chemical flooding (<1.5 psi/ft), surfactant sorption (<0.2 mg/g) and total injectant cost per barrel (<$15).

Key conclusions derived from this work can be summarized as follows:

a) The Purdue Berea CF tests show generally consistent pre-chemical flooding conditions, making this reference material well suited to investigate the relative effectiveness of different chemical formulations. The higher value of the initial water flood oil saturation, S_{orw} (~43%) compared to that of the Rock Hill site (~25%), suggests, however, that the recoveries measured on Berea core may represent an upper bound, and that the conditions for oil recovery may be more challenging in the reservoir core. Note that this effect is likely compounded by other differences between the two core materials, including the presence in the RH core of clay minerals.

b) For the different formulations examined in the testing program, a broad range in the performance parameters is observed (e.g. ROIP from 32% to 85%; surfactant sorption from 0.05 to 0.44 mg/g); cost per barrel from $11.4 to $27.5), reflecting the impact of many different factors. In particular:

   - Higher oil recoveries (as measured by high values of ROIP% and low values of S_{orc}) are associated with higher SP slug size, higher surfactant concentration, larger slug viscosity, and optimal salinity.
   - Surfactant sorption increases with increasing surfactant concentration and is affected by SP slug salinity. As a note, two of the three highest surfactant sorption values were measured in the tests that yielded the highest recovery.
   - Slug viscosity (which depends on polymer concentration and molecular weight) as well as the variables that control oil saturation in the core

affect the maximum pressure differential, with the highest values of dP measured in the three tests with the highest residual oil saturation (and lowest ROIP%).

c) With regard to the design of the SP slug, the results of the Berea CF tests indicate that:
   - The single surfactant solutions have inferior performance in terms of oil recovery compared to formulations involving a surfactant and a co-surfactant. Of the two primary surfactants considered in this study, S13D provides the most encouraging results when used alone.
   - The highest values of oil recovery are attained using S13D in combination with a co-surfactant (A6) and a co-solvent (L4-2).
   - Salinity adjustment is found to be essential to maximize the effectiveness of the injected chemicals, with the optimal SP slug salinity estimated at 17,500 ppm.

d) In three of the core flood tests performed, four of the five performance parameters exhibited values better or close to the target values. The most difficult performance metric to meet is the limitation on the pore pressure differential (above target value in all tests reported in this thesis). This remains a challenge to be addressed.

e) A comparison to data reported in the literature for 54 core flood tests performed under similar conditions (temperature and chemical slug salinity) indicate that in terms of tertiary oil recovery, the Purdue Berea CF data fall at the mid to high end of the range of the literature data.

f) In the only test performed using the reservoir core, oil recovery was found to be significantly lower than in the test on Berea core conducted using the same formulation. Additionally, although surfactant sorption was low, the total injectant cost of $32.2 per barrel of recovered oil was the highest of any of the tests performed and well outside the acceptable range, and the maximum pressure drop across the stack was also amongst the highest measured. This suggests that increased challenges are to be expected in recovering oil from the reservoir core.

5.2.3 Rheology of S13D Solutions

The last portion of the research involved rheological measurements on S13D solutions in DI water and two different brines (RH brine with 9.4 TDS and 17.5k brine), over a range of concentrations, up to neat solutions. These data were collected to support SAXS (Small-angle X-ray scattering) observations performed by the chemical engineering group of the Purdue EOR research team led by Professors Franses and Boudouris. In combination with the SAXS results, the rheological study was aimed at understanding the phase diagram of S13D, the primary surfactant used in this research. As discussed earlier, such an understanding is critical to several aspects of chemical EOR including development of slug formulations, preparation of surfactant flooding solutions, and interpretation of the behavior of phases that may form after injection of the slug in the rock formation.

This portion of the experimental program was performed in the Rheology Lab of Purdue's Lyles School of Civil Engineering, using a Physica MCR 301 rotational rheometer. Shear rate ramp tests were conducted on the fluid samples (based on visual observation) to obtain viscosity data, while oscillatory tests (amplitude and frequency sweeps) were performed to characterize the viscoelastic response of gel samples and gain insight on their microstructure. Frequency sweeps probed the 0.1-100 Hz spectrum. All tests were performed at 24°C.

The main conclusions from this work can be summarized as follows (note that since the testing program on the brine solutions is still underway the focus here is on the solutions in DI water):

a) The surfactant solutions in DI water exhibit distinct rheological responses depending on surfactant concentration. Specifically:
   - S13D solutions with concentrations up to 20wt% exhibit Newtonian behavior, with viscosity increasing with surfactant concentration. This increase reflects the increased volume fraction occupied by the micelles in the micellar solution.

- Beyond 20wt%, there is a step increase in the viscosity that suggests the occurrence of a structural transition. 25wt% and 30wt% solutions show shear thinning behavior.
- In gels formed at 37.5-40wt%, G' dominates over most of the frequency spectrum with increasingly elastic behavior as the frequency increases. A crossover at about 0.1Hz is observed which corresponds to a relaxation time on the order of 1.5 s. In general, the behavior is consistent with that reported in the literature for hexagonal liquid crystals.
- Distinct frequency response is observed for the 60-70wt% S13D solutions. While G' still dominates over a large frequency spectrum, eventually G'' exceeds G'. A low-frequency crossover is not observed over the examined frequency range, indicating a very long relaxation time. This behavior is consistent with data reported in the literature for lamellar liquid crystals.
- Data collected at 1Hz indicates that compared to the gels formed at 37.5-40wt%, at this frequency these gels exhibit lower values of the moduli and of the phase angle (more elastic response) in the LVE region, lower yield stress, and larger γ_{crit} (greater deformation required for solid to liquid transition).
- At 90wt% the solutions exhibits close to Newtonian behavior with viscosity approaching that of the neat surfactant.
- Two phase systems are formed at intermediate concentrations. Their characterization remains to be completed.

b) The boundaries corresponding to the transitions in rheological behavior as well as the types of structures identified through the rheological data are consistent with SAXS observations. In particular:
   - The step increase in viscosity observed at 25wt% aligns with the SAXS results which indicate the transition from micellar single phase solution

to two coexisting phases (micellar solution and hexagonal liquid crystal).

- SAXS result confirm the formation at of the two types of liquid crystals (hexagonal liquid crystal and lamellar liquid crystal) identified around 40wt% and 65wt% through the frequency sweeps.

c) Salinity affects the formation of the different phases, their rheological properties and the concentrations corresponding to their boundaries.

5.3 Recommendations for Future Research Work

The research performed for this thesis addressed three distinct areas relevant to the design of a chemical EOR formulation for the Pioneer Oil Rock Hill site. As a result, the scope of the work was limited and many opportunities for continued research remain. Some recommendations for future work, based on the key insights derived from the work performed, and challenges that remain to be addressed are discussed in the three sub-sections below.

5.3.1 Rheological Measurements in Support of Slug Design

a) In this research, rheological measurements were conducted on limited combinations of chemicals. Future work should consider expanding the viscosity parametric study to other materials of interest.

b) Iron, which is known to be present in the original RH brine, was not included in the synthetic RH brine. In the field, iron potentially poses a significant threat to polymer stability, and the impact of its presence on the behavior of polymer and polymer-surfactant solutions should be carefully evaluated.

c) To date, the rheological testing program on the polymer and polymer-surfactant solutions focused exclusively on viscosity measurements. Future work should examine elasticity effects on polymer behavior and assess their potential impact on mobility design.

d) Phase behavior studies indicate the formation, for some surfactant-oil-salinity combinations of a middle phase. It is reported by other researchers that this phase may be characterized by higher viscosity, thus impacting flow of the slug in the reservoir. The characterization of the rheology of this middle phase should be a focus of future work.

5.3.2 Purdue CF Data Analysis

Future work on the analysis of existing and future CF data should be aimed at maximizing the insights that can be gained from these lengthy and complex tests. In particular:

a) The work presented in this thesis focused primarily on the analysis of select summary performance parameters. Additional work is required to fully analyze the breakthrough curves and excess pore pressure development data generated form the individual tests. Such an analysis appears critical to obtain a better understanding of the chemical EOR process and to support modeling work.

b) When possible, the CF data should be integrated with forensic post test analyses of the cores. This would provide the research team with additional insights on test efficiency and directions to optimize the formulation.

c) The process of collecting CF data from the literature should continue to further expand the database against which the Purdue CF data can be evaluated.

d) Finally, it is recommended that in all future CF tests, measurements of pore pressure be routinely conducted at all ports along the core.

5.3.3 Rheology/structure study of surfactant phase diagram

a) The work performed to date in this area focused primarily on solutions of S13D in DI water. To better serve the overall goal of the Purdue EOR research team, it is of interest not only to complete the work on the brine (RH and optimal

salinity) solutions, but also to extend the study to the surfactant mixture selected for field trial, and to the selected surfactant-polymer combinations.

b) The work on S13D solutions in DI water should also be expanded to examine the variation in properties observed as a function of concentration within the single phases (e.g. the hexagonal and the lamellar liquid crystals).

c) In addition to experimental work, future research should address modeling of the viscosity and viscoelastic data, so as to infer additional structural information (e.g. shape of the micelles formed in the micellar solution, characteristic length scales of liquid crystals) in support of the SAXS measurements.

APPENDIX -BREAKTHROUGH CURVES OF PURDUE CF TESTS

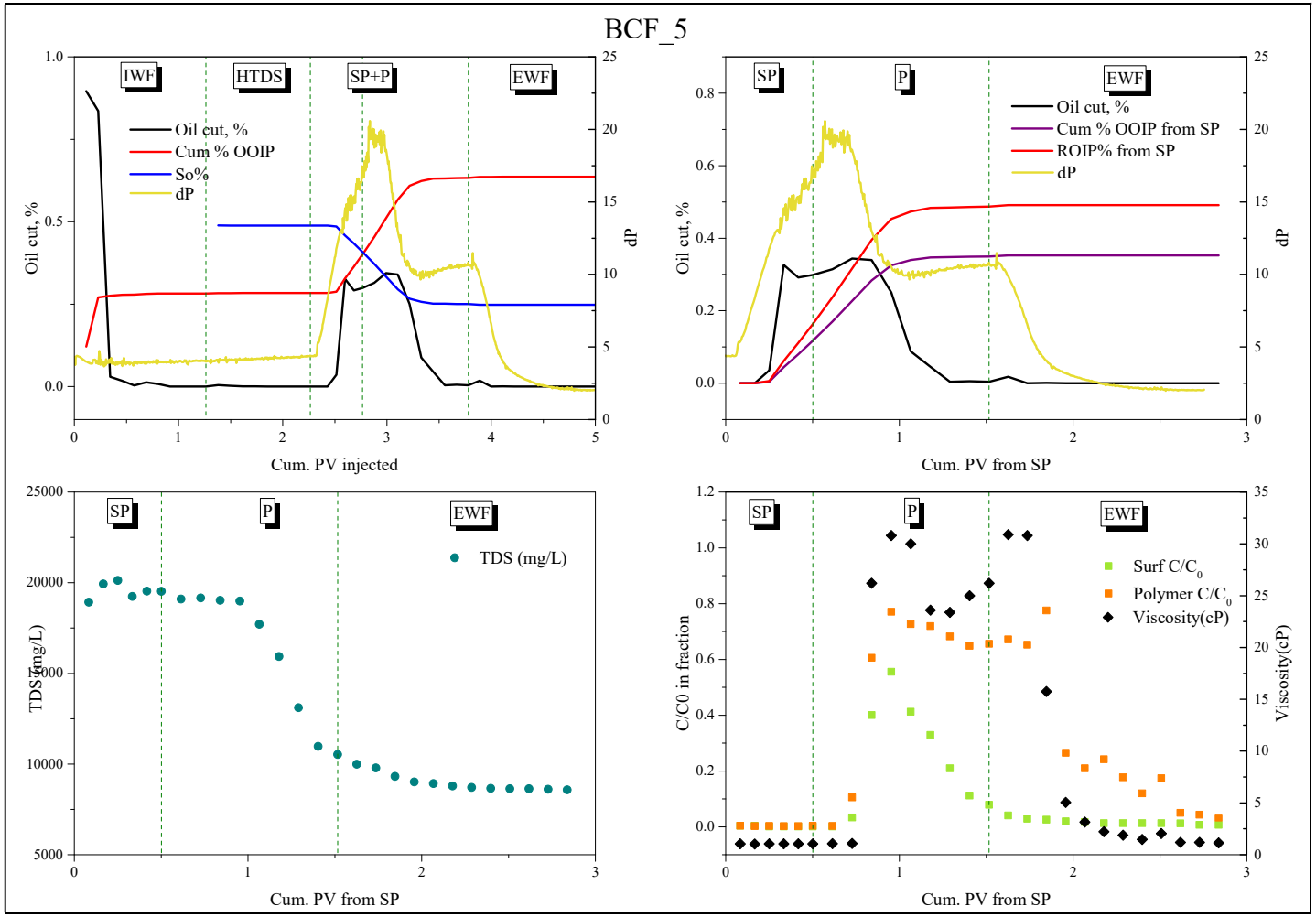

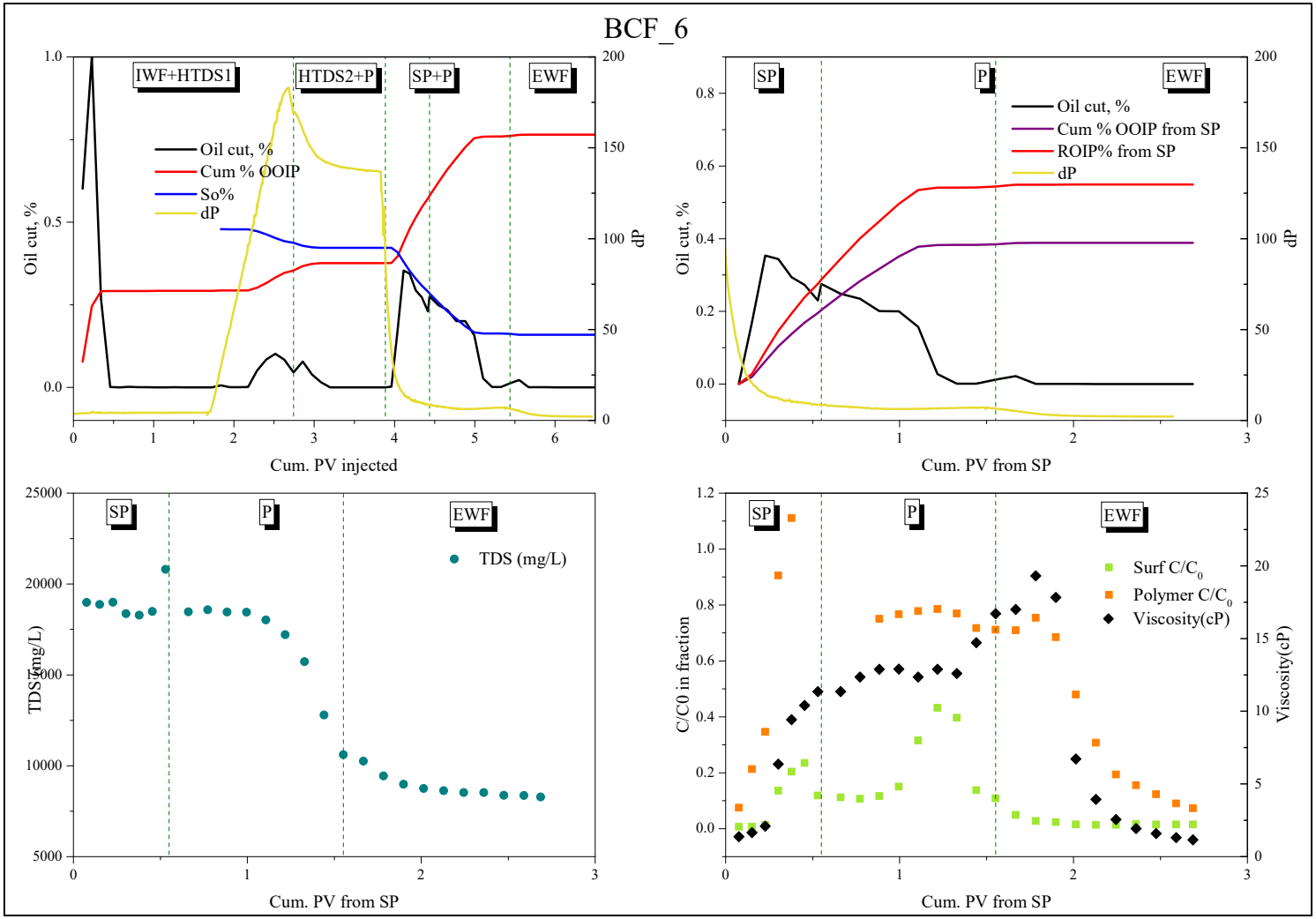

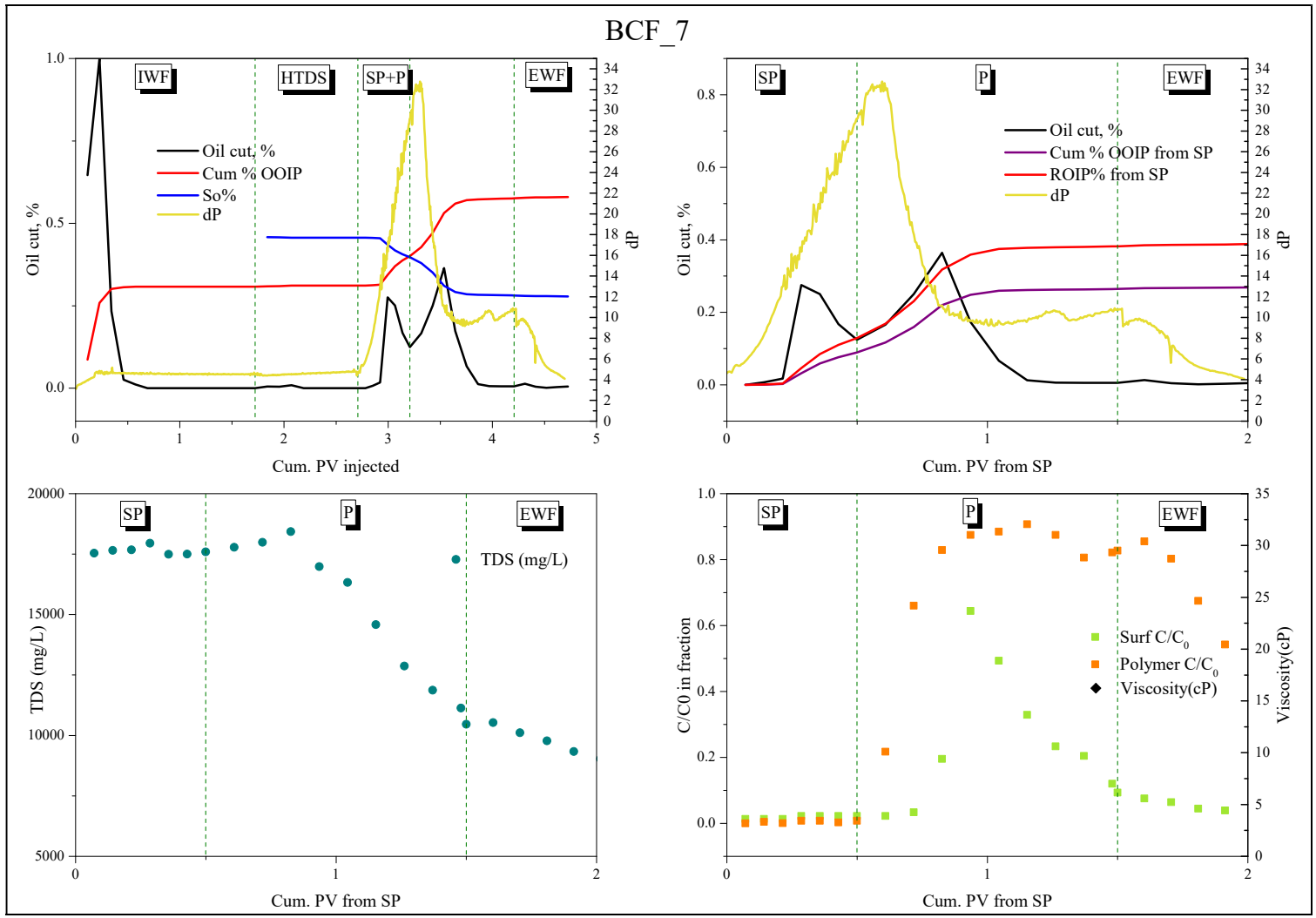

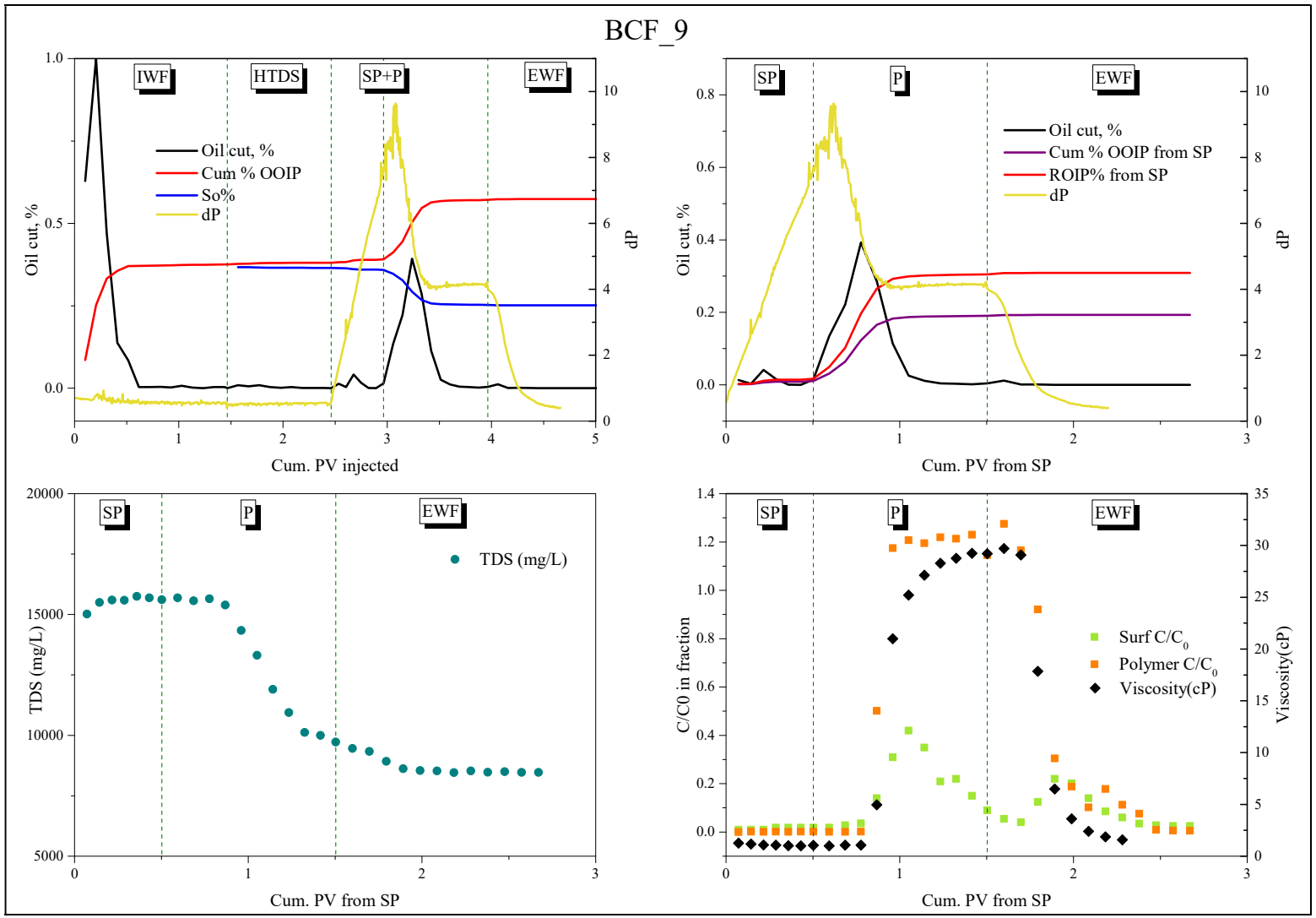

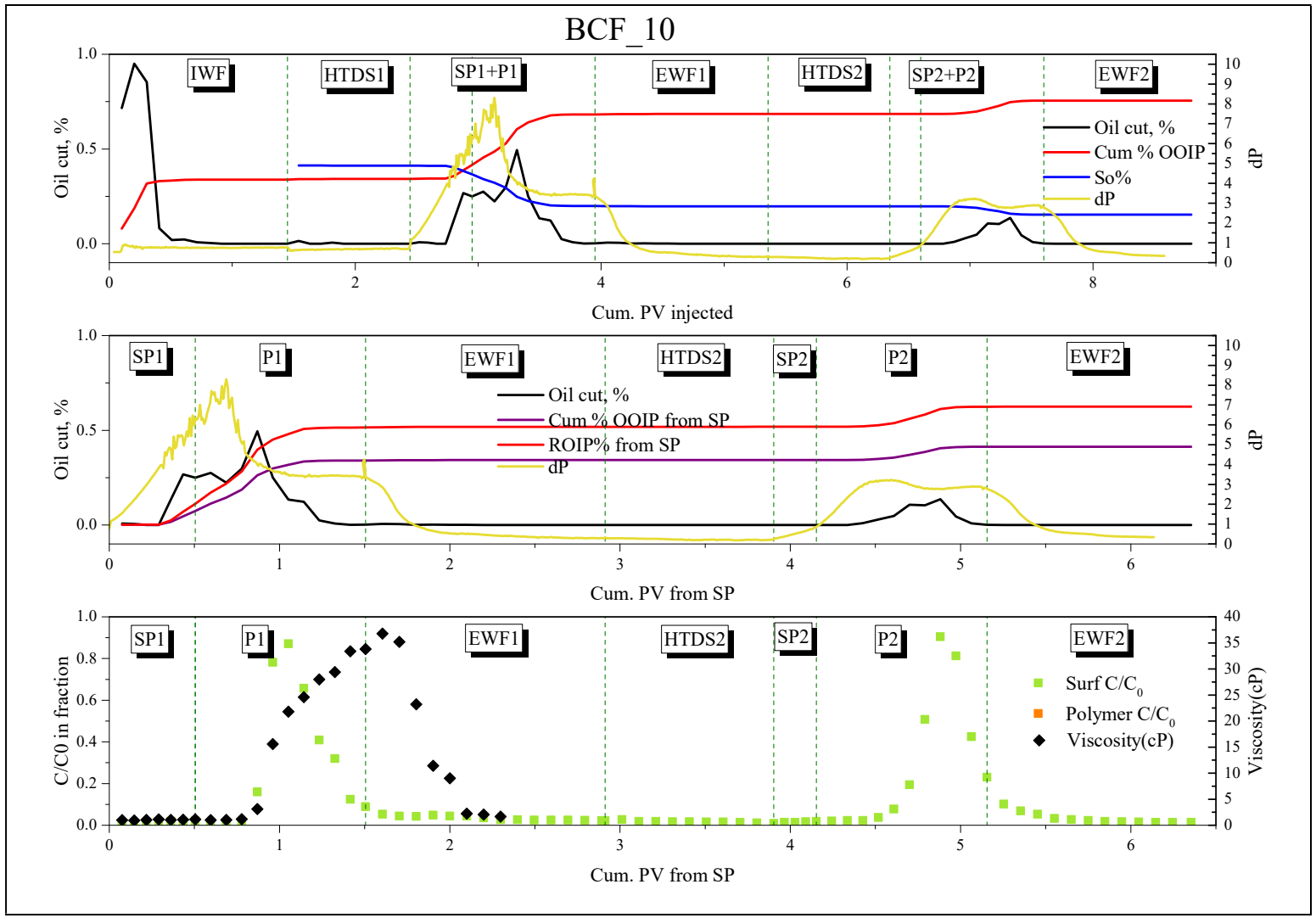

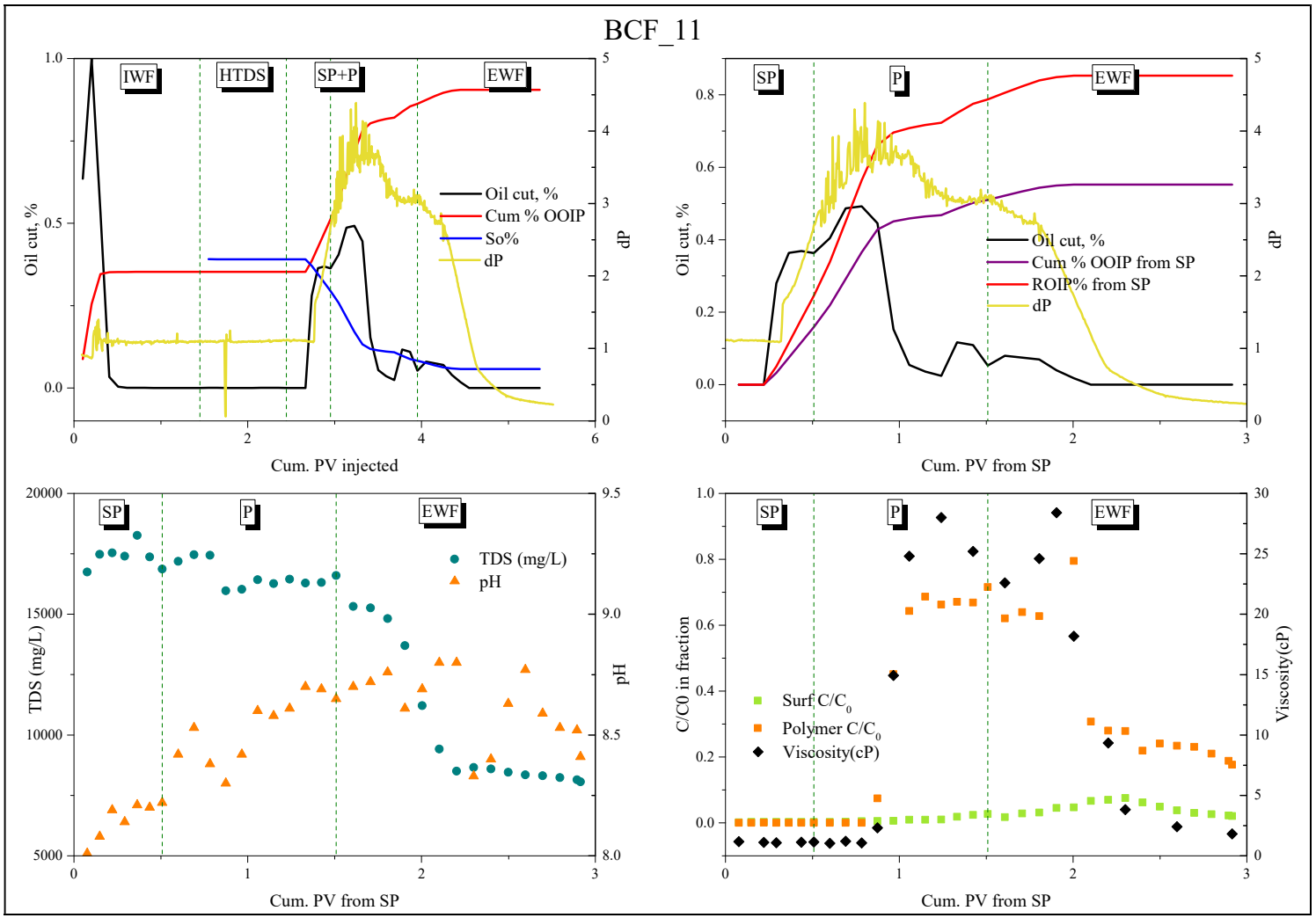

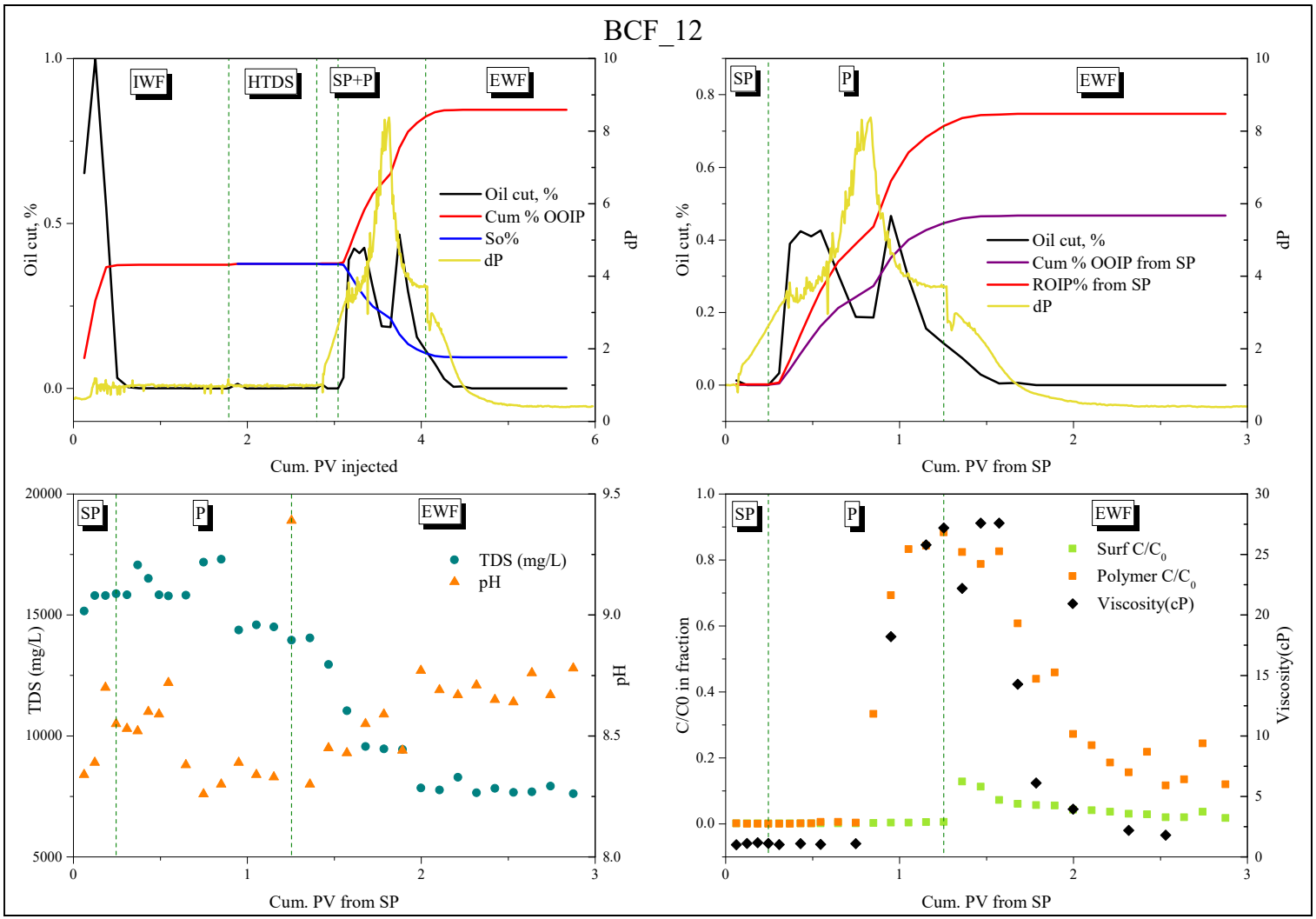

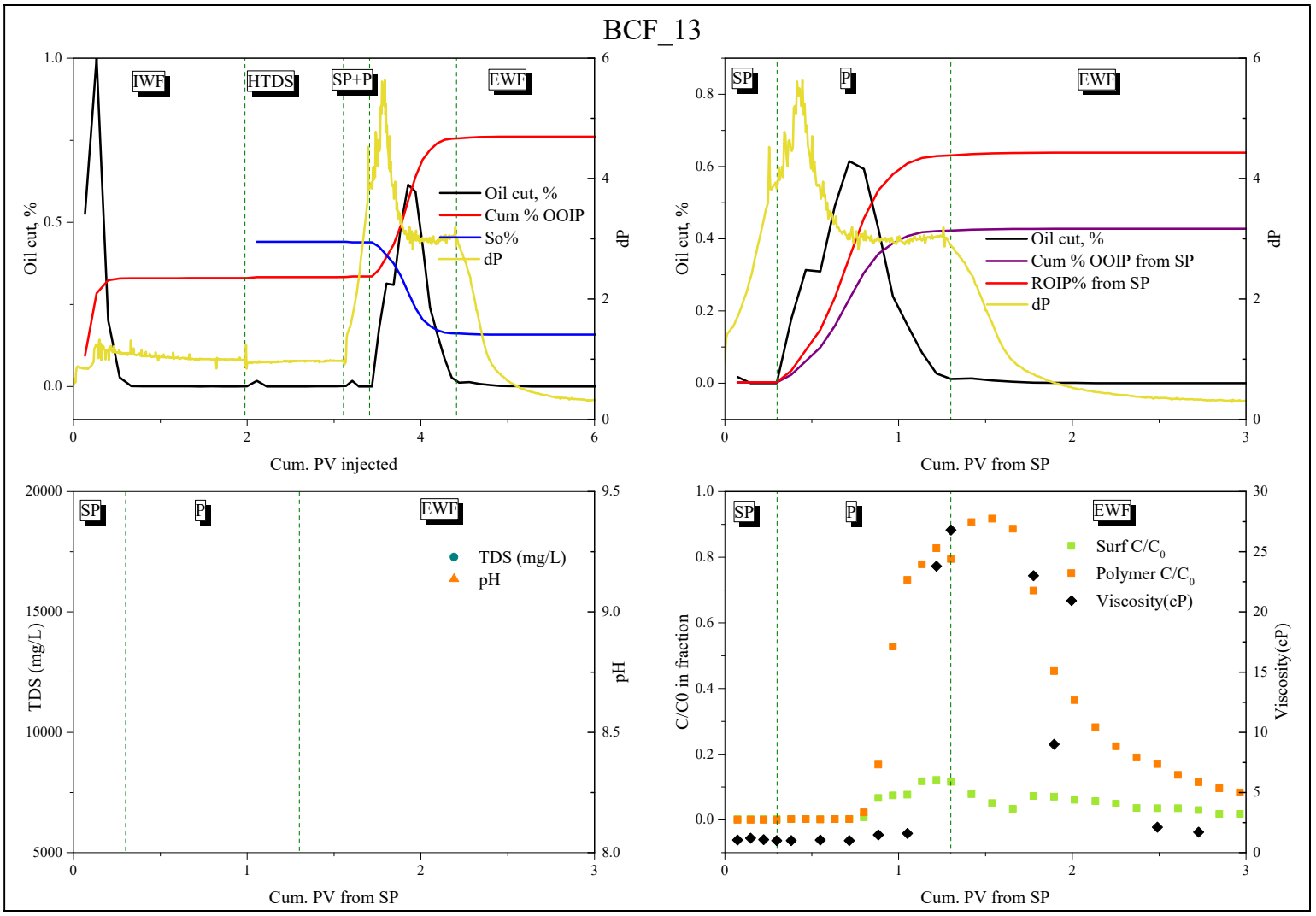

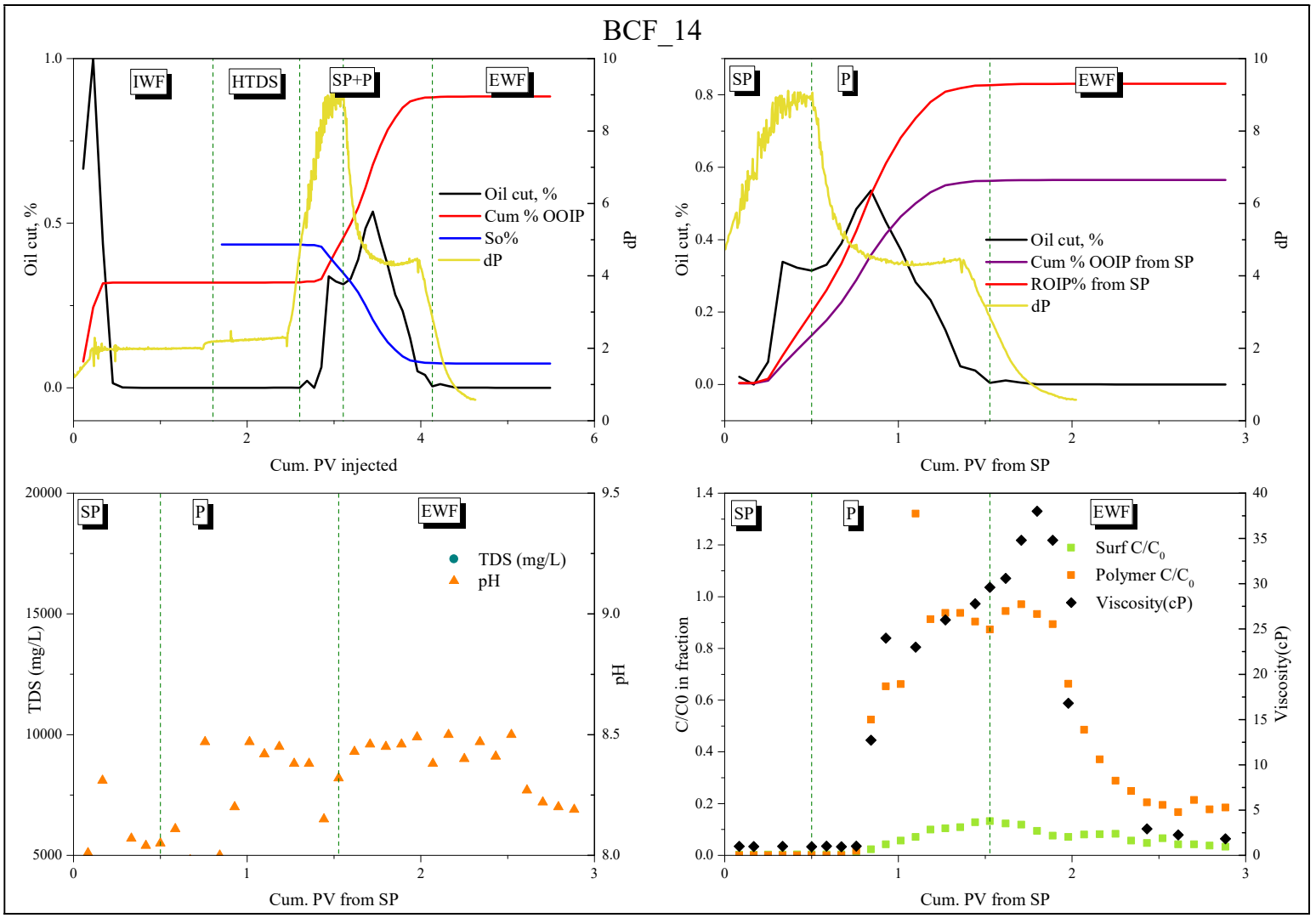

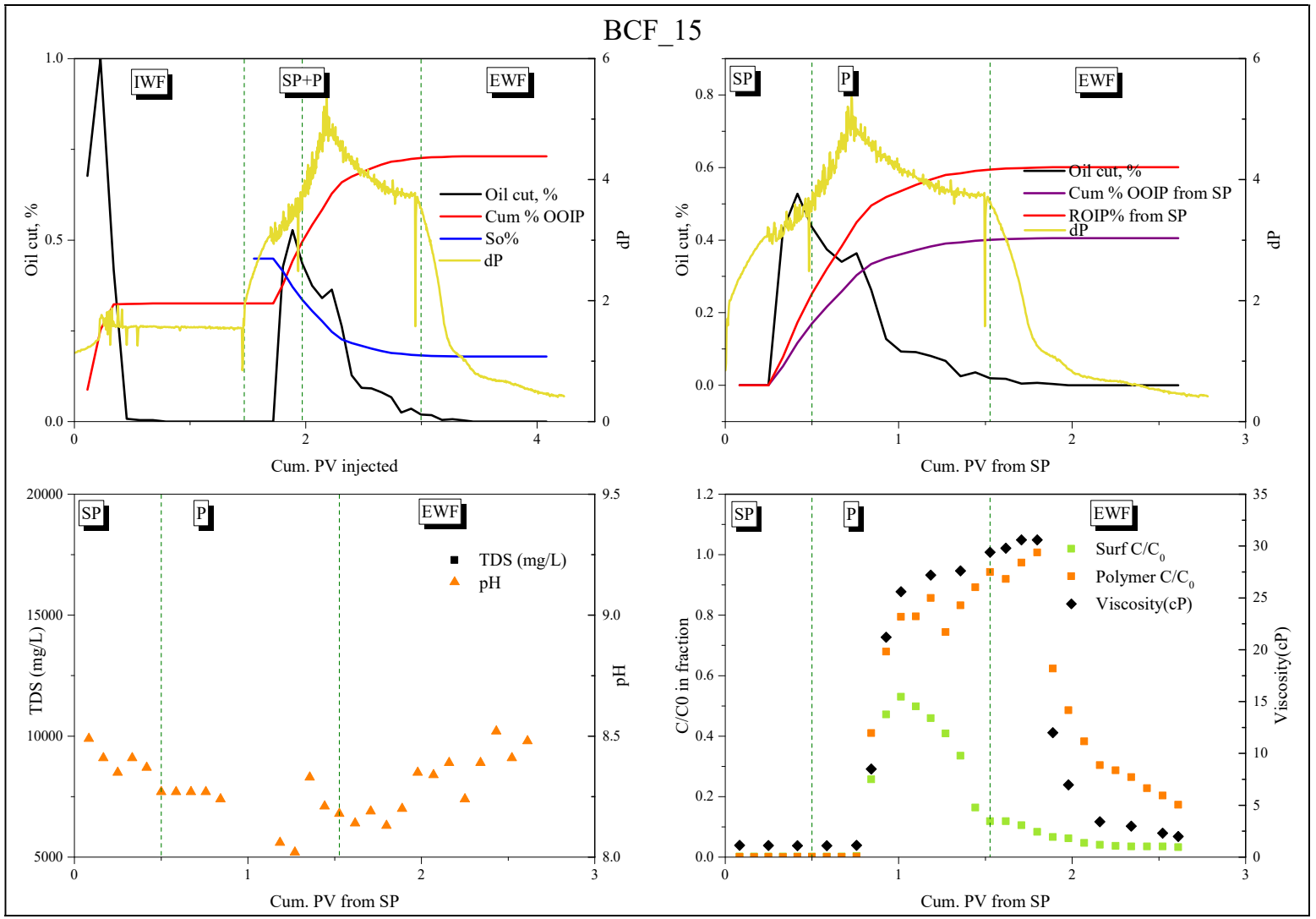

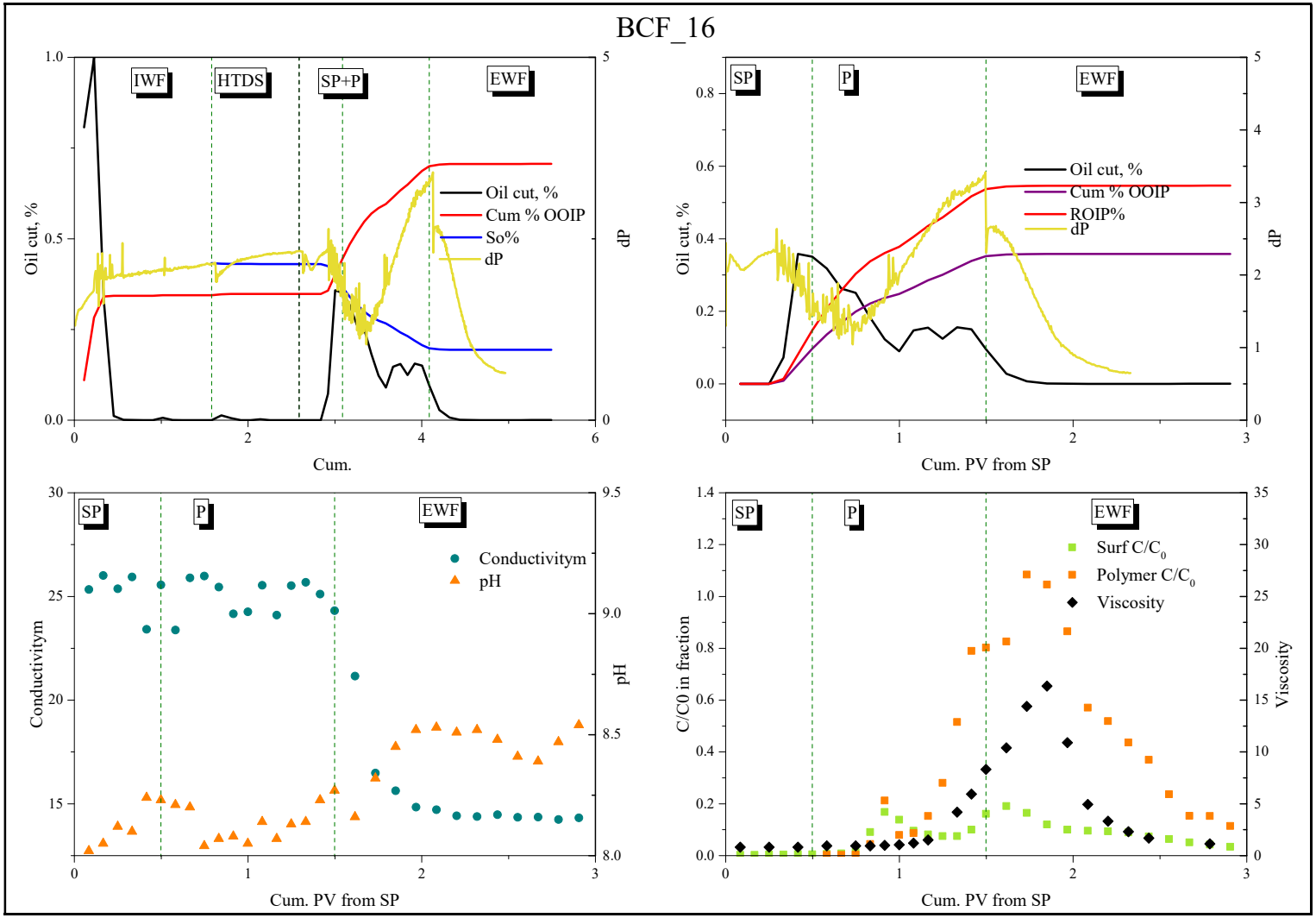

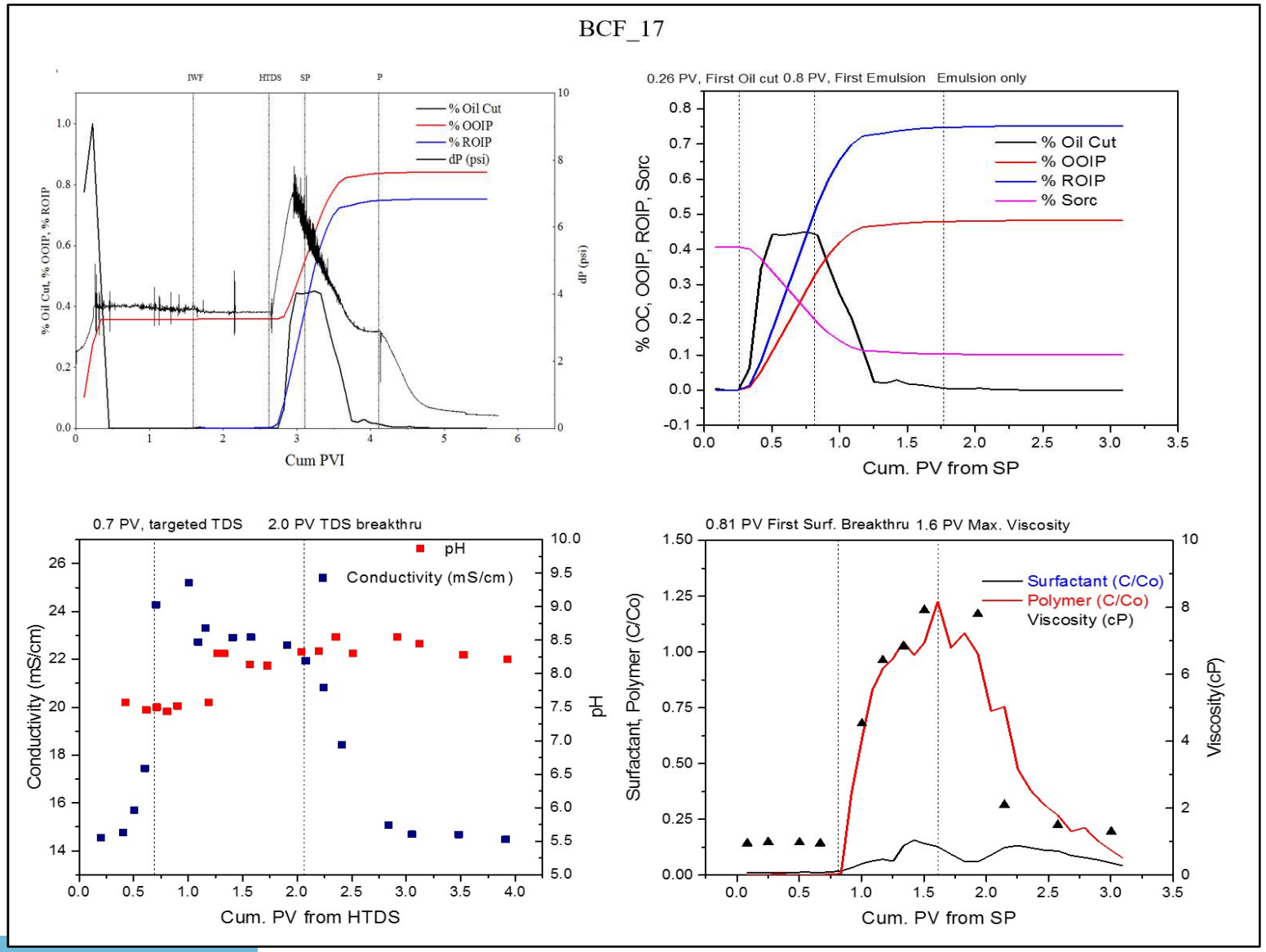

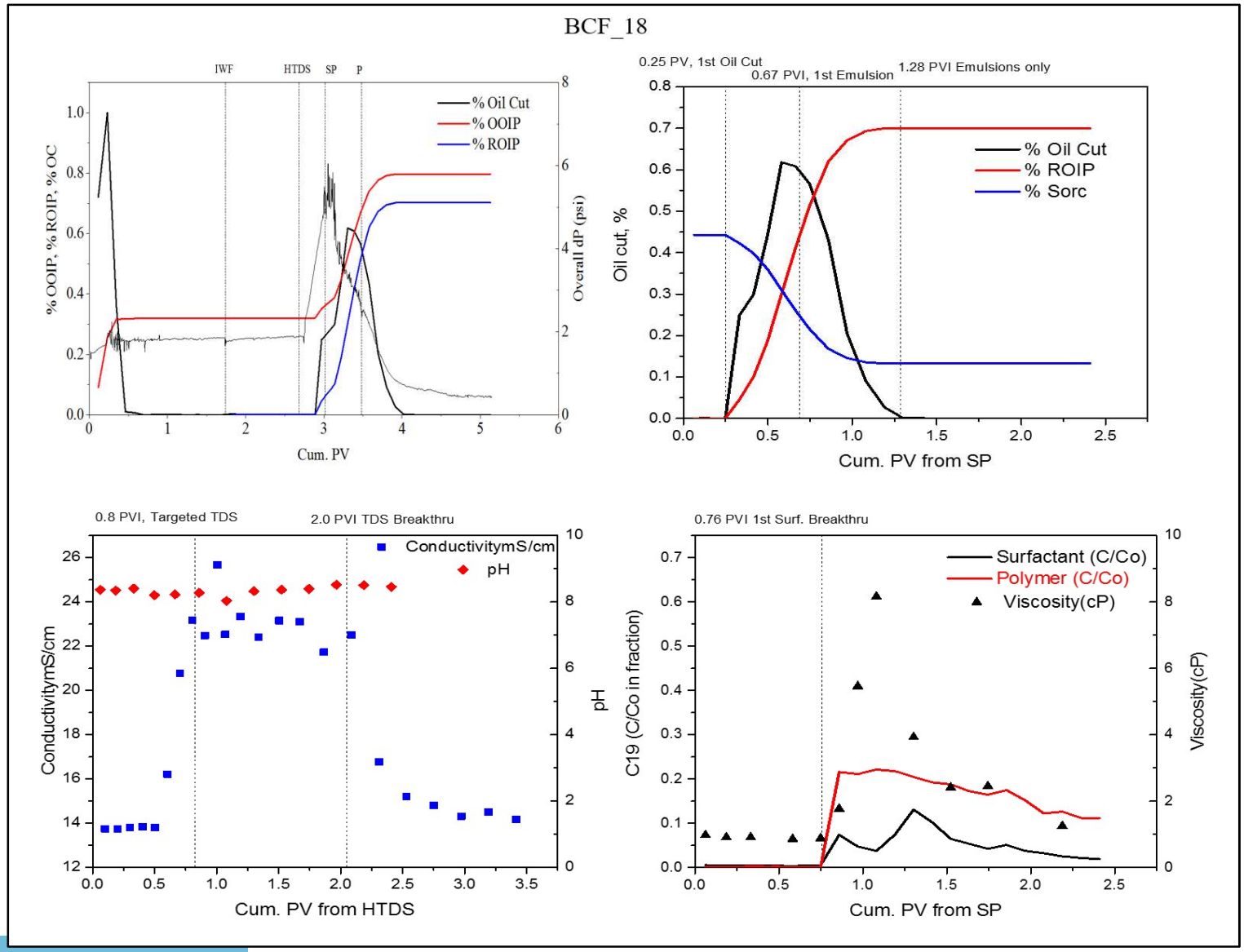

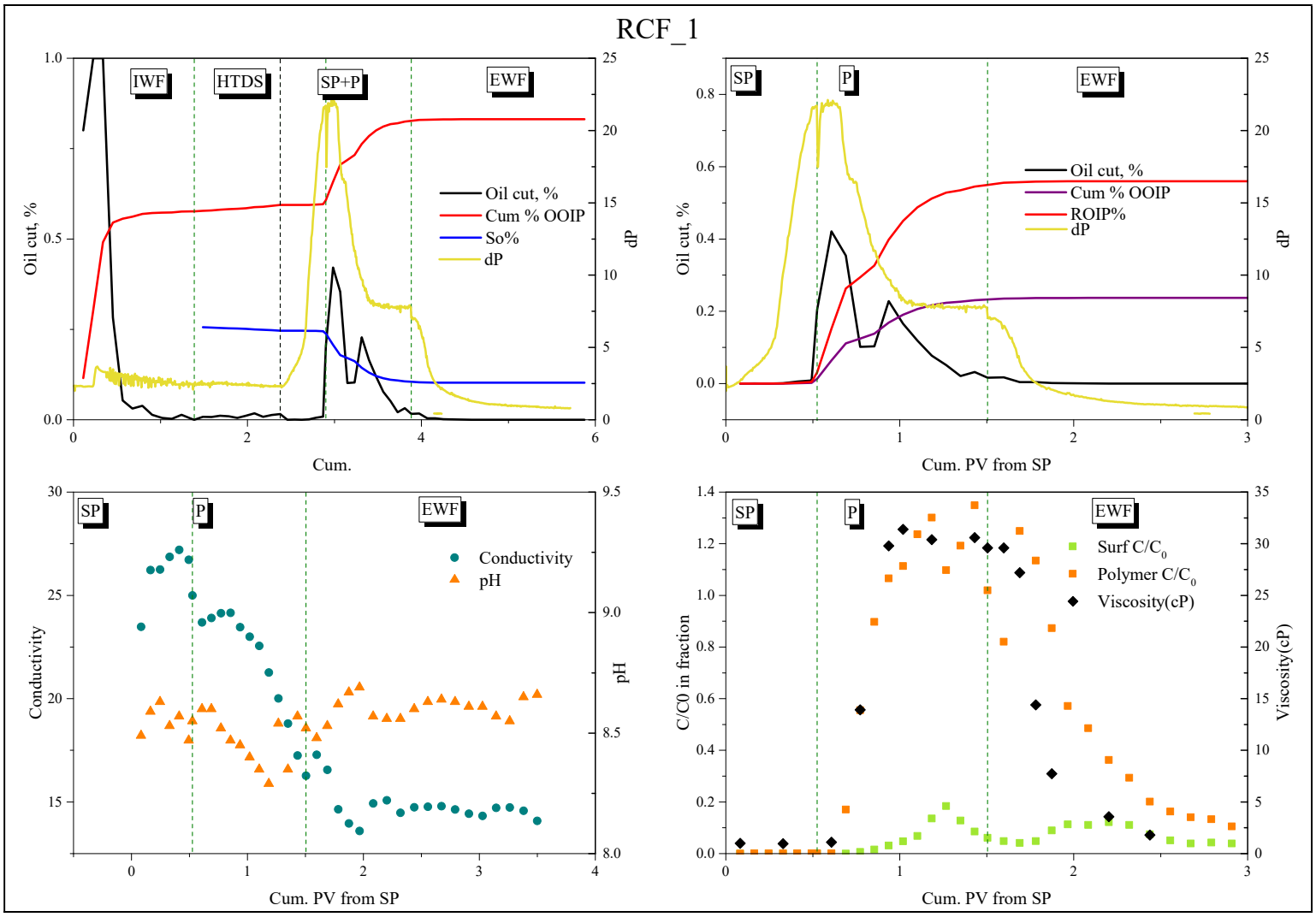

REFERENCES

[1] Green, D. W., & Willhite, G. P. (1998). Enhanced Oil Recovery. Henry L. Doherty Memorial Fund of AIME, Society of Petroleum Engineers. Retrieved from https://books.google.com/books?id=0cUWAAAACAAJ

[2] Patel, J., Borgohain, S., Kumar, M., Rangarajan, V., Somasundaran, P., & Sen, R. (2015). Recent developments in microbial enhanced oil recovery. Renewable and Sustainable Energy Reviews, 52, 1539–1558. https://doi.org/10.1016/j.rser.2015.07.135

[3] Doscher, T. M., & Wise, F. a. (1976). Enhanced Crude Oil Recovery Potential-An Estimate. *Journal of Petroleum Technology*, *28*. https://doi.org/10.2118/5800-PA

[4] Al Adasani, A., & Bai, B. (2011). Analysis of EOR projects and updated screening criteria. Journal of Petroleum Science and Engineering, 79(1–2), 10–24. https://doi.org/10.1016/j.petrol.2011.07.005

[5] Alvarado, V., & Manrique, E. (2010). Enhanced oil recovery: An update review. Energies, 3(9), 1529–1575. https://doi.org/10.3390/en3091529

[6] Babadagli, T. (2005). Mature Field Development - A Review. SPE Europec/EAGE Annual Conference. https://doi.org/10.2118/93884-MS

[7] Thomas, S. (2008). Enhanced oil recovery-an overview. *Oil & Gas Science and Technology-Revue de l'IFP*. Retrieved from https://ogst.ifpenergiesnouvelles.fr/articles/ogst/abs/2008/01/ogst07042/ogst07042.html

[8] Terry, R. (2001). Enhanced oil recovery. *Encyclopedia of Physical Science and Technology*. Retrieved from http://memberfiles.freewebs.com/50/69/68186950/documents/Enhanced Oil Recovery_EOR-1.pdf

[9] Levitt, D., Jackson, A., Heinson, C., Britton, L. N., Malik, T., Dwarakanath, V., & Pope, G. A. (2006, January). Identification and Evaluation of High-performance EOR Surfactants. In *SPE/DOE Symposium on Improved Oil Recovery*. Society of Petroleum Engineers.

[10] Flaaten, A. K. (2007). *Experimental Study of Microemulsion Characterization and Optimization in Enhanced Oil Recovery: A Design Approach for Reservoirs With High Salinity And Hardness* (Doctoral dissertation, University of Texas at Austin).

[11] Nasr-El-Din, H. A., Hawkins, B. F., & Green, K. A. (1991). Viscosity Behavior of Alkaline, Surfactant, Polyacrylamide Solutions Used for Enhanced Oil Recovery. *SPE International Symposium on Oilfield Chemistry*. https://doi.org/10.2118/21028-MS

[12] Levitt, D. B., Slaughter, W., Pope, G. A., & Jouenne, S. (2011). The Effect of Redox Potential and Metal Solubility on Oxidative Polymer Degradation. *SPE Reservoir Evaluation & Engineering*, *14*(3), 1–16. https://doi.org/10.2118/129890-PA

[13] Hornof, V., Neale, G. H., Chaaraoui, A., & Ottawa, U. (1983). Viscosity of Surfactant-Polymer Solutions. *SPE Oilfield and Geothermal Chemistry Symposium*.

[14] Nouri, H. H., & Root, P. J. (1971). A Study of Polymer Solution Rheology, Flow Behavior, and Oil Displacement Processes. *Proceedings of Fall Meeting of the Society of Petroleum Engineers of AIME*, (8). https://doi.org/10.2118/3523-MS

[15] Bataweel, M. A., & Nasr-El-Din, H. A. (2012). Rheological Study for Surfactant-Polymer and Novel Alkali-Surfactant- Polymer Solutions. *North Africa Technical Conference*. https://doi.org/10.2118/150913-MS

[16] Shupe, R. D. (1981). Chemical Stability of Polyacrylamide Polymers. *Journal of Petroleum Technology*, *33*(8). https://doi.org/10.2118/9299-PA

[17] Zhu, Y., Zhang, Y., Hou, Q., Yuan, H., & Jian, G. (2013). Effect of Main Factors on Oil Recovery of Surfactant-Polymer Flooding. *International Petroleum Technology Conference*.

[18] McCool, S., Walton, T., Willhite, P., Ballard, M., Rondon, M., Song, K., ... & Senior, P. (2012). *Bridging the Gap between Chemical Flooding and Independent Oil Producers*. University Of Kansas Center For Research Incorporated.

[19] Tagavifar, M., Herath, S., Weerasooriya, U. P., Sepehrnoori, K., & Pope, G. (2016). Measurement of Microemulsion Viscosity and Its Implications for Chemical. *SPE Improved Oil Recovery Conference*.

[20] Pope, G. A., Tsaur, K., Schechter, R. S., & Wang, B. (1982). The Effect of Several Polymers on the Phase Behavior of Micellar Fluids. *SPE Journal*.

[21] Fayers, F. J. (Ed.). (1981). Enhanced Oil Recovery: Proceedings of the Third European Symposium on Enhanced Oil Recovery, Held in Bournemouth, UK, September 21-23, 1981. Elsevier Scientific Publishing Company.

[22] Klinkenberg, L. J. (1941). The Permeability of Porous Media to Liquids and Gases. *Drilling and Production Practice*, 200–2013. https://doi.org/10.5510/OGP20120200114

[23] Wang, Y., Zhao, F., Bai, B., Zhang, J., Xiang, W., Li, X., & Zhou, W. (2010). Optimized Surfactant IFT and Polymer Viscosity for Surfactant- Polymer Flooding in Heterogeneous Formations. *SPE Improved Oil Recovery Symposium*, 1–11. https://doi.org/10.2118/127391-MS

[24] Enedy, S. L., Ali, S. M. F., & Stahl, C. D. (1982). Competing Roles of Interfacial Tension and Surfactant Equivalent Weight in the Development of a Chemical Flood. *Society of Petroleum Engineers Journal*. https://doi.org/10.2118/8898-PA

[25] Zhu, Y., Liu, X., Fan, J., & Exploration, P. (2015). Developments of ASP / SP Flooding Formulations for Huabei Fault Block Reservoir. *Society of Petroleum Engineers Journal*, 0–9.

[26] Guo, H., Dou, M., Wang, H., Wang, F., Gu, Y., Yu, Z., … Li, Y. (2015). Review of Capillary Number in Chemical Enhanced Oil Recovery. *SPE Kuwait Oil and Gas Show and Conference*. https://doi.org/10.2118/175172-MS

[27] Yang, Y. J., Chung, J., Philip, P. (2017) [Phase and Solution Behaviors of Aqueous Mixtures of a Propoxylated Surfactant]. Unpublished raw data.

[28] Otto, A., Du Plessis, J., & Wiechers, J. W. (2009). Formulation effects of topical emulsions on transdermal and dermal delivery. *International journal of cosmetic science*, *31*(1), 1-19.

[29] Rangel-Yagui, C. O., Pessoa-Jr, A., & Blankschtein, D. (2004). Two-phase aqueous micellar systems: an alternative method for protein purification. *Brazilian Journal of Chemical Engineering*, *21*(4), 531-544.

[30] Mezger, T. G. (2006). *The rheology handbook: for users of rotational and oscillatory rheometers*. Vincentz Network GmbH & Co KG.

[31] Mezzenga, R., Meyer, C., Servais, C., Romoscanu, A. I., Sagalowicz, L., & Hayward, R. C. (2005). Shear rheology of lyotropic liquid crystals: a case study. *Langmuir*, *21*(8), 3322-3333.

[32] Kang, K. C., Linga, P., Park, K. N., Choi, S. J., & Lee, J. D. (2014). Seawater desalination by gas hydrate process and removal characteristics of dissolved ions (Na+, K+, Mg 2+, Ca 2+, B 3+, Cl−, SO 4 2−). *Desalination*, *353*, 84-90.

[33] Marcus, Y. (1988). Ionic radii in aqueous solutions. *Chemical Reviews*, *88*(8), 1475-1498.

[34] Pathak, A. K. (2014). Conductance and bulk vertical detachment energy of hydrated sulphate and oxalate dianions: a theoretical study. *Molecular Physics*, *112*(11), 1548-1552.

[35] Yang, Y. J., Corti, D. S., & Franses, E. I. (2017). Effect of Triton X-100 on the stability of titania nanoparticles against agglomeration and sedimentation: A masked depletion interaction. Colloids and Surfaces A: Physicochemical and Engineering Aspects, 516, 296-304.

[36] Hiemenz, P. C., & Hiemenz, P. C. (1986). *Principles of colloid and surface chemistry* (Vol. 9). New York: M. Dekker.